LOW-OVERHEAD SCHEDULING FOR IMPROVING PERFORMANCE OF SCIENTIFIC APPLICATIONS

BY

VIVEK KALE

DISSERTATION

Submitted in partial fulfillment of the requirements
for the degree of Doctor of Philosophy in Computer Science
in the Graduate College of the
University of Illinois at Urbana-Champaign, 2015

Urbana, Illinois

Doctoral Committee:

Professor William D. Gropp, Chair
Dr. Bronis R. DeSupinski, Lawrence Livermore National Laboratory
Professor Maria Garzaran
Professor David Padua

Abstract

Application performance can degrade significantly due to node-local load imbalances during application execution on a large number of SMP nodes. These imbalances can arise from the machine, operating system, or the application itself. Although dynamic load balancing within a node can mitigate imbalances, such load balancing is challenging because of its impact to data movement and synchronization overhead. We developed a series of scheduling strategies that mitigate imbalances without incurring high overhead. Our strategies provide performance gains for various HPC codes, and perform better than widely known scheduling strategies such as OpenMP guided scheduling. Our scheme and methodology allows for scaling applications to next-generation clusters of SMPs with minimal application programmer intervention. We expect these techniques to be increasingly useful for future machines approaching exascale.

Acknowledgments

This work would not be possible without the help of many people. First, thanks to my advisor, Professor Bill Gropp, who provided me with several revisions to my thesis, several technical suggestions (including code development) throughout, and an initial and continual drive to learn new concepts and to solve challenging problems through a PhD. Additionally, I would like thank Professor Micheal Heath for helping to make the theoretical analysis part of this work more formal and systematic. Thanks to Simplice Donfack for his collaboration and support of the work on applying hybrid static/dynamic scheduling to dense matrix factorizations, and to Laura Grigori for overseeing a large portion of this work. Thanks also to Jim Demmel for discussing my work in the context of dense matrix factorizations, and for providing impetus for detailed investigation locality-based optimizations for dense matrix factorizations. I would like to especially thank Todd Gamblin for providing support for the software system that increased the applicability of this work and grew this work further, and to Bronis de Supinski for providing strategic research direction for runtime optimizations of our low-overhead scheduling techniques. Additionally, I'd like to thank Steve Langer who posed important questions to think about from an application programmer's point of view. I would also like to thank Martin Schulz for providing input on performance profiling, along with the LC division at Lawrence Livermore National Laboratory for providing technical support on the clusters at LLNL. I would also like to thank Torsten Hoefler for his input on performance modeling and theoretical analysis of low-overhead scheduling strategies. Thanks to my committee members David Padua and Maria Garzaran for their generous feedback and input throughout the dissertation process. Thanks to my labmates from the Scientific Computing Group at the University of Illinois at Urbana-Champaign for their feedback in practice presentations. Finally, this work would not be possible without the unconditional support and caring of family and friends throughout the PhD and the dissertation process.

Table of Contents

List of Tables

List of Figures

List of Abbreviations

MPI	Message Passing Interface
HPC	High Performance Computing
LDB	Load Balancer
static	OpenMP Static scheduling
dynamic	OpenMP Dynamic scheduling
guided	OpenMP Guided scheduling
half	Basic Hybrid Static/Dynamic Scheduling with 50% static fraction
besf	Basic Hybrid Static/Dynamic Scheduling
wSched	Weighted Factoring for Persistent Load Imbalances
uWldb	Weighted Hybrid Static/Dynamic Scheduling
sSch	Slack-Conscious Mixed Static/Dynamic Scheduling
sds	Staggered Static/Dynamic Scheduling.
combo	Example scheduler composition.

List of Symbols

τ	Time taken to complete the computational work of a dynamically scheduled task.
δ	Duration of excess work or idle time.
d	Number of tasks to be dynamically scheduled in a threaded computation region.
N	Number of loop iterations in a threaded computation region.
t_1	Length of time for a single loop iteration.
T_p	Time needed for computational work on p cores of a cluster's multi-core node.
S_i	Slack duration on process i.

Chapter 1

Introduction and Motivation

As applications become more sophisticated and architectures become more complex, a supercomputer may not be utilized to its peak performance [9,15, 29, 78]. Specifically, during application execution on a large number of processors, load imbalance can cause parallel efficiency of scientific applications to deteriorate with an increasing number of processors.

We focus on iterative MPI computations. Iterations may correspond to timesteps, numerical iterations, or both. In each iteration, steps involve synchronization across nodes, such as global reductions or near-neighbor communications. Broadly, applications with these characteristics can be called bulk-synchronous or loosely-synchronous.

Consider the kinds of load imbalances that arise in this context. Some imbalances arise somewhat randomly across individual cores. We can think of these as transient and uncoordinated imbalances. Examples of these types of imbalances are small, transient performance perturbances caused by time-shared operating system daemons, correctable hardware errors, variable memory access latencies, software floating-point exception handling, and dynamic CPU frequency management for power conservation [12, 61, 65, 70]. For brevity, we will call these variations *noise*, while noting that it is a generalization of the conventional definition of noise, which is typically associated with operating system daemons [12, 52, 72].

The other category of imbalances arises from *load variability*. Here, code executing on different threads takes different amounts of time, and so arrives at synchronization points at different times during each step. Many situations in which this happens involve persistent load imbalances. Persistent load imbalances have a (relatively) fixed pattern of load distributions across cores, over iterations of an application. The balance may shift somewhat across iterations, slowly, but the broad pattern remains similar. A major source of persistent load imbalances are the applications themselves. For example, application load imbalances exist in sparse matrix-vector multiplication used in quantum chromodynamics simulations [74] and N-body

force calculations used in molecular dynamic simulations [73]. Additionally, static variations in speeds of different cores may lead to persistent imbalances as well. Load variability also includes situations that are non-persistent imbalances. Here, the load variation significantly changes after every few iterations, such as in the case of adaptive mesh refinement [37].

A potential method for mitigating both of these categories of load imbalances is suggested by the fact that the number of cores per node is large and is steadily increasing over time [78]. Many machines with conventional processors have 32-64 cores per node, e.g., Cray's Titan, or IBM's Mira (BG/Q) [1,2]. Future versions of many-core processors, such as Intel's Xeon Phi, are likely to have several hundred cores per node [87]. It has been predicted that for an exascale machine, the number of nodes will not be much larger than today's petascale machines, but the number of cores per node will be substantially larger [9]. The existence of large numbers of cores within each node can be potentially utilized to reduce global load imbalance by dynamically equalizing the load within each node. This is the key approach that provides the context for this thesis.

The schematics in Figures 1.1 and 1.2 illustrate why our key approach mentioned above is potentially attractive. In these figures, the x-axis is time, and the y-axis is core number. A horizontal line represents the timeline of a core. A white space in the core's timeline represents the core's idle time. Consider the effects of system noise on overall performance, as shown in Figure 1.1a. On each timestep, a core on a different node experiences noise, given a system with a sufficiently large number of nodes. While on some iterations, no node may experience noise, and on other iterations multiple nodes might experience noise, the essential argument we are making is still valid. Even though the noise on any given core is rare and would not impact sequential computations significantly, the MPI synchronization between computations slows down the parallel program significantly. Our approach is illustrated by Figure 1.2b. If the load on the affected core can be re-distributed to the remaining cores within that node without much overhead, the overall impact of noise can be significantly reduced.

The schematic shown in Figure 1.2 applies for application-induced load imbalance, which is typically persistent. The performance is affected by the most heavily loaded core, as before. Again, if we could re-distribute the load within each node equally, the performance would be substantially improved. We make note that the indent on the node second to the bottom is due to differences in load across nodes, and handling this problem is complementary to this work. This re-distribution helps even for load variability that is not

persistent.

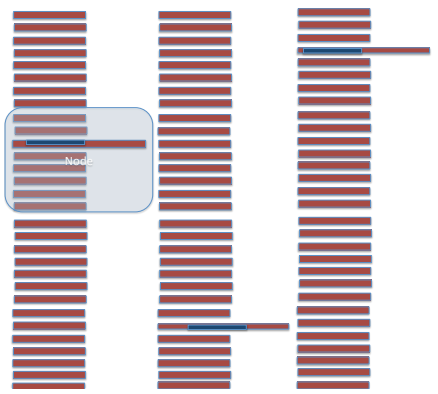

(a) Noise occuring on different nodes in different iterations delays every iteration.

(b) Execution times are significantly reduced, if we assume load can be perfectly re-distributed within each node.

Figure 1.1: Schematics of application timelines showing how impact of noise can be mitigated by idealized within-node work re-distribution.

(a) A modeled application timeline having persistent load imbalance across cores during execution.

(b) A modeled application timeline with work re-distributed across cores, to reduce load imbalance.

Figure 1.2: A modeled application timeline having load imbalance on some particular node through a re-distribution of work across cores within a node provides improved performance.

As a concrete example, consider the performance data shown in Table 1.2 for an N-body computation (a galaxy simulation) on a cluster named *cab*. Cab is an Intel Xeon Cluster with 16 cores per node. The table shows load imbalance during the application execution across all cores, in the form of the ratio of the load on the heaviest loaded core to the average load per core. This ratio captures the impact of load imbalance on execution time. As expected, the load imbalance increases as the number of cores increases in this strong scaling experiment.

To see how the above idealized approach will work for this example, we

assume that the load within each node is perfectly re-balanced without any overhead. For every node, we sum the load of each core on it. We then divide by the number of cores, to simulate the effect of an ideal within-node load balancer. In this scenario, the execution time will be decided by the most heavily loaded *node*. This leads to a substantial reduction in execution time, as shown in the table. This suggests that fixing within-node imbalance can be a powerful technique for improving program performance.

Num Nodes	**Num Cores**	**Across-core**
1	16	1.01
4	64	1.08
64	1024	1.41
1024	16384	1.45

Table 1.1: Standard load imbalance metric across all cores of multiple nodes of Cab.

Num Nodes	**Num Cores**	**Imbalance**	**Mitigated Imbalance**
1	16	1.01	1.00
4	64	1.08	1.04
64	1024	1.41	1.18
1024	16384	1.45	1.26

Table 1.2: Standard load imbalance metric taken across nodes (within each node, load is summed across cores) for the above N-body computation run on Cab, added to the rightmost column.

To be sure, for the persistent load imbalances of the kind seen in the N-body code, it is possible to use global across-node load balancing techniques. These could be overdecomposition-based measurement-driven load balancing techniques, such as those used in Charm++ [51]. Alternatively, they may be application-specific techniques, such as space-filling curve based techniques for Barnes-Hut N-body codes [92]. However, for the following reasons, the within-node dynamic load balancing is still attractive and necessary for persistent imbalances.

- Often, across-node load balancing requires significant effort. To use over decomposition based techniques, one has to change the programming model. Application-specific techniques may require significant effort. A within-node balancer can mitigate much of the imbalance with low programmer cost.

- Even if global load balancing is used, a significant residual imbalance remains because of imperfections in accurate predictions of load and imperfections in load balancing algorithms themselves.

- Global load balancers can be faster if they focus on partitioning work to the nodes (which are much smaller in number, compared with the number of cores), leaving the within-node imbalance for a within-node balancer.

- Often, applications with persistence still are not exactly repeating their behavior every time step. As particles move in N-body codes, for example, the load shifts slowly. This creates quasi-transient imbalance.

- Applications codes such as Adaptive Mesh Refinement, e.g., SAMRAI [37] or Shewchuck's triangulation programs [83], change behavior quickly as refinements and coarsenings are applied. A node may be a sufficiently large unit that these effects are neutralized, but work allocation to cores within a node must be changed after every refinement or coarsening.

Utilizing multiple cores to dynamically balance load within each node can be an effective technique for mitigating global load imbalance, without undue burden on the programmer. Although the potential of this idea of mitigating global load imbalance by dynamic load balancing within each node is attractive, its utility critically depends on whether the dynamic load balancing can be done effectively, and with low-overhead. Note that we assumed an idealized, perfect load re-distribution in the example and schematic above. The dominant methods for doing such load balancing, with minimal programming effort for the application programmer, are provided by OpenMP. However, as we show below, these methods are far from effective for our purpose.

We experiment with a single-node OpenMP implementation of two different codes, one a load balanced computation and the other a load imbalanced computation. With these codes, we try different ways to distribute work across cores, by running the code with OpenMP's three available schedulers.

As a representative of load imbalanced code, we consider the Barnes-Hut Lonestar benchmark [79], a code used in the context of galaxy simulation. We use the $100,000$ particle data set; this problem size is large enough to run out of cache and into main memory during application execution. For the load balanced code, we consider the NAS LU benchmark [50], a

code used within applications for solving a system of linear equations. We used problem class D for NAS LU code for the same reason as the problem size used for Lonestar Barnes-Hut code. Note that the purpose of applying dynamic load balancing to a load balanced code is to handle transient load imbalances, if they arise.

The below experiment is done on 1 node of Cab, which consists of two 8-core Intel Xeon chips with a CHAOS operating system. We use the Intel `icc` compiler, and use the `-O3` compiler optimization level. Also, we ensured that thread-to-core binding was on by setting the `GOMP_CPU_AFFINITY` OpenMP environment variable. The average of the timings across 25 trials is reported. For each trial, a separate job was submitted. The below is based on application execution time reported by the original code. We used `omp_get_wtime()` to gather the timings for each run.

Figure 1.4 shows the performance of different OpenMP scheduling strategies for Barnes-Hut and NAS LU. The OpenMP dynamic strategies make the performance substantially worse for NAS LU, and do not improve it to the extent expected for Barnes-Hut, as explained below. The first challenge for any load balancing strategy is in handling thread idle times due to load imbalances from the application or architecture. The method used to obtain the idle time is shown in Figure 1.3. The average thread idle time shown in blue in Figure 1.4 is the sum of idle times across all cores divided by the number of cores. The other time, shown in black, is average computation time per core, calculated as the difference between (a) the sum of execution times divided by the number of cores, and (b) the average thread idle time. Note that the sum of idle times across threads is the load imbalance that could be avoided. Thus, the average idle time across all threads is the overhead of idle time incurred during application execution. One might expect that dynamic scheduling would eliminate thread idle time. However, idle time can exist in dynamic scheduling due to task quantization [54], i.e., even with dynamic scheduling, each core except one may have idle time as large as the size of each dynamically scheduled task (a task is a chunk of iterations assigned at once).

The dynamic scheduling almost completely eliminated idle time for Barnes-Hut, but the total execution did not go down by the same amount, i.e., the black portion of the bar increased. For NAS LU, the execution time in both dynamic strategies is substantially worse than the static strategy.

What are the remaining overheads that cause the increased execution time in Figure 1.4? We first isolate the compute time of the application execution time, or the time spent doing the application's work. The compute

```
double idleTimeCost;

double t, idleTime;
int myTid, numThreads;
#pragma omp parallel private(myTid)
{
  myTid = omp_get_thread_num();
  numThreads = omp_get_num_threads();
#pragma omp for
for (i=0; i<n; i++)
  {
    c[i]+= a[i]*b[i];
  }
 idleTimes[myTid] = - omp_get_wtime();
} // threads synchronize here
t = omp_get_wtime();
for (tid=0; tid<numThreads ; tid++)
  {
    idleTimes[i] += t;
    idleTime += idleTimes[i];
  }
idleTimeCost += idleTime/numThreads;
```

Figure 1.3: Calculation of the total overhead of thread idle time for an MPI+OpenMP code.

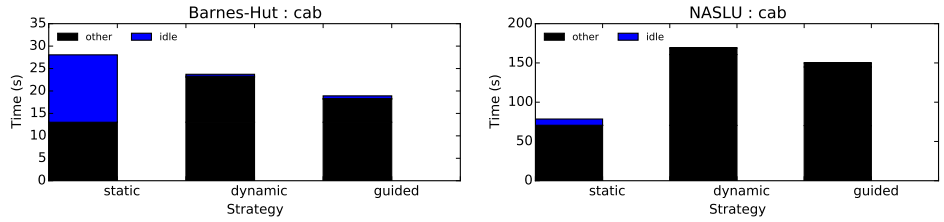

Figure 1.4: Breakdown of execution time for a load imbalanced code (left) and a load balanced code (right) on cab, shown for the three available OpenMP scheduling strategies.

time for each strategy is calculated by obtaining the time for execution using OpenMP static scheduling when run on 1 core of a node, and dividing this time by the number of cores the experiment was run with. Figure 1.5 shows compute time in blue at the bottom of each bar.

One source of overhead is synchronization overhead, which is the time taken during application execution for coordination of threads to share the queue of work. We measure the synchronization overhead using HPC-Toolkit [3], which provides call-path profiles of functions invoked during application execution; we focus on those functions invoked from the OpenMP

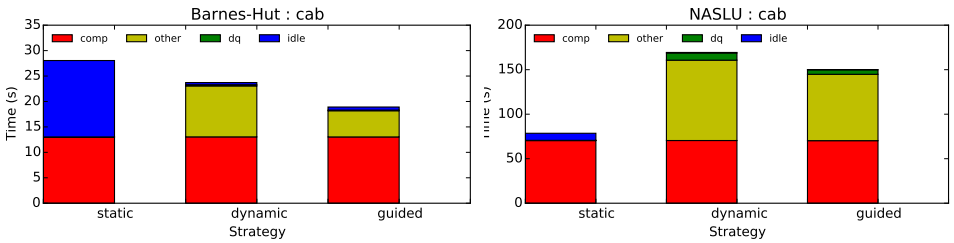

Figure 1.5: Breakdown of time. Synchronization overheads are shown in green.

runtime. The call-path profiles tell us the percentage of execution time and the total execution time taken for all invocations of the `omp_lock()` function within the OpenMP runtime, which is invoked each time a thread retrieves a chunk of work from the queue. This percentage provides the synchronization overheads of each scheduling scheme. From Figure 1.5, we see the synchronization time, shown in green in the graph just below the idle time. Synchronization overhead only exists when using dynamic or guided scheduling; for the static scheduling scheme, threads do not use a shared lock to retrieve their iterations, in the beginning of execution, and therefore this cost of assigning work to threads does not exist.

While seemingly insignificant, these synchronization overheads account for approximately 5% percent of execution time for the NAS LU and the Barnes-Hut code. The overhead of synchronization is larger for the load balanced code NAS LU. This may be partly because the iterations are more finely quantized, and partly because all threads access the lock at the same time, since the threads are done with their local work at roughly the same time.

The above problem of synchronization overhead is inevitable for supercomputer nodes with larger numbers of cores. The reason can be seen by breaking down the synchronization overhead into its two components: 1. the function call overhead that each thread must incur when it enters and exits the lock function, i.e., the locking function call overhead, and 2. the time that threads spend waiting for another thread in the critical section to make the lock available, i.e., the serialization overheads. While the locking function call overheads stay constant, the serialization overheads will only become larger with an increasing number of cores, since more threads will have to wait for the lock. Thus, we can project a larger contribution of this synchronization overhead as we run the code on supercomputer nodes with more cores.

However, as can be seen in Figure 1.5, the synchronization overhead alone does not account completely for the performance degradation with OpenMP dynamic scheduling and OpenMP guided scheduling. Since dynamic scheduling may lead to accessing a cache line that may be in another core's cache, the remaining overheads are likely from data movement.

To confirm the impact to data movement, we measured the L2 and L3 cache misses for the threaded computation regions of each application using PAPI [17]. We measured the cache misses by starting the PAPI counters just before the threaded computation region, and stopping the PAPI counters just after the threaded computation region. We used `PAPI_counter_start()` and `PAPI_counter_stop()` for counter functions, defined in the high-level interface. Before we started the PAPI counter, we invoked the function `PAPI_thread_self()`. We used the PAPI counters `PAPI_L2_TCM` and `PAPI_L3_TCM` for the L2 and L3 cache misses, respectively. At the end of each threaded computation region, we took the sum of cache misses across all threads, and reported the sum across all threaded computation regions, for each threaded computation region. The cache misses are the total cache misses across all cores. Figure 1.6 shows the L2 and L3 cache misses for the Barnes-Hut code (left) and NAS LU (right).

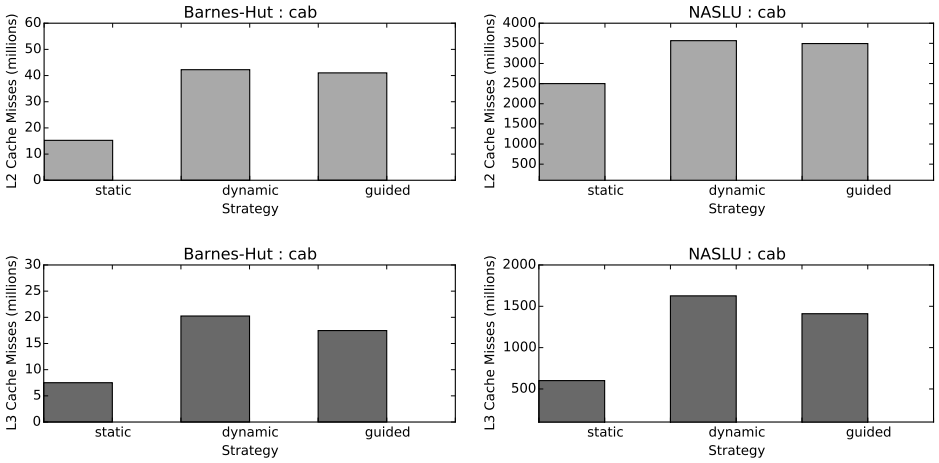

Figure 1.6: Cache misses with L2 misses on top and L3 on bottom, for different OpenMP scheduling strategies.

The results from Figure 1.6 suggest that the performance degradation of OpenMP dynamic scheduling and guided scheduling, with respect to OpenMP static scheduling, is due to the significantly higher L2 and L3 cache misses observed when using OpenMP dynamic and guided scheduling. Specifically, dynamic scheduling has roughly 4.0 times higher L2 cache

misses over static scheduling, and 3.5 times higher L3 cache misses over static scheduling. The cost of data movement does not decrease significantly with OpenMP guided scheduling. OpenMP guided scheduling has 3.5 times higher L2 cache misses compared to OpenMP static scheduling, and 2.8 times higher L3 cache misses compared to OpenMP static scheduling. The cost of coherence cache misses increases with increasing numbers of cores. The reason is that the probability that a core selects a tasklet that it did not execute in the last invocation of the threaded computation region (this incurs coherence cache misses) increases with increasing numbers of cores.

1.1 Cache Miss Calculations

To check that the cache misses in Figure 1.6 are in fact impacting performance and can explain most of the performance loss quantitatively, we show calculations for NAS LU. We obtain the time for an L2 cache miss and for an L3 cache miss on Cab using the specification sheet for Cab's node architecture [60], along with Intel's forum post reply referring to this specification sheet that gives the information needed [24]. In the architecture specification sheet, the processor frequency is 2.66GHz. The forum post indicates that the L2 remote cache miss latency is 100-300 cycles, so we use the mean cycle time of 200 cycles. The time to remote DRAM, i.e., the L3 cache miss latency, is 100 nanoseconds.

We need to account for 485.52 - 83.53 - 24.65 = 376 seconds of time spent in dynamic scheduling. Note that we do not need the execution time breakdown here, since this code exhibits low idle time. Cache miss time for the L2 cache is $\frac{200}{2.66\times10^9} \cdot (3845 \times 10^6 - 2257 \times 10^6) = 65$ seconds. This leaves 376 - 65 = 311 seconds to account for. Cache miss time for the L3 cache is $(100 \cdot 10^-9) \cdot (1676 - 631) \times 10^6 = 97$ seconds. This now leaves 311 - 97 = 214 seconds to account for. The time of L3 cache misses may be much higher than 100 nanoseconds, because access to main memory by multiple threads requires threads to wait in the memory queue. In the worst case, i.e., when all threads access main memory simultaneously, the latency to memory is a factor of $(16 + (16 - mem\_queue\_depth) \times 100)$ nanoseconds of the original latency, where mem_queue_depth = 12 on this machine.

To check that memory bandwidth was the factor for the increase in time for L3 cache misses, we ran STREAM [66] on one core of Cab and on all cores

of Cab. We recorded the bandwidth for both runs. The memory bandwidth of STREAM triad run on one core is 14,837.24 MB/s, but the memory bandwidth of STREAM triad run on 16 cores is only 103,669.71 MB/s, a 7x improvement in memory bandwidth rather than a 16x improvement. The effective memory latency increases by a factor of 2.4x, giving 238 seconds instead of 97 seconds for the cache miss time for L3. The remaining time is now 311 - 238 = 73 seconds. This may be due to the L2 cache miss latency being higher (also, note that the L2 cache miss latency was reported at 1 core). Another cause could be TLB misses, although we to tried reduce their impact by using huge pages for the runs.

While the above is a rough estimate, it helps explain the performance degradation. Additionally, in terms of order of magnitude, the calculations show that the timings shown in yellow for NAS LU in Figure 1.5 are mostly attributed to data movement.

Thus, current OpenMP schedulers do not solve the performance problem for next-generation clusters of SMPs. We have identified three challenges to obtaining good performance using dynamic load balancing within a node: (1) idle time due to load imbalances from the application or system noise, (2) data movement overhead, and (3) synchronization overheads from runtimes. These challenges provide motivations for developing a new set of schedulers, which balance the tradeoff between load balance and locality that works for any application-architecture pair.

To summarize, we first argued for the importance of handling within-node load imbalances, and how they could mitigate the performance loss due to global load imbalances. We describe these schematically for both transient and persistent imbalances, using NAS LU and N-body code, respectively. We further showed that using OpenMP scheduling strategies to do this dynamic load balancing is problematic because they add significant data movement overheads. Given the above challenges, the objective of this thesis is to:

Design a set of new scheduling strategies that handles all three causes of performance loss, i.e., thread idle time, data movement, and synchronization overhead, simultaneously, for any application and architecture, in the context of an MPI+OpenMP application.

Thus, we ask: can we combine a static and dynamic scheduling scheme that simultaneously reduces load imbalances and scheduler overhead, in an intelligent manner?

The key idea of our solution is to allocate to threads a fixed fraction of OpenMP loop iterations statically, and schedule the remainder dynamically. We define the ratio of static loop iterations to all loop iterations as the *static fraction* (and the ratio of dynamic iterations to all iterations as the *dynamic fraction*). The scheduling schemes developed throughout this thesis are an elaboration of this basic idea.

1.2 Contributions

The main contributions of this thesis are:

- An experimental method to determine parameter values of our strategy which achieves the tradeoff between load balance and locality;
- A runtime determination of scheduler parameters for maximizing both load balance and locality, given partially transient and partially persistent load imbalance;
- A performance model and theoretical analysis of scheduler parameter values for our strategy for any number of nodes;
- analysis and experimentation of the tradeoff between locality and load balance for coarse-grained application-generated imbalances;
- A methodology to provide for continual innovation of new scheduling strategies through a combination of basic strategies developed, and to provide a way to integrate into existing OpenMP or MPI runtimes, or any exascale runtime.

Low-overhead dynamic scheduling has far-reaching implications because it allows us to utilize the existence of multiple cores on a node to mitigate the effects of load imbalances. Since the number of cores is expected to grow far more rapidly than the number of nodes in future generations of hardware [9, 29, 78], future machines will be able to prevent effects of load imbalances from propagating to other nodes by off-loading delayed work to other cores *within* the node. If integrated with MPI and OpenMP implementations, our techniques will avoid the scaling wall due to load imbalances for several generations of machines to come.

1.3 Thesis Outline

The remainder of this thesis is organized as follows. Chapter 2 describes the problem of transient load imbalance, introducing a basic low-overhead hybrid static/dynamic scheduling strategy along with some variants, for empirically tuning the tradeoff between load balance and locality. It then also describes the enhancements to the basic scheduling strategy.

Chapter 3 discusses runtime adjustments to our low-overhead scheduling strategies that can handle a mixture of imbalances due to transient noise and persistent (core) noise. Chapter 4 discusses a scheduling technique that uses a model-guided tuning of our scheduler's parameters and optimizes the scheduler for each MPI process. Chapter 5 describes techniques and optimizations for reducing the loss of spatial locality in hybrid static/dynamic scheduling. Chapter 6 describes how our techniques would be used by an application programmer, along with a description of how different scheduling strategies can be composed. Chapter 7 provides a literature survey of relevant related work. Finally, Chapter 8 concludes this thesis, including broader impact and possible future directions and extensions of this work.

Chapter 2

Hybrid Static/Dynamic Scheduling

In the previous chapter, we highlighted three challenges for current OpenMP loop schedulers. In this chapter, we show an intuitive diagram and model for OpenMP static scheduling and OpenMP dynamic scheduling. With this, we present our solution of mixed static/dynamic scheduling using OpenMP static and dynamic scheduling to obtain the benefits of static and dynamic scheduling, which can address the challenges of static and dynamic scheduling. Given this mixed static/dynamic scheduling scheme, we ask how to select the static fraction, and suggest a basic strategy of exhaustive search. We apply the resulting scheduling strategy to the NAS LU and Barnes-Hut code in Chapter 1. We proceed to describe a 3D regular mesh code, and apply our static/dynamic scheduling technique to this code. In this part of the chapter, we describe our own implemented scheduling library, which allows for providing locality across timesteps for the dynamic section of the scheduler, and allows for simultaneously tuning different parameters of the scheduler. Finally, we discuss our approach applied to dense matrix factorizations, highlighting a Communication-Avoiding LU code which has our hybrid static/dynamic scheduling approach applied to it. We particularly show its competitive performance over two widely-known implementations of LU factorization, one from Intel's MKL library for numerical linear algebra codes, and the other from University of Tennessee's PLASMA runtime.

2.1 Basic Mixed Static/Dynamic Scheduling Technique

Given the thesis objective to design a set of new scheduling strategies that handle all three causes of the problem, i.e., thread idle time, data movement, and synchronization overhead, simultaneously, for many applications and platforms, in the context of an MPI+OpenMP application, we propose a new scheduling scheme.

Figure 2.1 shows a schematic of an OpenMP statically scheduled

threaded computation region's invocation, when using 4 threads, followed by an MPI communication function invocation. The figure depicts an invocation of the threaded computation region on an arbitrary I^{th} invocation on one of the MPI processes. The x-axis is time, and the y-axis is different threads within the process, each with its own hardware resource. When no noise occurs during a threaded computation region, and each loop iteration takes an equal amount of time, this computation proceeds efficiently without any idle time on any thread, as shown on the top part of Figure 2.1.

The lower part of the figure shows what happens when a noise event affects one of the cores. As can be seen, the noise event causes all other threads to wait at the thread barrier. This in turn causes other MPI processes to wait within MPI communication. This waiting of other MPI processes delays the application's critical path, just as we saw in Figure 1.1.

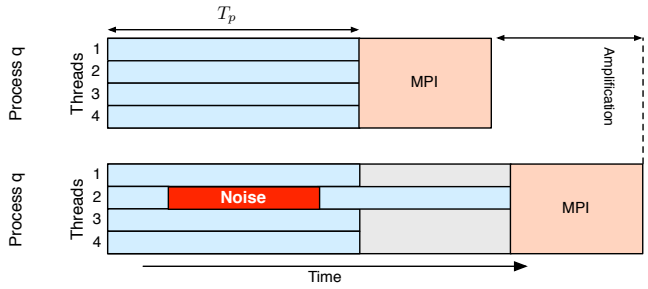

Figure 2.1: Impact of performance irregularities for static scheduling.

Figure 2.2 shows a schematic of a dynamically scheduled (OpenMP) threaded computation region's invocation, when using 4 threads. The lower part of the figure shows what happens when a noise event affects one of the cores. In this specific case, the extra delay caused by the noise event on thread 2 is reduced by the other 3 threads doing the work that thread 2 would have done if this threaded computation region were statically scheduled. Essentially, dynamic scheduling has moved the excess work, induced by noise, off the application's critical path, and consequently has reduced the impact of amplification. However, this dynamically scheduled strategy incurs scheduling overhead, which increases the time taken to execute the code. The scheduler overhead, as noted in Chapter 1, is caused by data movement and synchronization. The data movement overhead is induced by a thread switching to spatially unrelated loop iterations, and is reflected in the increased width of each computation block. The synchronization overhead is incurred at the beginning of execution of each loop iteration. This

scheduling overhead causes each iteration to be dilated, causing a significant performance degradation.

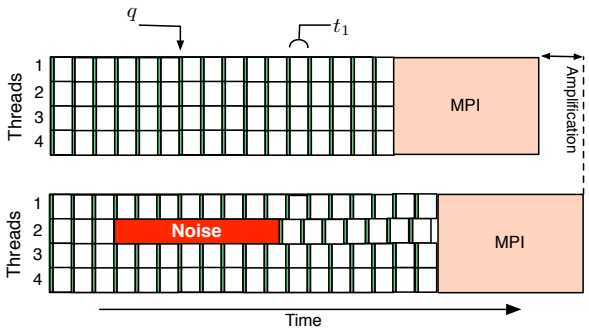

Figure 2.2: Dynamic scheduling of one invocation of a threaded computation region on an arbitrary MPI process.

In Chapter 1, we asked how we can combine static and dynamic scheduling in a way that reduces overhead for HPC applications. Because many synchronous MPI applications involve an outer iteration followed by a synchronization across all threads, we combine static and dynamic scheduling in a way that allows for maximum performance gains in this context. We *intelligently* combine static and dynamic scheduling by making each thread first do a pre-assigned fraction of the loop's iterations statically, and then do the remaining part dynamically. Figure 2.3 illustrates our approach on a simple threaded computation region on a single node. By dividing the iterations into a statically allocated subset and a dynamically allocated subset, we reduce the overhead in the static component, while utilizing the dynamic component for acheiving load balance. We thus hope to combine the best of both scheduling strategies. We refer to this strategy as *mixed static/-dynamic scheduling*, and we explore this idea further in the context of the N-body and NAS LU code described in Chapter 1.

The question is, *how do we select the appropriate static fraction*? In the next section, we discuss an empirical method to tune the above scheduler's static fraction, effectively developing a scheduler that aims to overcome the 3 challenges described in Chapter 1.

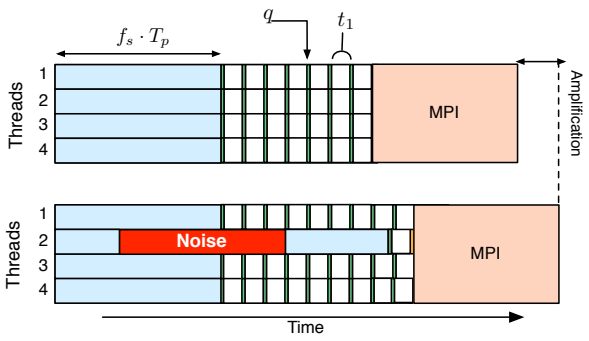

Figure 2.3: Using mixed static/dynamic scheduling to handle load imbalances across cores.

2.2 Results for Barnes-Hut and NAS LU with Mixed Static/Dynamic Scheduling

As a first approximation for the static fraction for the scheduler, we choose 50%. This can be implemented by splitting the data parallel loop shown in Figure 2.4 into two OpenMP loops: the first statically scheduled, and the second dynamically scheduled, as shown in Figure 2.5.

```
#pragma omp parallel for schedule(static)
   for(int i=0; i<n; i++)
      c[i] += a[i]*b[i];
```

Figure 2.4: OpenMP loop with static scheduling.

```
#pragma omp parallel for nowait
  for (int i = 0; i < n/2; i++)
      c[i] += a[i]*b[i];

#pragma omp parallel for schedule(dynamic)
  for (int i = n/2; i < n; i++)
      c[i] += a[i]*b[i];
```

Figure 2.5: OpenMP loop modified for mixed static/dynamic scheduling.

We refer to this strategy as Mixed Static/Dynamic Scheduling, and label it *half* in the graphs for brevity. We expect *half* to cut the dynamic scheduling overhead in half. Figure 2.6 shows the performance of this strategy along with multiple OpenMP strategies on *Cab* for Barnes-Hut and NASLU codes. For the Barnes-Hut code, the *half* scheduling improves performance 10.1%

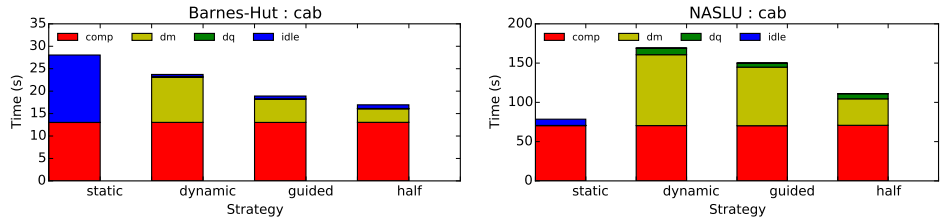

Figure 2.6: Set $f_s = 0.5$: In *half*, threads do the first half of their iterations statically. See rightmost bar in the bar graph.

over OpenMP guided, due to preservation of locality across invocations of threaded computation regions, and thus less data movement across invocations of the threaded computation region. We see that using the *half* scheduling strategy, we get a relatively large 41% gain over OpenMP static. For the NAS LU code, the *half* scheduling still has relatively high overhead compared to OpenMP static scheduling.

2.2.1 An Empirical Method for Finding the Best Static Fraction

Is a 50% static fraction best? The best static fraction depends on the characteristics of the application and the platform. One way to solve this problem would allow the user to set the static fraction. This strategy, taken by itself, is referred to as *Hybrid Static/Dynamic Scheduling*. The user then uses this strategy to tune the static fraction experimentally, trying static fractions between 0.0 and 1.0, e.g., in increments of 0.01 (the increment is configurable), and use the best performing one (for each node) during application execution. We vary the static fraction environment variable in increments of 0.01. We use an increment of 0.01 to get enough data points to understand performance characteristics, but we note that more refinement gives more improvement. This strategy is called the *best static fraction*, or *besf*. Its application to the data parallel loop in Figure 2.4 is shown in Figure 2.7.

Figure 2.8 shows wall clock time for the Barnes-Hut code for different static fractions. Each data point is an average over 10 trials. Also, fully dynamic scheduling (static fraction is 0%) is better than fully static scheduling (rightmost data point), but the static fraction of 49% gives even better performance.

Figure 2.9 shows wall clock time for the NAS LU code for different static fractions. The fully static scheduling is significantly better than fully dynamic. The static fraction of 96% is the best performing. When com-

```
double fs = get_env_var(STATIC_FRACTION);
#pragma omp parallel nowait
{
#pragma omp for
  for (int i = 0; i < fs*n; i++)
      c[i] += a[i]*b[i];
}

#pragma omp parallel
{
#pragma omp for schedule(dynamic)
  for (int i = fs*n; i < n; i++)
      c[i] += a[i]*b[i];
}
```

Figure 2.7: OpenMP statically scheduled loop transformed for hybrid static/dynamic scheduling.

pared with its performance improvement over 100% dynamic, the difference between the performance of the best performing static fraction and performance of 100% static may appear small, but we still get a significant improvement.

Comparing the two performance curves of N-body and NAS LU suggests that load balanced computations have a line graph for varying static fractions that is shaped like a *reverse checkmark*, and load imbalanced codes have a performance curve for varying static fractions that is shaped like a *fat (forward) checkmark* (the checkmark is fat because it has a rounded bottom). The two performance curves also show that the best performing static fraction varies for different applications.

The static fraction used in the *besf* scheduling strategy for Barnes-Hut and NAS LU is the minima of the curves in Figure 2.8 and Figure 2.9, respectively.

Figure 2.10 shows the performance of Barnes-Hut and NASLU with the best static fraction strategy added. Using *besf* for Barnes-Hut improves performance 52% over OpenMP static, and also improves performance 29% over OpenMP guided scheduling. More importantly, our *besf* strategy now also provides non-trivial performance benefits for NAS LU: we get (a somewhat unexpected) 8.4% gain over OpenMP static. The idle time (blue) in the figure for NAS LU with static scheduling is likely due to the incidental imbalance not coming from the application.

Figure 2.11 shows the L2 and L3 cache misses for N-body and NAS LU, with the best static fraction strategy added to the rightmost bar. The *best*

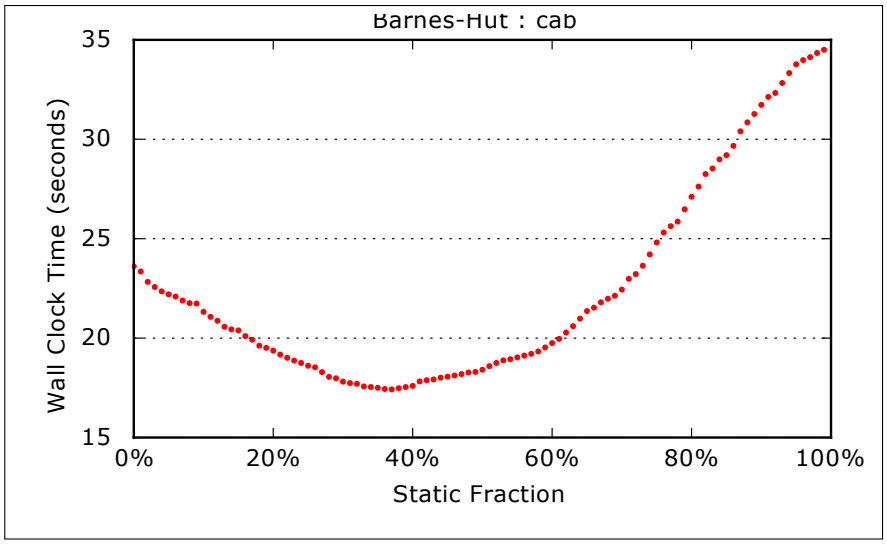

Figure 2.8: Performance for different static fractions when using hybrid static/dynamic scheduling for Barnes-Hut.

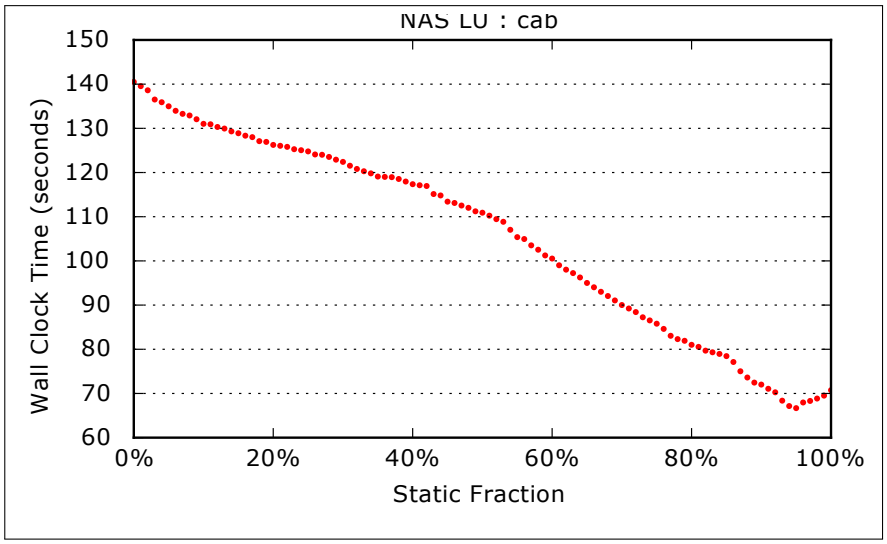

Figure 2.9: Performance for different static fractions when using hybrid static/dynamic scheduling for NAS LU.

static fraction, or *besf*, strategy has significantly less, i.e., 62% less, L2 cache misses than *guided* scheduling, but only a somewhat small amount more, i.e., 17% more, L2 cache misses than OpenMP *static* scheduling, helping to explain why the *besf* strategy improves performance over OpenMP static scheduling.

Although our strategies (*half* and *besf*) reduce cache misses through the statically scheduled part, the dynamically scheduled part still incurs cache

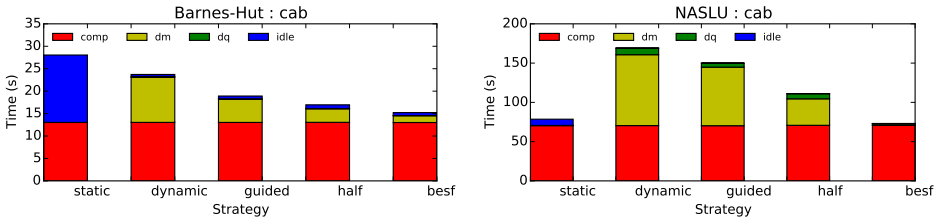

Figure 2.10: Execution time breakdown with the *besf* strategy added on the rightmost bar.

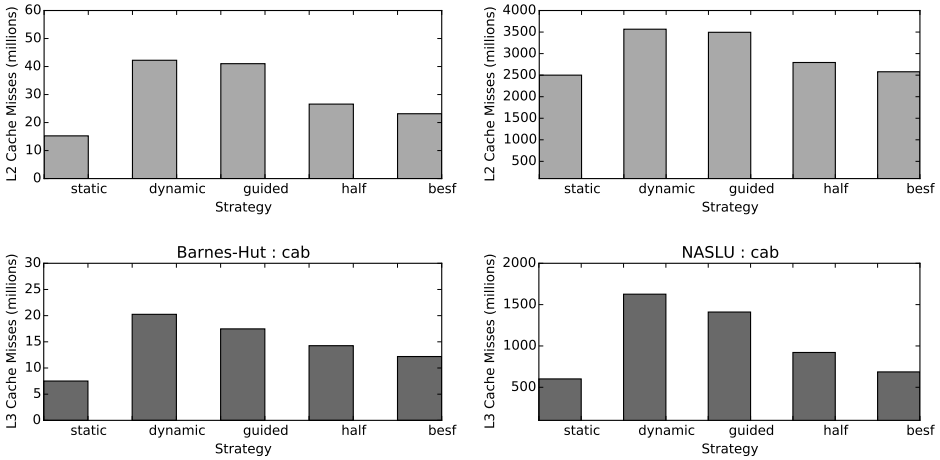

Figure 2.11: L2 cache misses shown in the top graphs; L3 in the bottom. The *best static fraction* strategy is added on the rightmost bar.

misses because of the loss of spatial locality. We describe a scheme to reduce these further in Chapter 5.

We next apply our strategy, with empirical determination of best static fraction, to several NAS benchmarks. Table 2.1 and Table 2.2 respectively show the performance improvement of our scheduling technique over OpenMP static scheduling on the NAS benchmarks for an Intel Westmere 16-core node (cab) and an IBM BG/Q 16-core node (rzuseq). As can be seen in Table 2.1, the gains for the CG benchmark are large on the Intel Westmere machine due to the scheduler's handling of application load imbalance of NAS CG along with load imbalance due to performance irregularities arising from OS noise. As seen in Table 2.2, while the BG/Q machine has low noise [12], the scheduler still achieves significant performance gains for CG because of its ability to handle the application load imbalance of CG.

SP	BT	LU	FT	CG	MG
4.14%	5.42%	5.57%	5.31%	14.67%	9.48%

Table 2.1: Table showing performance gains over OpenMP static for NAS benchmarks with *besf* on cab.

SP	BT	LU	FT	CG	MG
-1.09%	-1.05%	-1.62%	-1.59%	7.93%	5.04%

Table 2.2: Table showing performance gains over OpenMP static for NAS benchmarks with *besf* on rzuseq.

2.3 Study with MPI Code And Outer Iteration Locality

We next introduce a variant of the hybrid scheduling strategy. We use an MPI regular mesh computation to study the performance of this strategy. We then study the performance impact of our strategy on one node, followed by a scalability study that shows how the amplification problem is controlled.

2.3.1 A Scheduler for Outer Iteration Locality

When we use hybrid static/dynamic scheduling with OpenMP, the loop iterations in the dynamic section are selected by threads somewhat randomly. In particular, when execution returns to the next outer iteration, the scheduler has no memory of the allocation of the previous outer iteration. Iteration I may be executed by thread a in one outer iteration of an MPI region, but it may be executed by a completely different thread b in the next. This loss of locality is detrimental for NUMA-like machines and platforms with first-touch page allocation policies, as well as for TLB misses and other factors. Our next scheduling strategy addresses this loss of locality by keeping track of the thread on which each loop iteration was executed before.

We implemented the technique for supporting dynamic scheduling of computation with a queue that was shared among threads. Each element of the shared queue (we refer to the element as a tasklet) contains the specification of the work for which the thread executing this tasklet is responsible, and a flag indicating whether the tasklet has been completed by a thread. In order to preserve locality so that in repeated computations the same threads can get the same work, we also maintain an additional tag specifying the last thread that ran this tasklet. In the execution of each

iteration of an MPI+pthreads program, there are 3 repeated phases: MPI communication, statically scheduled computation, and dynamically scheduled computation. In the first phase, thread 0 does the MPI communication for border exchange. During this time, all other threads typically wait at a thread barrier. In the second phase, each thread does all work that is statically allocated to it. Once a thread completes its statically allocated work, it immediately moves to the third phase, where it starts retrieving the next available tasklet from the queue shared among other threads, which it repeats until the queue is empty. As in the completely static scheduled case, after threads have finished computation, they must wait at a barrier before continuing to the next iteration. The percentage of dynamic work, granularity/number of tasklets, and number of queues per node, are specified as parameters.

An additional scheme extends this strategy to improve outer iteration locality. In this scheme, each tasklet in the queue has an extra field, or *tag*, that records the thread ID that executed the tasklet in the previous outer iteration. In the third phase, when a thread retrieves a tasklet from the queue, the scheduler attempts to first give it a tasklet having a *tag* equal to its thread ID. Only if such a tasklet is not available are other tasklets assigned. We refer to this strategy as *scheduling with locality tags*, or simply *scheduling with locality*.

2.3.2 MPI Regular Mesh Computation

Our model application is an exemplar of regular mesh code. For simplicity, we will call it a Jacobi algorithm, as the work that we perform in our model problem is the Jacobi relaxation iteration in solving a Poisson problem. However, the data and computational pattern are similar for both regular mesh codes (both implicit and explicit) and for algorithms that attempt to divide work evenly among processor cores (such as most sparse matrix-vector multiply implementations). Many MPI implmentations of regular mesh codes traditionally have a pre-defined domain decomposition, as is seen in many libraries and microbenchmark suites [86]. This optimal decomposition is necessary to reduce communication overhead, minimize cache misses, and ensure data locality. In this work, we consider a slab decomposition of a 3-dimensional block implemented in an MPI/pthreads hybrid model, an increasingly popular model for taking advantage of clusters of SMPs. We use a problem size and dimension that can highlight many of the issues that we see in real-world applications with mesh computations implemented in

MPI: specifically, we use a 3D block with dimensions $64 \times 512 \times 64$ on each node for a fixed 1000 iterations. With this problem size, we can ensure that computations are done out-of-cache so that it is just enough to excercise the full memory hierarchy. The block is partitioned into vertical slabs across processes along the X dimension. Each vertical slab is further partitioned into horizontal slabs across threads along the Y dimension. The slab domain decomposition across processes is shown in Figure 2.12, while the full hybrid process-thread domain decomposition is shown in Figure 2.13.

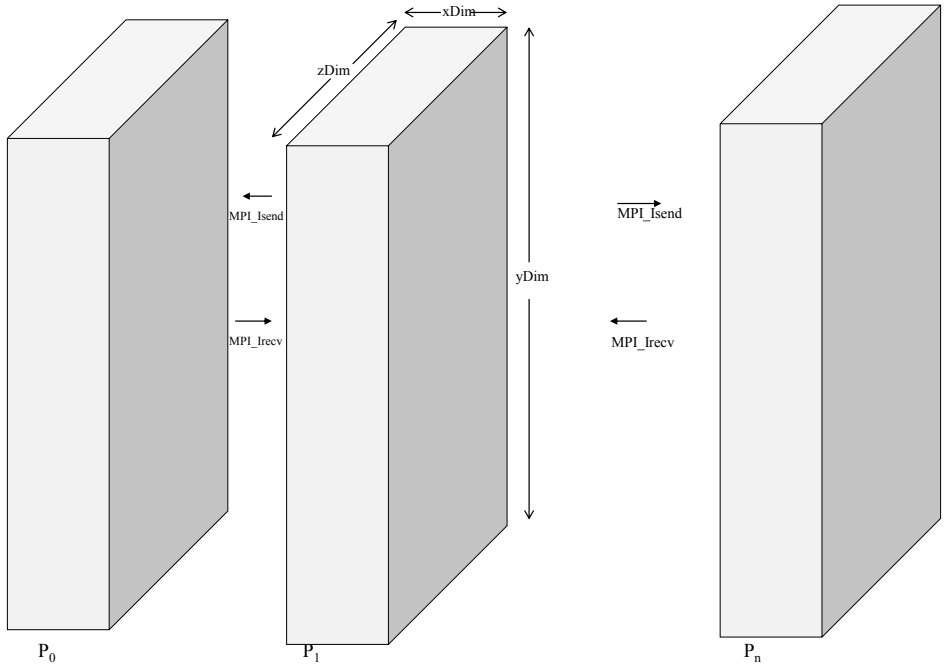

Figure 2.12: 3D stencil domain decomposition across MPI processes.

We use the slab decomposition strategy for the regular mesh because of its simplicity to implement and to tune parameters in our search space, and because it is a common way to partition meshes in Lattice-Boltzmann codes [93]. A MPI border exchange communication occurs between left and right borders of blocks of each process across the YZ planes. The border exchange operation uses an MPI_ Isend and MPI_Irecv pair, along with an MPI_Waitall. We mitigate the issue of first-touch as noted in [78] by doing parallel memory allocation during the initialization of our mesh. For such regular mesh computations, the communication between processes, even in an explicit mesh sweep, provides a synchronization between the processes. Any load imbalance between the processes can be amplified, even when using a good (but static) domain decomposition strategy. If even 1% of nodes are

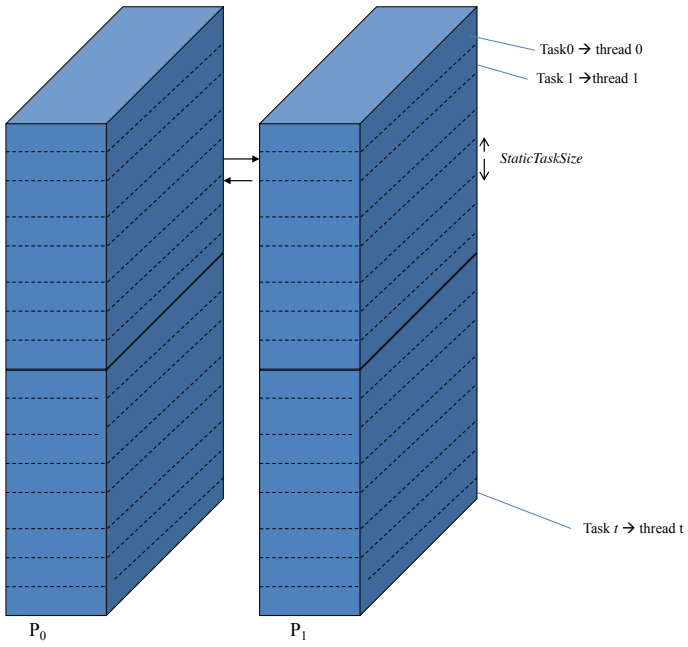

Figure 2.13: 3D stencil domain decomposition across MPI processes, along with thread partitioning of work within each MPI process.

affected by system interference during one iteration of a computationally intensive MPI application on a cluster with 1000s of nodes, several nodes will be affected by noise during each iteration. Our solution to this problem is presented in the section that follows.

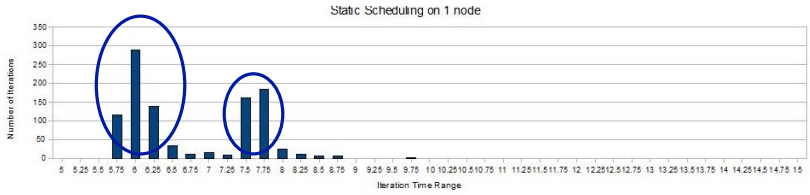

Figure 2.14: Histograms for static scheduling on 1 node, showing bi-modal distribution.

Figure 2.15 and 2.16 shows the domain decomposition for a 3D stencil, with the dynamic scheduling and locality-aware scheduling srategy applied, respectively.

Figure 2.17 shows the domain decomposition for a 3D stencil, with our mixed static/dynamic scheduling strategy applied to the 3D stencil.

Through our experimental studies of tuning our dynamic scheduling strategy, we pose the following questions:

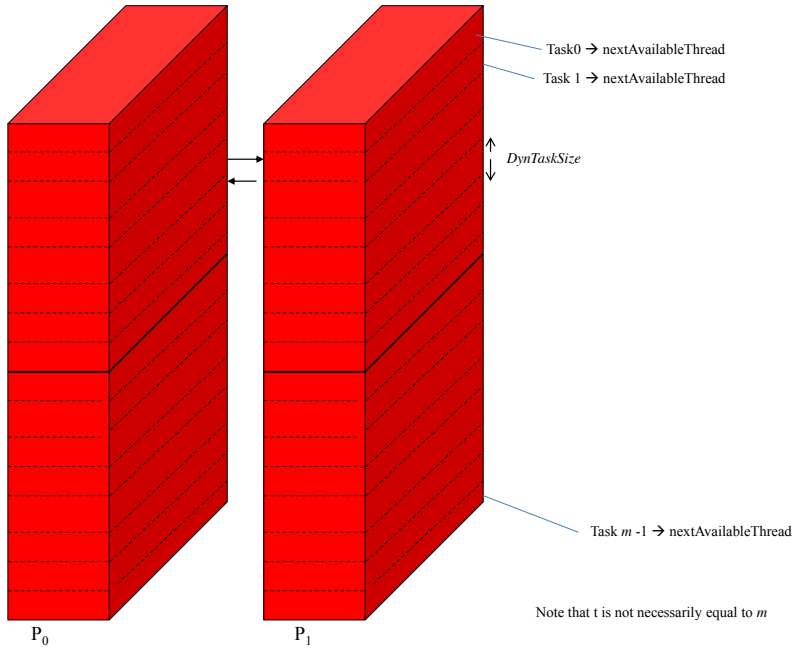

Figure 2.15: 3D stencil decomposition with a dynamic scheduling strategy applied.

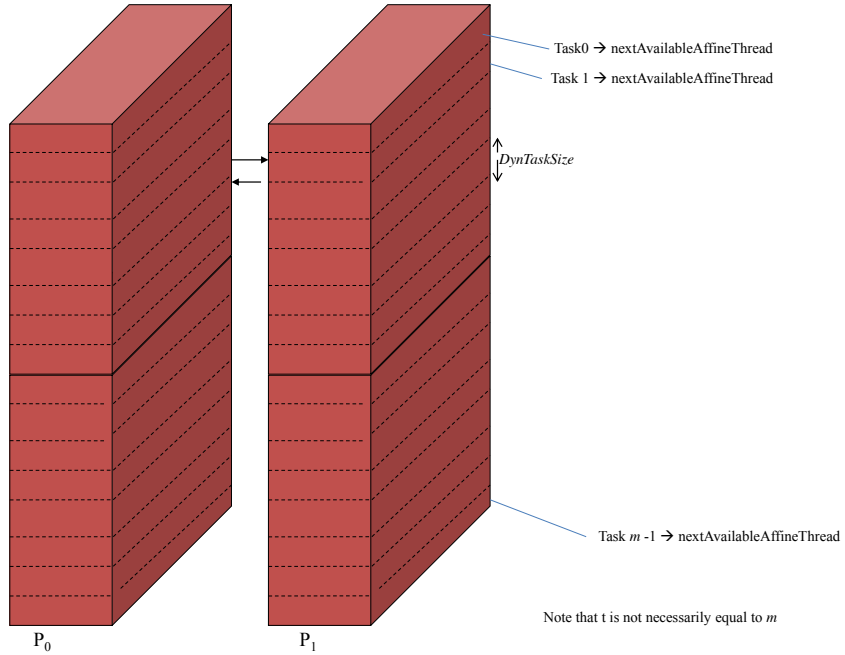

Figure 2.16: 3D stencil decomposition with a locality-aware scheduling strategy applied.

1. Does partially dynamic scheduling improve performance for mesh computations that have traditionally been completely statically scheduled?

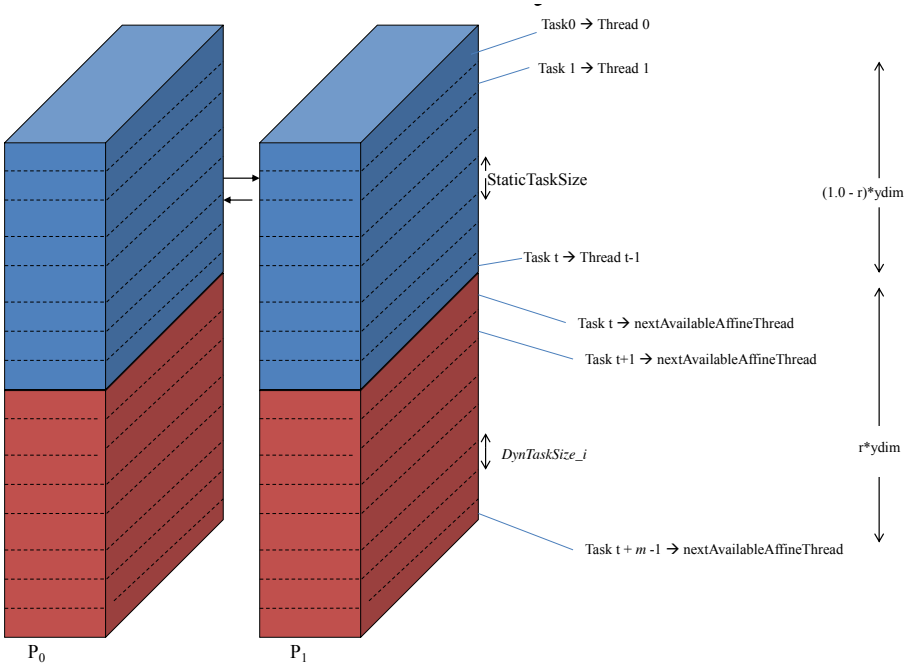

Figure 2.17: 3D stencil decomposition with our mixed static/dynamic scheduling strategy applied.

2. What is the tasklet granularity that we need to use for maintaining load balance of tasklets across threads?

3. In using such a technique, how can we decrease the overhead of synchronization of the work queues used for dynamic scheduling?

4. What is the impact of the technique for scaling to many nodes?

In the subsections that follow, we demonstrate the benefits of partially dynamic scheduling on one node, describe the effect of task granularity, and examine the impact on MPI runs with multiple nodes. Our experiments were conducted on a system with Power575 SMP nodes with 16 cores per node, and the operating system was IBM AIX. We assign a compute thread to each core, ensuring that the node is fully subscribed (ignoring the 2-way SMT available on these nodes, as there are only 16 sets of functional units). If any OS or runtime threads need to run, they must take time away from one of our computational threads.

1. 0% dynamic: Slabs are evenly partitioned, with each thread being assigned one slab. All slabs are assigned to threads at compile-time.

2. 100% dynamic + no locality: All slabs are dynamically assigned to threads via a queue.

3. 100% dynamic + locality: Same as 2, except that when a thread tries to dequeue a tasklet, it first searches for tasklets that it last executed in a previous jacobi iteration.

4. 50% static, 50% dynamic + locality: Each thread first does its static section, and then immediately starts pulling tasklets from the shared work queue. This approach is motivated by a desire to reduce overhead in managing the assignment of tasks to cores.

For the cases involving dynamic scheduling, we initially assume the number of tasklets in the queue to be 32, and that all threads within an MPI process share one work queue. Rather than using convergence criteria, we preset the number of iterations to allow us to verify our results more easily, and we use 1000 iterations to capture the periodicity of the noise induced by the system services during a trial [12]. For case 4, i.e., 50% static, 50% dynamic+locality, locality across timesteps is preserved not just due to the locality tags, but also (inherently) through the static section assigning the same set of iterations to threads on all timesteps. Figure 2.18 below shows the average performance we obtained over 40 trials for each of these cases. Using static scheduling, the average execution time was about 7 seconds of wall-clock time. From the figure, we can see that the 50% static, 50% dynamic scheduling gives significant performance benefits over the traditional static scheduling scheduling case. In our 40 trials, we obtained 6 lucky, or low-noise, runs in the range 6 - 6.5 seconds. The remaining 34 runs were between 7 - 8 seconds. Using fully dynamic scheduling with no locality, performance was slightly worse than the statically scheduled case, and for this case, there were also some small performance variations (within 0.2 seconds) across the 40 trials. Using the 50% dynamic scheduling strategy, the execution time was 6.53 seconds, giving us over 7% performance gain over our baseline static scheduling. Thus, using a reasonable partially dynamic scheduling strategy can reduce performance variation and improve average performance.

In all cases using dynamic scheduling with locality, thread idle times (not shown here) contribute to the largest percentage overhead. The high overhead in case 2 is likely attributed to the fact that threads suffer from doing work not local to a core. Because some threads suffer coherence cache misses while others do not, the overall thread idle time, due to threads waiting at barriers, could be particularly high.

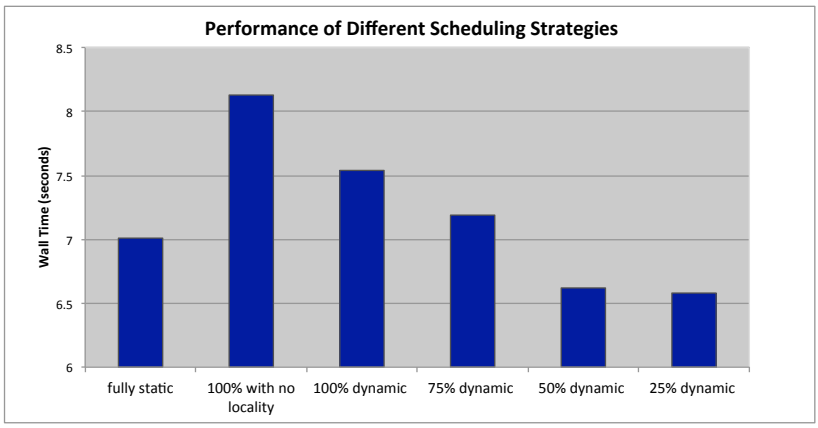

Figure 2.18: Performance for different scheduling strategies on a single node of IBM Power5+ cluster of SMPs.

2.3.3 Tuning Tasklet Granularity for Reduced Thread Idle Time

As we noted in the previous section, the thread idle times account for a large percentage of the execution time for the case of dynamic scheduling with locality.

As a first strategy, we varied the number of tasklets in the queue, using size 16, 32, 64, 96, and 128 tasklets as our test cases; the number of planes per tasklet was 32, 16, 8, 4, and 2. A second strategy, which we call skewed workloads, addresses the tradeoff between fine-grain tasklets and coarse-grain tasklets. In this strategy, we use a work queue containing variable-sized tasklets, with larger-sized tasklets at the front of the queue and smaller-sized tasklets towards the end. Specifically, we use 4 sets of size 16 tasklets in the beginning of the queue, 8 sets of size 8 tasklets in the next section of the queue, and 16 sets of size 4 tasklets in the final section of the queue. Skewed workloads reduce the contention overhead for dequeuing tasklets, seen when using fine-grained tasklets, and also reduces the idle time of threads, seen when using coarse-grained tasklets.

In Figure 2.19, we see that as we decrease the planes per tasklet from 32 to 16, we obtain significant performance gains, and the gains come primarily from the reduction in idle times. Overall, we notice that the performance increases rapidly in this region. As we further decrease the planes per tasklet from 16 to 4, performance starts to decrease, primarily due to the contention for retrieving the tasklets. We also see that performance of the skewed strategy, especially with 50% dynamic scheduling, is comparable to that of 64 tasklets.

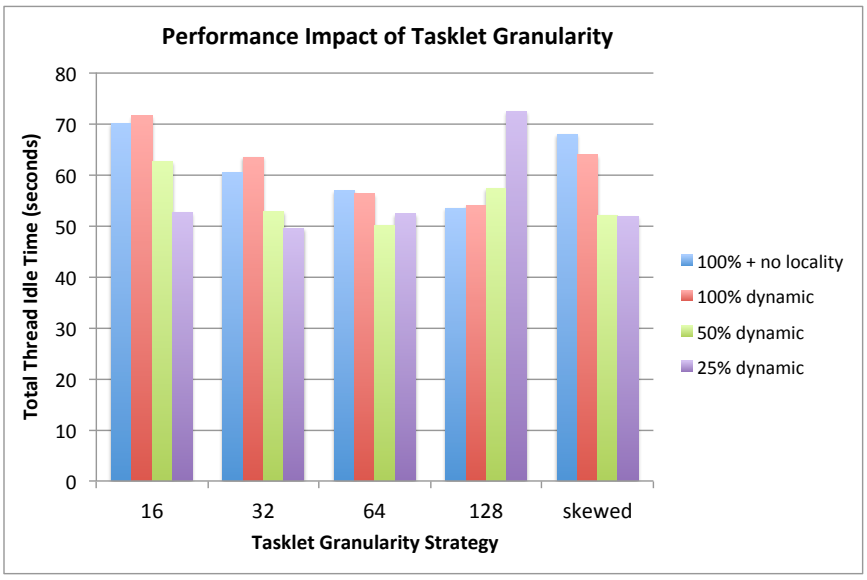

Figure 2.19: Performance for scheduling with different numbers of planes per tasklet.

Figure 2.20 shows iteration time histograms, which show how using 50% dynamic scheduling provides better absolute performance and less performance variation than both 100% dynamic scheduling without locality (topmost histogram), and 100% dynamic scheduling with locality (middle histogram). To understand how tuning with a skewed workload benefits performance, Figure 2.20 shows the distributions of timings for the 1000 iterations of the Jacobi algorithm, comparing static scheduling (top), 50% dynamic scheduling with fixed size tasklets (middle), and 50% dynamic scheduling with skewed workloads (bottom). Using static scheduling, the maximum iteration time was 9.5 milliseconds (ms), about 40% larger than the average time of all iterations. Also, the timing distribution is bi-modal, showing that half of the iterations ran optimally as tuned to the architecture (running in about 6 ms), while the other half were slowed down by system noise (running in about 7.75 ms). Using 50% dynamic scheduling, the maximum iteration time is reduced to 8.25 ms, but it still suffers due to dequeue overheads, as can be seen by the mean of 7.25 ms. By using a skewed workload strategy, we see that the max is also 8.25 ms. However, the mean is lower (6.75 ms) than that seen when using fixed-size tasklets, because of the lower dequeue overhead that this scheme achieves. The skewed workloads provided 7% performance gains over the simple 50% dynamic scheduling strategy, which uses fixed-size coarse-grain tasklets of size 32. Furthermore, the reduced maximum time when using dynamic scheduling indicates that our dynamic

scheduling strategy better withstands perturbations caused by system noise than does static scheduling.

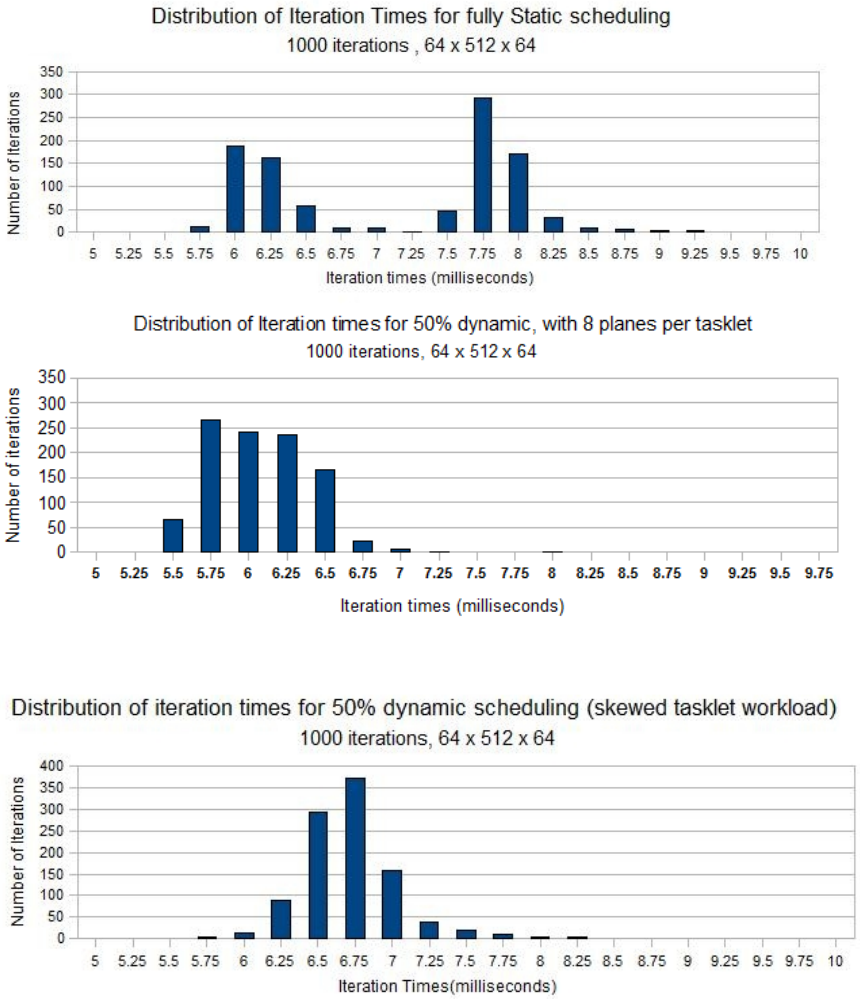

Figure 2.20: Iteration timing histograms of 3D regular mesh run on single node of IBM Power 5+ cluster, where each histogram corresponds to a different scheduling strategy applied to the 3D regular mesh.

2.3.4 Using Our Technique to Improve Scalability

We next explain the problem of how noise affects scalability, and follow that with a performance study that demonstrates how mixed static/dynamic scheduling improves scalability.

The Problem of Noise Amplification And Scalability

The transient imbalances are not a problem in sequential programs, and only a problem at large-scale. This is because of the way randomness of noise interacts with global synchronizations in parallel programs. As illustrated in Figure 1.2b, the chance that a synchronized iteration experiences a noise-related delay increases with the number of nodes. This is especially true if the noise is caused by OS daemons that are uncoordinated across nodes. As an example, consider a system in which an OS daemon executes approximately once every second on a node. Assume that the duration of the noise event is 5 ms. Let us assume that the application takes 10 ms for each iteration before it synchronizes via an MPI collective call. In this scenario, most iterations of a single-node execution will be unaffected by noise. So, if we run this program for 1000 iterations, it would take 10 seconds without any noise. Since there will be 10 noise events in 10 seconds, the execution time will be 10.05 seconds, which is a small acceptable loss of performance.

Consider now the application running on thousands of nodes in a weak scaled fashion. Since noise is uncoordinated, in every iteration there is a high likelihood that there is at least one processor affected by noise. Therefore, each iteration is delayed by 5 milliseconds, taking 15 ms instead of the 10 ms; this is a high, unacceptable performance loss. This is referred to as the noise amplification problem in literature. It was discovered by Petrini et al [72]. We will next illustrate how our dynamic schedulers help mitigate the amplification problem.

Scaling Performance of Different Schedulers

To understand whether our technique improves scalability, we measured execution time of stencil code with different scheduling strategies on varying number of nodes of a cluster. We used a weak scaling version of the code. So, ideally the execution should remain the same as we increase the number of nodes. We report the performance over 1000 iterations. One core of a node was assigned as a message thread to invoke MPI communication (for border exchanges) across nodes. We used the hybrid MPI/pthread programming model for implementation.

Figure 2.21 shows how as we increase the number of nodes, using 50% dynamic scheduling almost always outperforms the other strategies and scales well. At 64 nodes, the 50% dynamic scheduling gives us a 30% performance improvement over the static scheduled case. As we see for the case with

static scheduling, a small overhead due to system services is amplified at 2 nodes and further degrades as we move up to 64 nodes. In contrast, for the 50% dynamic scheduling strategy, the performance does not suffer as much when increasing the number of nodes, and our noise mitigation techniques benefits are visible at 64 nodes.

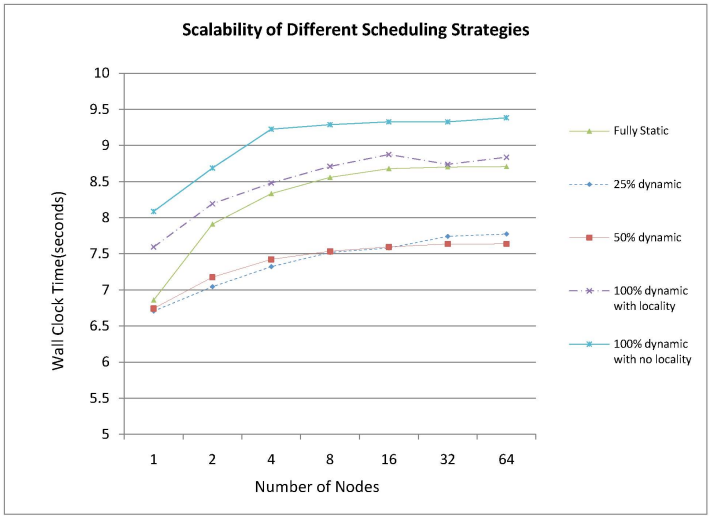

Figure 2.21: Scaling behavior of different scheduling strategies.

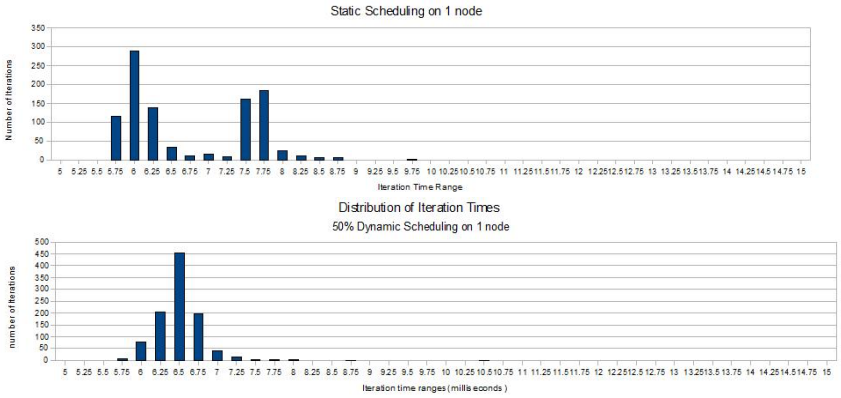

Figure 2.22: Performance consistency is maintained for mixed static/dynamic scheduling for 1 nodes.

To understand why the performance of mixed static/dynamic scheduling is better compared with static scheduling, we examine the histogram of the thousand individual iteration times. The bin size we used was 250 milliseconds, or 0.25 seconds. As seen in the top figure of Figure 2.22, on one node, with static scheduling, some iterations take as little as 5.75

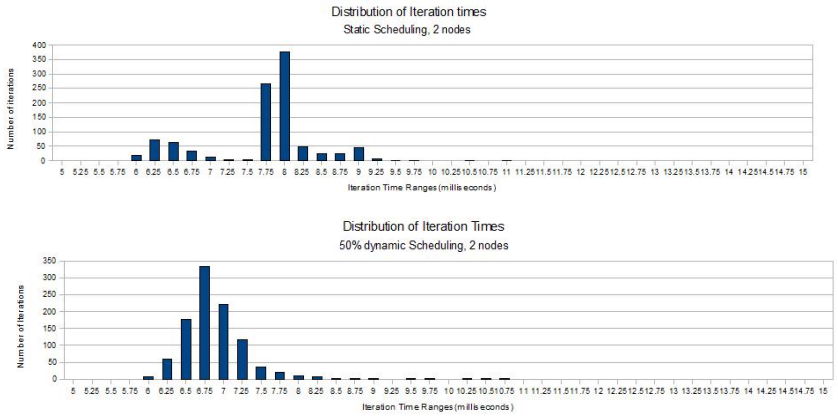

Figure 2.23: Performance consistency is maintained for mixed static/dynamic scheduling for 2 nodes.

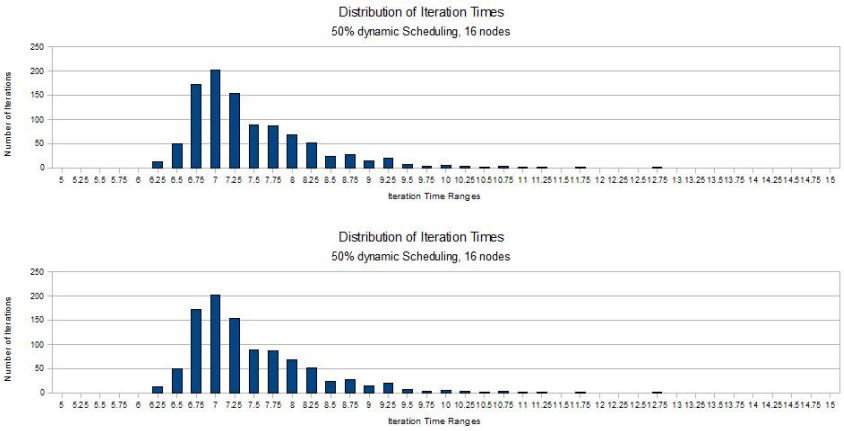

Figure 2.24: Performance consistency is maintained for hybrid static/dynamic scheduling for 16 nodes.

milliseconds, while a small number take as large a time as 9.25 milliseconds. Note the bi-modal nature of the distribution, with the primary mode around 6 ms, and the secondary one around 7.75 ms. The latter corresponds to iterations that are affected by noise.

As we scale up to 64 nodes in Figure 2.25, the average execution time increases significantly with static scheduling, as shown by the red arrow. With mixed static/dynamic scheduling on one node, as shown on the top right histogram, the distribution is clearly uni-modal. Iterations affected by noise do not take significantly longer time than the normal iterations because extra work is spread across all cores. In the rare case when noise happens near the end of the iteration, dynamic scheduling cannot mitigate

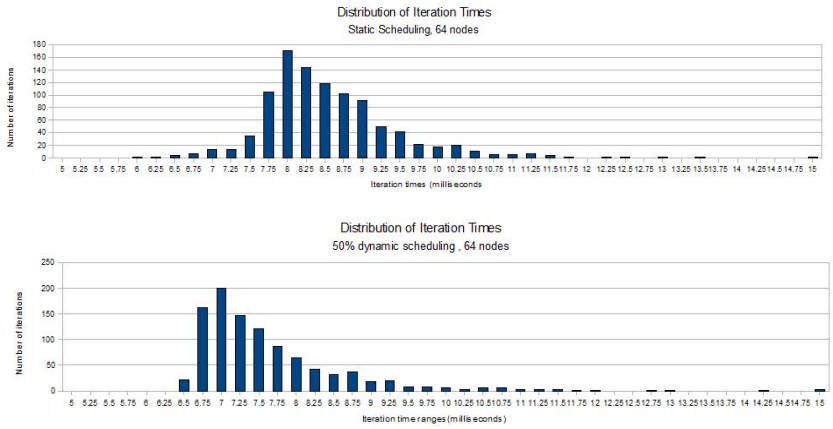

Figure 2.25: Performance consistency is maintained for hybrid static/dynamic scheduling for 64 nodes.

its impact, which is why a few iterations take a long time.

The mode is 6.5 ms which is larger than the 6 milliseconds primary mode for static scheduling because of the overhead of dynamic scheduling, but much smaller than the secondary mode of static scheduling of 7.75 ms.

Compared to the top histogram of Figure 2.25, the bottom histogram of Figure 2.25 shows that the distribution has shifted significantly to the right for static scheduling. This makes sense since each nodes noise event occurs at different times. The chain of dependencies through MPI messaging for border exchanges compounds the delay across nodes in consecutive iterations. With dynamic scheduling, the distribution has not shifted as much. For example, the mode, i.e., the tallest bar of the histogram, only shifted from 6.75 ms to 7.00 ms. This is because in each iteration, the node that experiences noise mitigates its effect by scheduling delayed tasklets to its other threads. Generally, performance variation increases for static scheduling with increasing numbers of nodes, but is maintained for mixed static/dynamic scheduling with increasing numbers of nodes.

2.4 Results for Numerical Linear Algebra

Considering the application of our scheduling strategies to the 3D regular mesh computation in Section 2.2 and Section 2.3, we apply our scheduling strategies to dense matrix factorization computations, e.g., LU factorization, QR factorization, Cholesky factorization, a class of numerical linear algebra computations [89]. Dense matrix factorization computations form an important class of numerical linear algebra computations because of their use in

scientific applications [30], and because of their criticality to execution time within such scientific application [26]. An example of a scientific application using a dense matrix factorization computation (specifically, LU factorization) is the simulation of air flow across an airplane's wing for aiding the design and engineering of an aircraft [26, 41, 42].

We focus on dense LU factorization computation, and specifically consider a highly optimized, i.e., Communication-Avoiding, LU factorization computation [36]. We apply our hybrid static/dynamic scheduling strategy to CALU by modifying the multi-threaded (dynamically scheduled) Communication-Avoiding LU factorization numerical algorithm described by Donfack *et al.* [28] so as to have the beginning portion of the work of the algorithm statically allocated to threads, and the remainder dynamically allocated.With this modification, we try different static fractions in increments of 0.05, and use the best performing static fraction for our runs.

Figure 2.26 and Figure 2.27 show comparisons of performance of the hybrid static/dynamic scheduled implementation of CALU to widely used LU factorization library implementations, one the implementation in the Intel Math Kernel Library (MKL) [48], and the other the implementation in the Parallel Linear Algebra Software for Multi-core Architectures library (PLASMA) developed by Dongarra *et al.* [7,39]. The hybrid static/dynamic scheduled version of CALU is 30% faster than PLASMA and 34% faster than MKL for the largest matrix size of 15,000 on the 48-core AMD Opteron machine, as seen in Figure 2.27. The hybrid static/dynamic scheduled version of CALU is 20% faster than PLASMA and 21% faster than MKL for the largest matrix size of 15,000 on the Intel machine, as seen in Figure 2.26. The results show that the performance benefits of our low-overhead scheduling approach over the statically scheduled approach increase with increasing matrix sizes. The results also show that our approach provides more significant benefits over the dynamically scheduled versions of CALU for an architecture with a larger number of cores.

The histograms in Figure 2.28 show the distribution of execution times for 5000 independent executions of the CALU code on a single node of an 24-core AMD Opteron cluster, for static, dynamic, and hybrid static/dynamic scheduled versions of CALU. For hybrid static/dynamic scheduling approach, we only considered a 90% dynamic scheduling due to machine usage constraints. The performance of the executions using static scheduling is multi-modal, showing the impact of various sources of load imbalances on the machine. The load imbalances come from both the application and the architecture. The performance variations are small for dynamic scheduling,

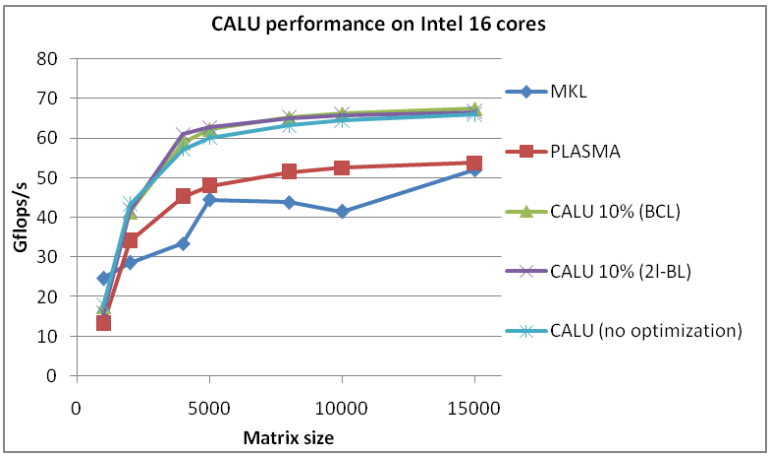

Figure 2.26: Performance of Hybrid Static/Dynamic Scheduled CALU, MKL and PLASMA on the 16-core Intel machine.

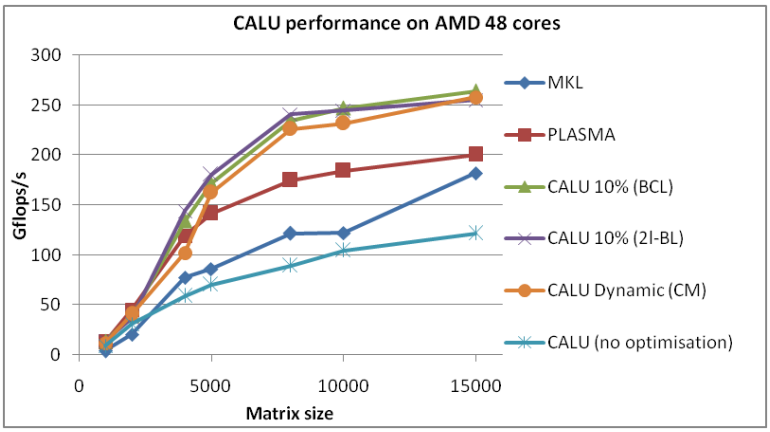

Figure 2.27: Performance of Hybrid Static/Dynamic Scheduled CALU, MKL and PLASMA on the 48-core AMD Opteron machine.

but because of the overheads that dynamic scheduling incurs, performance degradation increases. Both the performance variations and absolute performance are least when mixed static/dynamic scheduling is used.

As Section 2.3 suggests, the distribution of execution times can show potential impact to scalability; having high within-node average performance and low within-node performance variations across executions is desirable for maintaining high performance when running an application at large scale. The hybrid static/dynamic scheduled CALU has high within-node performance and lowest standard deviation across execution times in Figure 2.28, suggesting its benefits to performance when used at large scale.

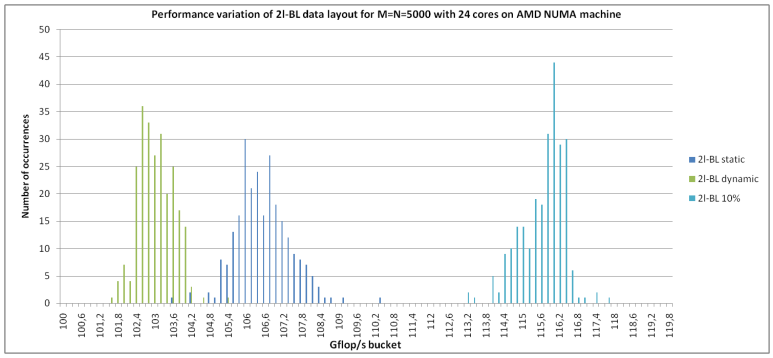

Figure 2.28: Performance variation of CALU on an AMD Opteron 24-core node of a cluster.

2.5 Conclusions

In this chapter, we introduced a dynamic scheduling strategy that can be used to improve scalability of MPI implementations of regular meshes. To do this, we started with a pthread mesh code that was tuned to the architecture of a 16-core SMP node. We then incorporated our partially dynamic scheduling strategy into the mesh code to handle inherent system noise. With this, we tuned our scheduling strategy further, particularly considering the grain size of the dynamic tasklets in our work queue. Finally, we added MPI for communication across nodes and demonstrated the scalability of our approach. Through proper tuning, we showed that our methodology can provide good load balance and can scale to a large number of nodes of our cluster of SMPs, even in the presence of system noise.

The problems remaining are handling persistent load imbalances more effectively in the presence of transient load imbalances, and the reducing the large search space for tuning the scheduler. The subsequent chapters address these problems.

Chapter 3

Weighted Hybrid Scheduling

In the previous chapters, we saw how infrequent uncoordinated noise can be amplified on synchronous MPI programs running on a large number of processors. We also developed a hybrid scheduling strategy that combines both static and dynamic allocation of loop iterations to cores within a node that handles dynamic load balancing without adding significant overhead. The nature of noise considered in the last chapter was such that only a small number of processors/nodes are affected by it in every outer iteration, i.e., between MPI synchronizations. This is low-frequency, high-amplitude noise; by high-amplitude, we mean that the duration of the noise is long enough to significantly delay the iteration. However, another kind of noise exists: namely high-frequency, low-amplitude noise. This can arise from short-duration daemons that execute frequently enough that they affect every node in each iteration. As we will see, on many platforms, such daemons run on a fixed subset of cores of each node. From the application's point of view, this has the effect of slowing down those cores. Slow cores may also arise from other architectural factors such as low-priority hardware threads, e.g., Power7. [91]. We next focus on how to handle such persistent difference in effective speeds of cores. This chapter is based on material published in an early paper [52], and so it uses the tasklet-based scheduling technique of Chapter 2. The tasklet-based scheduling technique described in Chapter 2 is referred to as micro-scheduling in this chapter.

Our key contribution in this chapter is an augmentation of our reactive, queue-based micro-scheduling approach with a form of pro-active load-balancing. Pro-active load balancing adjusts load before the application time step begins, while reactive load balancing adjusts load during the time step. Pro-active load balancers can assign work to each core in proportion to its availability with respect to OS daemons running on it. We refer to this augmented load balancing strategy as weighted micro-scheduling.

We show the benefits, over our original solution, for aiding noise mitigation by:

1. Discussing an implementation of this technique that is portable and efficient for regular computations.

2. Validating our implementation's efficiency by comparing it against industry standard scheduling such as OpenMP guided scheduling.

3. Showing how we can tune our scheduler using a weighted factoring approach [47] that assigns less work to slower cores and more work to faster ones.

3.1 Platforms Considered

The two platforms that we consider are ORNL's Cray XT5 machine (Jaguar) and TACC's SUN constellation cluster (Ranger). Each node of Jaguar consists of twelve cores, 16 GB of memory, and a peak FLOP rate of 124.8 Gflop/s per core. The nodes run a specific version of the SuSE Linux operating system. An in-depth performance comparison of the two supercomputers is presented in [11].

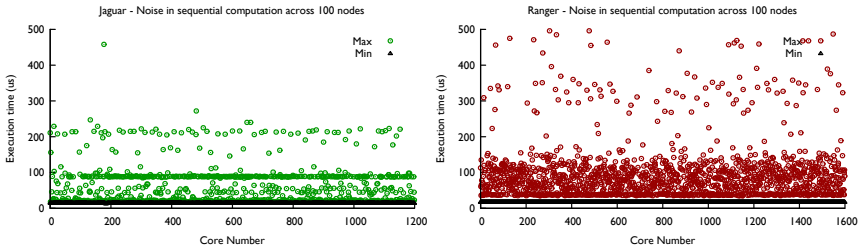

(a) Jaguar. (b) Ranger.

Figure 3.1: System noise plotted against all ranks for a 100 node run for Jaguar and Ranger.

Each node of Ranger consists of 16 cores, with a peak flop rate of 147.2 Gflop/s per node. The frequency of each core on Ranger is 2.3 GHz and allows for four floating point operations per clock period. All cores within a node share 32 GB of memory. On Ranger, the operating system used is the Linux kernel (release 2.2) from kernel.org and is open-source.

A characterization of system noise for Jaguar and Ranger was done through the use of a square root computation run for several thousand iterations on each core. This represents the fixed work quantum (FWQ) method of recording noise. The timings for the sequential computation for each iteration on each core of the machine were recorded.

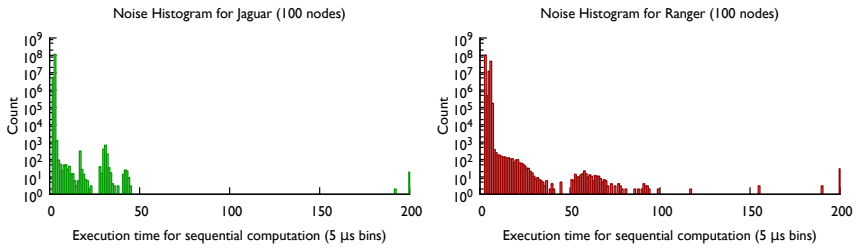

Figure 3.2: Histograms for the execution time of a sequential computation performed to record noise events on Jaguar (left) and Ranger (right). The labels on the x-axis are bin-numbers.

Figure 3.1a shows the minimum and maximum execution times for the work quantum on 1,200 cores (100 nodes) of Jaguar For most cores, the maximum time spent in execution is several times the best execution period (14–15 μs). We can also see the impact of two specific daemons of 100 μs and 200 μs durations, respectively. Figure 3.1b shows a similar plot of the minimum and maximum execution times for 100 nodes or 1,600 cores of Ranger. For Ranger, the maximum execution times are random for different cores, but the spread is denser in the 17–100 μs region. These top bands in the graph show that the noise events are confined to a small subset of cores on each node. This same is also seen in the results by Bhatele et al. [11] for these two machines.

In order to get a better idea of the distribution of timings, we place the execution times for the sequential computation for all cores across all iterations into 5 μs bins and histograms were plotted for the two machines. The histograms were shown in Figure 3.2. The labels on the x-axis are bin-numbers, so the label "60" corresponds to a bin representing execution time between 300–305 μs. Also, note that the scale on the y-axis is logarithmic. If there were no noise, the histogram would have only a couple of occupied bands corresponding to times around 15 microseconds. And indeed, a majority of iterations are in the leftmost bins for both machines. But as the spread of the bins shows, noise does affect many cores and iterations. The Jaguar plot (left) shows four distinct peaks, the last three of which possibly correspond to specific daemons that have a high frequency. The Ranger plot (right) shows a spread from 15–200 μs and then a smaller distribution around 300 μs.

Given a noise-free machine and a scientific application without load imbalance, intra-node static partitioning and inter-node domain decomposition will be most effective. Owing to the load imbalance induced by the operat-

ing system, dynamic scheduling can be beneficial to improve performance of scientific applications [14]. As we saw in Chapter 1, this dynamic scheduling scheme needs to incur low overheads to offer performance benefits for synchronous MPI applications.

Understanding the characteristics of variations helps us to further fine-tune the scheduling schemes, which is important to reduce costs of the scheduler. Each characteristic of the noise pattern of a platform suggests the importance of a particular feature of our scheduler. In previous chapters, we designed schedulers to handle the noise pattern where the noise on any given core is an infrequent event. Within this pattern, there could be several variations: when a platform has several different noise events of different lengths, a dynamic scheduling strategy with an assortment of task granularities can be used; if there are only a few different noise events, each with relatively similar durations, then we can tune the task granularity.

Yet, none of the scheduling schemes we have developed have used the noise characteristic of persistence due to core speed variation that is observed in Figure 3.1a and Figure 3.1b. The next section extends the lightweight scheduling scheme described in Chapter 2 so that it can mitigate imbalances due to a mixture of peristent core noise and transient noise, and, as we note at the end of the chapter, can also be used to handle a mixture including persistent application imbalance.

3.2 Scheduling Techniques

Locality-sensitive scheduling aims to schedule work on cores that executed this work in a previous time step. This optimization aims to improve temporal locality, and has been shown to provide benefits in [54].

Our basic scheduler [54] uses a queue to assign chunks of work to cores. Each queue is implemented as an array of pointers to data structures we call *tasklets*. A *tasklet* is a fine-grained piece of computation that keeps track of its movement across cores of a node. A queue can consist of an assortment of tasklets of different lengths. These tasklets are dynamically scheduled across cores of a node, but are aware of their movement across cores of a node.

In this work, we improve our technique by augmenting the statically scheduled stage of the computation with weighted scheduling. Our previous work assumed that a noise event was equally likely to delay computation of any core of a node, and that a dynamic scheduler could, in theory, handle noise events of any duration and any frequency. Yet, short-duration, high

frequency events are fine-grained enough that the application quantization of tasklets limits the ability to distribute the noise across cores evenly. Our previous work did not handle short-duration, high-frequency noise events specially.

We address the case when a core is continuously impacted by short-duration, high-frequency noise events. We observe that a core effectively becomes "slow" when there are many such OS daemons that are bound to that particular core and must be frequently time-sliced with the actual computation. Due to the many different system services that are running on that core, we observe that the core may have a higher chance of performance degradation during a time step. Finally, only a subset of cores tend to have several OS daemons running on them, while the remaining cores are relatively unoccupied by such system services [72]. If we know that some cores are always slower than others, we can employ a strategy to offload some work from the slow cores, and move that work onto faster cores.

Putting both techniques together, we use a prescriptive load balancing technique in the first stage of the computation to mitigate system noise, followed by a reactive load balancing technique in the second stage of the computation. This strategy tries to reduce the amount of work done on those cores that are heavily occupied by the OS services.

Using weighted scheduling, we obtain performance gains when we are able to predict which processors likely remain slow throughout the duration of the application time step. This allows all processors on the node to start their work at the same time in the subsequent dynamic scheduling stage. If we know this information before an application time step begins, we can reduce the chance that the slow core(s) impacts the collective iteration time across all cores. This can be done by using a form of measurement-based load balancing as in Charm++ [51].

Weighted scheduling works well because it offloads work proportionally to the speed of a processor. Its advantage over dynamic scheduling arises from the fact that it involves no dequeue overheads for locking and unlocking the work queue. Weighted scheduling tries to ensure that the slow core's static section will not be the cause of timestep slowdown. If we do not handle the slow cores differently, we essentially create a predictable load imbalance. This will lead to a much higher dynamic fraction, with associated overheads. This increases the chance that the dynamic load balancing may not be able to restore balance. In this case, there is no way for the other cores to "steal" the work from the static section. However, weighted scheduling does also have its shortcomings. Noise events may not necessarily be restricted to

one, or a subset, of the cores on a node. Thus, the predetermined weighted factoring will serve little purpose. In addition, weighted scheduling does not handle low-frequency, long-duration noise events. These low-frequency, long-duration noise events that can happen on any core are seen on both Jaguar and Ranger, and thus should not be ignored.

The set of cores that are slow varies for different platforms. Even for a particular platform, the set of cores that are slow can change over the course of days or weeks. To handle both of these issues, we run an initial loop with a square-root computation to gather the speeds of each core before the application begins. We also allow for adjustment of weights during runtime, to handle the case when the speeds of the cores change during execution of the program.

Also, for the dynamic scheduling stage, we make use of a more systematic auto-tuning methodology to find the best scheduler parameters. The tuned parameters include the average tasklet granularity and tasklet granularity distributions. We use a shell script that runs before execution of the program, to tune the parameters. In the future, we plan to make our auto-tuning more sophisticated.

3.2.1 Allocating Iterations Based on Weights

We should assign fewer iterations to slower cores, and more iterations to faster cores. In this section, we describe how to calculate the number of iterations assigned to each core, based on the history of the computation, i.e., of previous outer iterations. For the micro-scheduler described Chapter 2, recall that the total number of loop iterations was denoted as N, and the number of cores was p. Given a static fraction f_s, the number of iterations assigned to each core is $\frac{N \cdot f_s}{p}$. Thus, the i^{th} core begins with iteration $i \cdot \frac{N \cdot f_s}{p}$. How do we calculate the starting iterations for each core, in terms of weighted scheduling?

For weighted scheduling, we measure the time taken by static iterations for each thread, s_i, with equal allocation as in Chapter 2. The weight for the i^{th} thread, w_i, is calculated as: $w_i = \frac{avg\{s_i\}}{s_i}$. The slower cores which had a larger value of s_i have a smaller weight, as we desired. The number of iterations k_i allocated to the i^{th} thread is then given by: $k_i = w_i \cdot \frac{f_s \cdot N}{p}$. A prefix sum of k_i gives the starting iteration for each thread. This needs to be stored in an array that is calculated at the end of the experimental uniform allocation phase of the computation. This process of adjustment can be repeated across outer iterations. In this case, the new k_i is calculated

by multiplying the old k_i by w_i.

3.3 Results for Weighted Hybrid Scheduling

To assess the effectiveness of the proposed technique, we apply it to a three-dimensional 7-point stencil computation. The computation and its domain decomposition for the MPI-only (no pthreads) implementation is shown in Figure 3.3. A one-dimensional slab decomposition of the data array is done and a slab is assigned to each MPI task. In the hybrid MPI+pthreads implementation, each thread is assigned a portion of the slab as shown in Figure 3.4. Each compute thread corresponds to a core of a node of the cluster. Each MPI process corresponds to a node of a cluster. We make note that there are ways to optimize the process/thread aspect ratio, but we use the simplest one here, as we see that tuning in this search space does not give a large performance difference for our particular stencil code.

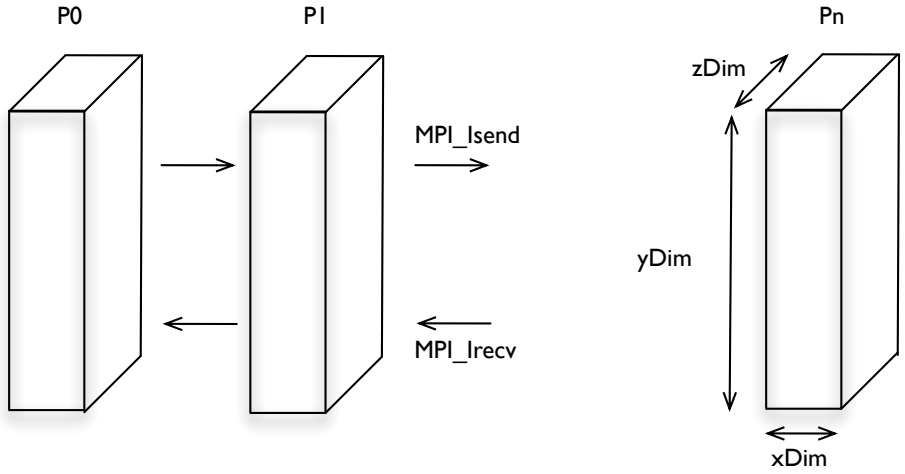

Figure 3.3: MPI domain decomposition used for the 3D Stencil code.

Figure 3.5 shows the MPI+pthreads implementation that uses weighted scheduling in the first stage of the computation. Here, w denotes the weight of the work assigned to a particular thread. We run the 3D stencil computation for 1000 iterations, and use a problem size of $64 \times 32 \times 64$ for each core, regardless of the machine on which we test. By ensuring that we consider a dense matrix with regular computation, we can more easily isolate the problem of noise for different machines. Below, we show how each of the two schedulers perform with respect to the baseline static scheduling. We also show a comparison to commercial schedulers, such as OpenMP guided scheduling [23] and the TBB affinity scheduler [80]. Through careful tuning

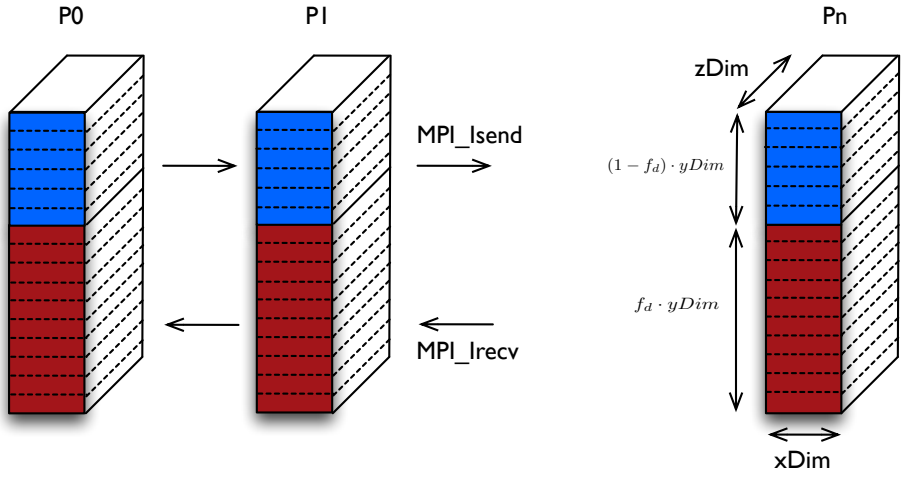

Figure 3.4: Hybrid MPI+pthreads domain decomposition with micro-scheduling used for the 3D Stencil code. The dynamic fraction is denoted by f_d.

of the parameters shown in Figure 3.5 in our experimentation, we can obtain significant performance benefits for the stencil application.

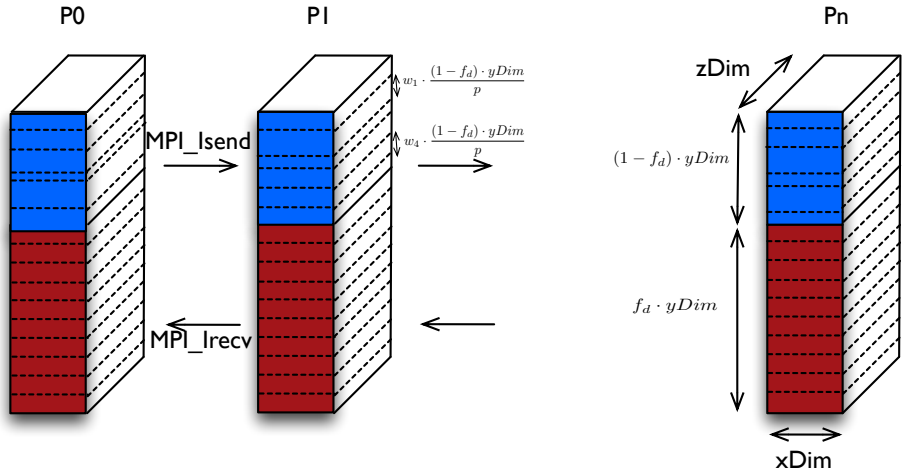

Figure 3.5: Hybrid MPI+pthreads domain decomposition used with weighted static and dynamic micro-scheduling for the three-dimensional 7-point stencil computation. The dynamic fraction is denoted by f_d, and the weight of thread 1, as shown in this diagram, is denoted by w_1.

We now discuss the performance of weighted scheduling, micro-scheduling, and our combination of the two schedulers, called weighted micro-scheduling. Figures 3.6 and 3.7 show the performance of the stencil computation described above, using the various schedulers on Jaguar

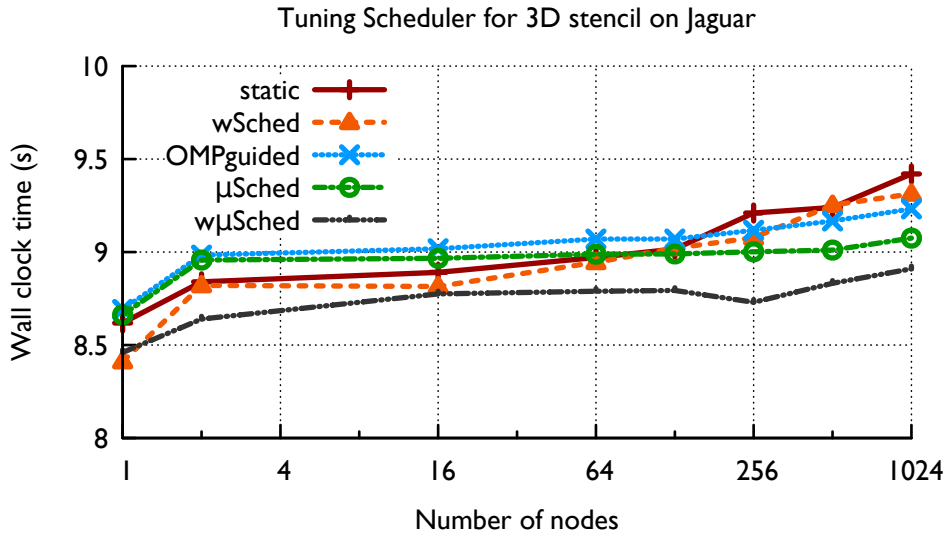

Figure 3.6: Performance of the stencil computation on Jaguar for various scheduling techniques.

and Ranger. On Jaguar, we ran the stencil code on up to 1024 nodes and Ranger, we ran on up to 512 nodes.

3.3.1 Weighted Scheduling

Running on 512 nodes of Jaguar, weighted scheduling gives a benefit of 6% over the baseline static scheduling (Figure 3.6). This is somewhat better than the performance gain with micro-scheduling. Since OS noise typically affects a subset of the cores on a node [11], weighted scheduling is primarily beneficial at the beginning of the computation. By offloading work from the noisy cores of Jaguar, we have provided a solution that is better than micro-scheduling in the sense that it avoids dequeue overheads that the non-noisy cores would otherwise have to suffer.

Running on 512 nodes of Ranger, weighted scheduling gives almost no performance benefit over the baseline static scheduling (Figure 3.7). There is a smaller benefit from weighted scheduling on Ranger since noise can occur on any core of a node, rather than being restricted to a subset of cores. Unlike micro-scheduling, weighted scheduling incurs no dequeue overheads. Weighted scheduling incurs idle time due to measurements that may mispredict weights, or because of low-frequency noise events that affect only a few time steps. Because our scheduler is conservative, the performance loss of trying to use weighted scheduling on Ranger is very low.

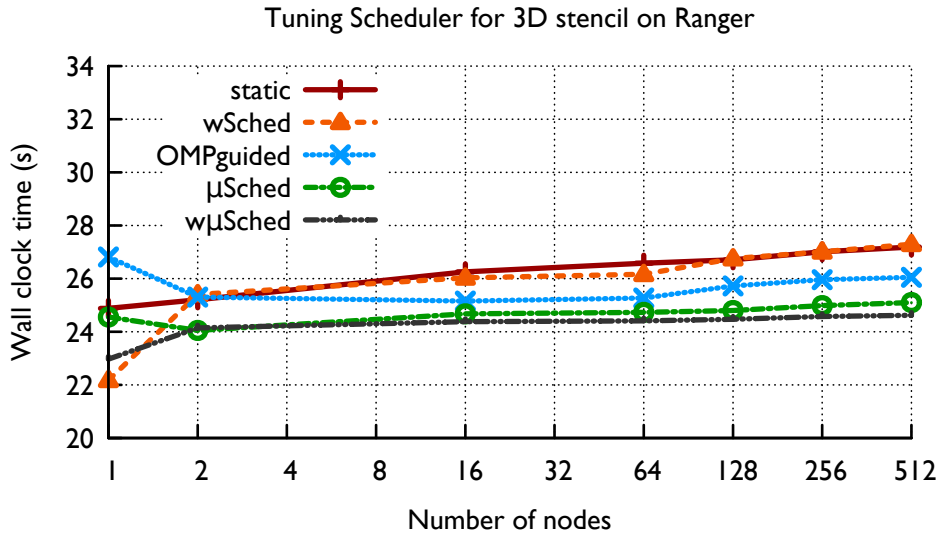

Figure 3.7: Performance of the stencil computation on Ranger for various scheduling techniques.

3.3.2 Micro-scheduling

To assess the effectiveness of tuned micro-scheduling, we use an automated tuning to search for the best parameters for the dynamic scheduler on each architecture. Micro-scheduling provides for the most performance benefit on Ranger, with 12% performance improvement on 512 nodes. This is likely due to the fact that any core on a Ranger node can get perturbed by a noise event, not a specific subset of the cores. Because the noise interruptions occur over a range of short and long durations, rather than over a fixed duration, the task granularity cannot be determined ahead of time. By using variable-sized tasks, we are able to handle these variable-length noise events. It should be noted that the use of variable-sized tasks resembles guided scheduling, as implemented in OpenMP.

On Jaguar, the tuned micro-scheduling strategy is less effective. The reason is that the noise events happen on only some subsets of cores. These noise events are also probably of higher frequency. While using variable sized tasks can help address the issue of variable duration noise events, we believe that our strategy of using variable-sized tasklets does not help as much due to the fact that our implementation is likely not tuned carefully. With further tuning of the tasklet length distribution in the queue (effectively, finding the right "assortment" of tasklet lengths), micro-scheduling can provide for better performance on Jaguar. However, this will require more investigation, and we leave this as future work for now.

3.3.3 Weighted micro-scheduling

As the preceding sections show, noise that occurs sporadically on any core of a node can be mitigated by micro-scheduling, and noise that is restricted to run on a subset of nodes is well-mitigated by weighted scheduling. However, in practice, production HPC clusters may not have a clear distinction between the case of noise being focused on a subset of the cores versus the case where noise occurs sporadically on any core of a node [72].

For example, noise events on a production HPC cluster may be more *likely* (rather than restricted) to occur on one core than the other. Thus, using either of the schedulers in isolation does not necessarily provide for significant performance gains. To what extent can we combine these two different schedulers to get the best of both worlds? We now discuss the results obtained when we combine the weighted scheduler and micro-scheduler.

On Jaguar, we observe that noise happens on some cores more than others. Specifically, cores 0, 6, and 9 are slowest. This is 3 out of the 12 cores that could potentially finish late and cause a slowdown. By using weighted micro-scheduling on 512 nodes of Jaguar, we get a performance improvement of 12% over the baseline static scheduling. This is significantly better than the performance that we get with using the weighted scheduler (7%) or the micro-scheduler (9%). In this case, the knowledge that these cores are noisy allows us to reduce the time for each time step. In addition, dynamic scheduling handles low-frequency, small duration noise events occurring on any core.

On 512 nodes of Ranger, weighted micro-scheduling yields a performance improvement of 16.6%, which is a slight improvement over the 14.1% improvement we get with just micro-scheduling. All cores are almost equally noisy, although core 0 has slightly more noise than other cores. Weighted scheduling (offloading work from core 0) does help to mitigate high-frequency, short duration noise on core 0. However, the benefit from weighted scheduling is still not significant; the benefits obtained through micro-scheduling still dominate in the results for Ranger.

A key observation we make here is that while weighted scheduling is not very successful on Ranger, our combined weighted micro-scheduler also does not hinder performance, compared to the corresponding results for the weighted scheduler or micro-scheduler. Thus, our solution of combining weighted and micro-scheduling is portable; when we do not have "slow" cores on a node, the weighted scheduling portion of the combined weighted micro-scheduler does not induce unnecessary overhead. Further, our scheduler

can handle static and dynamic variations that are likely to arise in future architectures due to semiconductor process variation, cache error correction, etc.

3.3.4 Experimentation with Varying Problem Sizes

In this section, we present the impact of application parameters on the performance of our scheduling techniques. We vary the problem size and the computation per timestep. In order to isolate performance efficiency of our scheduler from the efficiency of the MPI runtime, our experiments are performed on one node.

3.3.5 Impact of Memory Accessed per Time Step

Figures 3.8 and 3.9 illustrate the impact of varying the problem size in this stencil computation on each of the machines. In the figures, the third cluster of bars from the left indicates the baseline problem size. As is seen in these figures, our strategies are competitive with and seem to perform better than OpenMP static scheduling and OpenMP guided scheduling. By varying the problem size, we test how time for memory access impacts our strategy. Results from both Jaguar and Ranger, with a small problem size, suggest that system noise is a factor in performance. The reduced benefit for larger problem sizes is likely due to the fact that performance is already impacted by limited effective memory bandwidth. Leaving aside these nuances, the broad conclusion from this data is good or better compared with OpenMP strategies, over a range of problem sizes.

3.4 Discussion

This work builds on work from previous chapters, which used our scheduling techniques for hybrid MPI+pthread programs. We aim to build a more acceptable strategy for use at the application level. There are two methods behind each of these techniques: the first is auto-tuning and the second is measurements of performance taken from previous application time steps.

Offline auto-tuning happens for the dynamic phase, while online auto-tuning is used for the static region. Auto-tuning is important because system noise typically does not change during the execution of the program. For a long running application, the subset of processing elements that are slower may change. Furthermore, if there is a large noise event that spans several iterations, the scheduling techniques will offer no benefit. In this

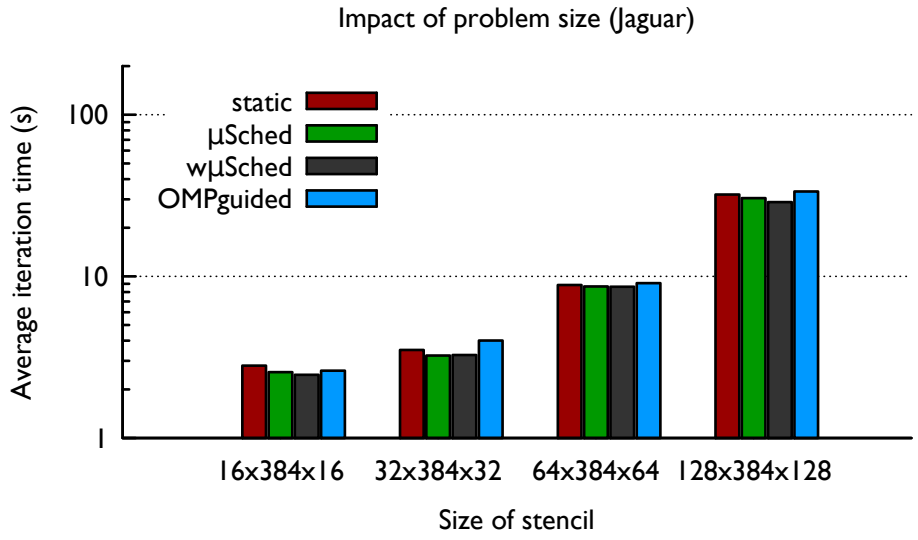

Figure 3.8: Impact of problem size on Jaguar for 3D Stencil with different load balancing strategies.

case, we need a measurement-based load balancing technique such as in Charm++ [51] that adaptively adjusts to situations where cores are constantly slowed down by operating system events, even across time steps. We must move work away from those "slow" processing elements.

There is no proactive load measurement involved in our solution of weighted scheduling. An intelligent load balancer like that in Charm++ uses sophisticated techniques to implement load balancing strategies by collecting load balancing information from previous iterations [10, 57, 94]. The nature of load imbalances our strategies are designed to deal with is not predictable. However, if we can find a pattern in the noise events, an intelligent measurement-based technique that uses periodic load balancing may be advantageous. Further, our technique can be used in conjunction with Charm++'s measurement-based load balancers.

Finally, performance tuning a scheduler for a given operating system is a difficult task. If applications are sensitive to the operating system on which they are running, the argument for portable application code is further justified. The rapid pace of innovation of computer architectures is clearly evident, and can change over just a year's notice. This requires one to re-tune application codes continually for these new architectures. Unlike the pace of innovation for architectures, an operating system can change underneath within weeks. Furthermore, operating systems are programmed by humans. This further adds complications because humans make mistakes, thereby

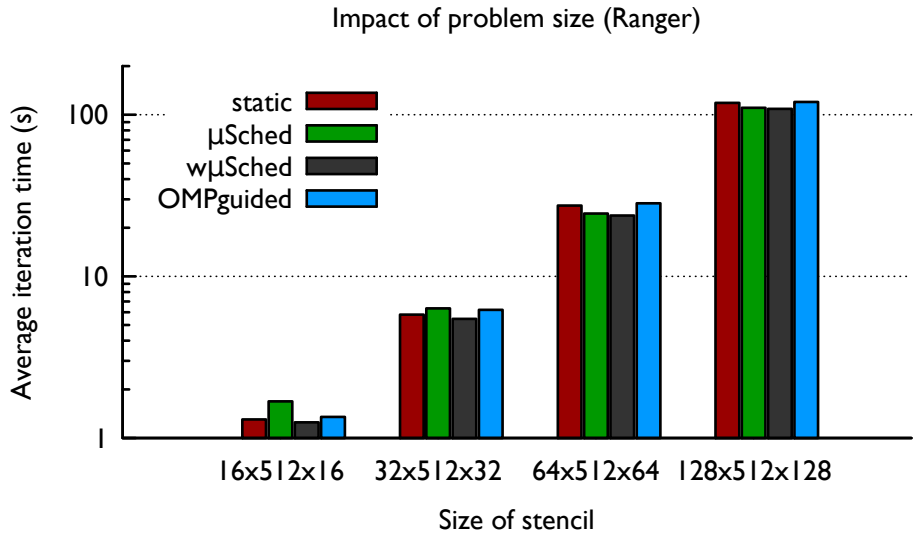

Figure 3.9: Impact of problem size on Ranger for 3D Stencil with different load balancing strategies.

causing performance (or correctness) bugs in kernel software. Therefore, strategies such as that described in this chapter that automatically adapt to variabilities, are desirable.

Chapter 4

Slack-Conscious Hybrid Static/Dynamic Scheduling

Consider again the basic hybrid scheduling approach that we developed in Chapter 2. By combining static and dynamic scheduling, we were able to control overhead while providing dynamic load balancing. We saw that it is necessary to reduce the dynamic fraction, and therefore the number of dynamically scheduled iterations to the minimum value that is adequate to contain the load imbalance. The method that we used for finding this value of the dynamic fraction was an exhaustive enumerative search. Further, once the dynamic fraction was decided, the same dynamic fraction was used on all nodes.

In this chapter, we first develop a model-based method to determine the dynamic fraction; an empirical search can still be performed near the optimal dynamic fraction determined by the model. Next, we explore the following question: If we allow the dynamic fraction to be different on different nodes, can the dynamic fraction be further reduced, along with reducing the overhead associated with dynamic scheduling? What we need is a technique that uses *minimally* dynamic scheduling on a node, minimizing delay added to the critical path due to either noise or overhead. As we demonstrate, in hybrid parallel applications, the mixture of static and dynamic work that minimizes the average-case runtime varies by each threaded region as well as by node. Specifically, we show that the percentage of dynamic work that minimizes the *average-case* runtime for a threaded computation region in a *noisy* system depends on each node's communication deadline.

The main contributions of this work are:

- A model-based determination of scheduler parameters based on noise, scheduler overhead and the communication deadline;
- A *minimally dynamic* scheduling policy that minimizes the average-case runtime of noisy hybrid applications;
- A tuning technique that enables the above scheduling policy by coupling shared memory and distributed runtimes;

- A compiler transformation that automatically generates self-tuning OpenMP loops to implement our scheduling policy.

The remainder of this chapter is organized as follows. The next section discusses the model of computation we consider throughout this chapter. Section 4.2 develops a model for a minimal value of the dynamic fraction that can ensure that the impact of noise is minimized, given the expected duration of the noise event. Sections 4.3 and 4.4 describe an opportunity to minimize the dynamic fraction further by allowing it to be different on different processes based on a communication deadline. Section 4.5 presents our implementation. Section 4.6 discusses our experimental results. Finally, Section 4.7 concludes this chapter.

4.1 Performance Perturbances

Recall the following simple bulk-synchronous code that performs a local computation at each MPI process, followed by a global communication, where each MPI process is assigned to a core of a node in a cluster:

```
for (int i = 0; i < n; i++)
  c[i] += a[i]*b[i];

MPI_Operation;
```

On a cluster of multicore nodes, this example code could be written using hybrid MPI+OpenMP by adding a `#pragma omp parallel for` before the loop. Assume that doing this will execute the loop with a static schedule, which distributes the iterations evenly among threads. With the `#pragma omp parallel for` added before the loop, the loop becomes a *threaded computation region*. Threads participating in the threaded computation region are called a *team*. Assume that an MPI process contains one team, and each node of a cluster runs one MPI process. After a thread has completed its assigned loop iterations, it waits, i.e., idles, at a team-wide barrier. Then, each such team running within an MPI process participates in MPI communication, dictated by `MPI_Operation`. As shown by Hoefler et al. [46] and in Chapter 2, the above code is prone to noise propagation that causes slow down at scale.

4.2 Model-Based Determination of Minimal Dynamic Fraction

We now establish the theoretical foundations for our technique which builds on hybrid scheduling. We assume that applications execute bulk-synchronously, as computation phases followed by communication phases. We refer to each bulk-synchronous step as a timestep, and we refer to an iteration as one unit of work in an OpenMP loop.

We use a simple model for noise, computation, and the fraction of dynamic work used. We denote t_1 as the duration of a single iteration of a loop, on one core. We denote the total execution time of a single bulk-synchronous step, consisting of N loop iterations on p cores, as T_p. We denote the expected noise delay as δ. We define the portion of dynamically scheduled work done in a threaded computation region as the *dynamic fraction*, and denote it as f_d. The portion of statically scheduled work in a threaded computation region is the *static fraction*, and we define it as $1.0 - f_d$. Table 4.3 provides an overview of all parameters used in the following analysis.

At sufficient scale, noise of length δ occurs with virtual certainty within each timestep. In principle, at least one process in the job will be affected by noise with duration δ during each threaded computation region. When this noise impacts some particular node during a timestep, the noise can occur on any of the cores of that node. We assume in our model that for the node that is impacted by noise during an outer iteration, only one core within that node suffers the noise event.

4.2.1 Using a Model for Hybrid Scheduling

In the absence of dynamic scheduling, when noise occurs on a core, the critical path will be delayed by δ time units (see Figure 4.2). Therefore, making at least δ time units worth of work dynamic will allow other cores to absorb the delayed work to minimize the critical path delay on this node. Since each thread has $\frac{Nt_1}{p}$ amount of computation, the relationship between the delay and dynamic work can be expressed as:

$$f_d \frac{Nt_1}{p} \geq \delta \tag{4.1}$$

$$f_d \geq \frac{p\dot{\delta}}{Nt_1} \tag{4.2}$$

Although the above is an inequality, increasing the dynamic fraction further does not improve performance. Thus, to achieve our goal of using the

Model outputs	
f_d	Fraction of work scheduled dynamically
f'_d	Fraction of work scheduled dynamically, reduced for slack
Model inputs	
q	Overhead of dequeueing single iteration
δ	Expected noise duration
δ_i	Expected noise duration on node i
T_p	Execution time on p cores with fully static scheduling and no noise
N	Total number of iterations across all threads
Change quantities	
Δ_f	Change in dynamic fraction
Δ_η	Change in execution time of computation region
τ	Sequential time for dynamic work moved
Other variables	
t_1	Duration of one loop iteration on one thread (running on one core)
d	Duration of one dynamic iteration on onethread
η	Compute delay due to noise and scheduling overhead
α_i	Delay added to the critical path by node i

Table 4.1: Overview of all model parameters.

minimal amount of dynamic scheduling, we consider the above relationship as an equality throughout the remainder of the section.

A minor variant of this model is described in [54] for understanding the experimental data, but is not used as a part of a runtime strategy for producing the results, and was not connected to the experiments. Furthermore, even if we did attempt to use this model by itself for applications, this model is overly simplistic. To begin with, it assumes that dynamic scheduling is free, i.e., that no queueing overhead exists.

With dequeue overhead, each dynamically scheduled iteration takes slightly longer than a statically scheduled iteration. So, we should use slightly fewer dynamic tasks to absorb the same amount of noise. Let d represent the execution time of one dynamically scheduled iteration, p be the number of cores, and let q represent the scheduler queueing overhead of a single iteration. Given t_1 and q, d can be approximated as:

$$d = t_1 + q \tag{4.3}$$

We want to use just enough dynamic scheduling so that the scheduler can parallelize any work displaced by a noise event of length δ. On any one

thread, there are $f_d \frac{N}{p}$ dynamically scheduled iterations. So:

$$\delta = df_d \frac{N}{p}$$

$$\delta = f_d \left(\frac{Nt_1}{p} + q\frac{N}{p} \right)$$

$$f_d = \frac{p\delta}{N\left(t_1 + q\right)} \tag{4.4}$$

This is more aggressive and uses significantly less dynamic scheduling than that in Equation (4.2), by taking into account the dequeue overhead. Still, a limitation of the above is that the dynamic fraction is constant for all invocations of a threaded computation region. This limitation can be addressed by using run-time predictions of values of noise, dequeue overhead, and compute time per thread, for a given threaded computation region. We refer to the adaptation of the dynamic fraction based on the parameter estimation of noise, dequeue overhead and the per-thread compute time as static-hybrid scheduling.

As described in the beginning of the section, using the dynamic fraction f_d on all nodes insulates us from the expected noise δ. What is the computational delay η when one node experiences noise? This delay consists of two components: one is the extra work done by the remaining $p-1$ cores on a node that experience noise, and the other is the dequeue overhead experienced by every core on every node. Adding those up, we get a computational slowdown of:

$$\eta = \frac{\delta}{p-1} + \frac{f_d N q}{p} \tag{4.5}$$

where $\frac{\delta}{p-1}$ is the overhead of work displaced by noise, and $f_d N q$ is the added dequeue overhead. In the average case, many nodes will suffer performance degradation due to the dequeue overhead, which can be significant. The question then becomes whether we can reduce scheduling overhead further.

4.3 Communication Deadlines and Slack

In the simple example code that we showed at the beginning of the chapter, we used MPI_operation as a standin for any across-node synchronization. However, when the MPI operation is a time-consuming collective operation, it creates an opportunity to reduce the dynamic fraction further. Because a node typically must wait for information from other nodes to make progress on a collective operation, it may sometimes be able to tolerate a delay in

arriving at the collective operation without impacting the completion time of the collective operation.

4.3.1 Characterizing Slack

We first show that the slack in collective operations is of significant duration. Figure 4.1 illustrates the slack distribution across different MPI processes for a simple broadcast implementation. The threaded computation within each MPI process is shown in light blue rectangles. The arrows indicate MPI messages. The idle time spent waiting for messages inside MPI calls is shown in orange, and this time is the *slack*. The root of the broadcast can start immediately and thus has no slack. The other processes exhibit slack depending on the process arrival pattern and the communication pattern. Note that communication patterns are specific to the broadcast implementation of the collective within the MPI implementation.

The key to acheiving *minimalistic* dynamic scheduling is knowing the amount of time available before the communication deadline. Figure 4.4 shows a near-optimal case, where the computation ends *just* before the deadline. To do this for every dynamic execution, we must predict the duration of the slack. However, slack is *not* the same on all processes, and it can also vary over time. The question is how predictable slack is, and whether it is different enough across different processes to make separate, per-process adjustments of the dynamic fraction.

Collective	**max**	**avg (σ)**	σ_i
`Allreduce`	307	199 (.792)	.102
`Alltoall`	280	149 (.821)	.176
`Barrier`	250	139 (.178)	.061
`Allgather`	268	189 (.527)	.115
`Reduce_scatter`	459	296 (.649)	.129

Table 4.2: Slack statistics (in μs) across MPI processes.

To characterize the variability of slack on a single process and across processes, we performed a simple experiment in which we ran 1000 iterations of a simple computation, followed by an MPI collective call, and measured the slack on each process. Table 4.2 shows the results for running on 512 nodes of a Blue Gene/Q system.

The second and third columns show the maximum and average slack observed across MPI processes. We also show the standard deviation across MPI processes in parentheses in the third column. We see that there is a

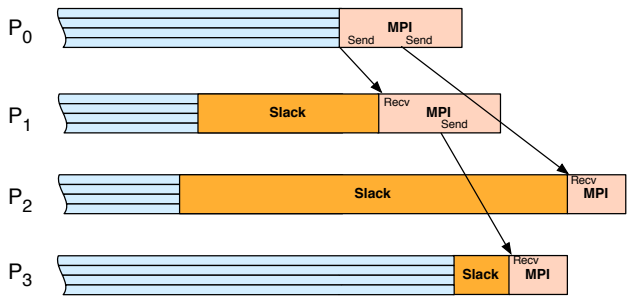

Figure 4.1: Slack in a binomial broadcast tree with four processes.

wide range of slack values across MPI processes. The last column shows the process-internal standard deviation σ_i across iterations, averaged across MPI processes. The intra-process deviation across time is small. Given this, our goal is to predict the slack as accurately as possible during runtime, and also to ensure that this prediction incurs minimal overhead.

4.3.2 Existing Thread Scheduling Policies In the Context of Slack

We now show how different existing scheduling strategies handle noise, in the context of slack. Figure 4.2 shows a team of statically scheduled threads in a timestep of an MPI+OpenMP application, without noise occuring (top) and with noise occuring (bottom), with the slack factor added. If uninterrupted by noise, the threads finish simultaneously and start the MPI communication. If a noise event occurs in one of the threads during the computation, the statically scheduled work is delayed. In the case that the noise consumes less time than the slack, the critical path is unaffected and the noise is *absorbed*. If the noise duration exceeds the slack, then the MPI work on the application's critical path is delayed, which *amplifies* the noise, i.e., delays another process. Absorption and amplification has been studied extensively in the literature [46, 72].

Figure 4.3 shows the same work dynamically scheduled, where the work is broken into fine-grained chunks of iterations. Threads obtain these work units from a *work queue*. The time required to pull work from the queue is called *dequeue overhead*. If noise occurs on a thread, the "lost" work will be picked up by other threads, and the noise is consequently mitigated. Thus, dynamic scheduling allows some noise to be absorbed even if it would exceed the slack if static scheduling were used. However, dynamic scheduling adds a queueing cost and data movement overhead to the overall execution.

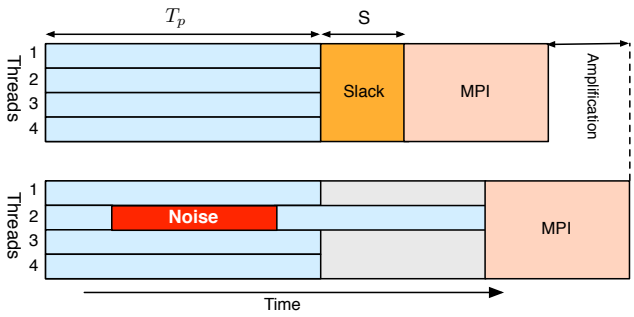

Figure 4.2: Impact of performance irregularities for static scheduling, with slack factor added.

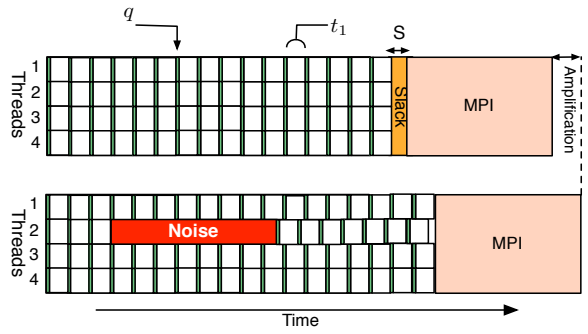

Figure 4.3: Resilience to performance irregularities with dynamic scheduling, with slack factor added.

The overhead caused by this cost depends crucially on the granularity of the work, but can be significant for loops typically found in computational science applications [27, 54].

To reduce queueing cost, we can schedule a large fraction of the iterations statically and schedule only a minimal number of iterations dynamically. We call this mechanism *Hybrid Static/Dynamic Scheduling*, or *Hybrid Scheduling*. Figure 4.4 illustrates this technique. Here, only the second part of the workload is scheduled dynamically. The first part, shown in blue, is scheduled statically, without any overhead. The noise event causes load imbalance, but the dynamic scheduling moves excess work off the critical path. Additionally, the schedule still incurs some dequeue overhead, but much smaller than that of a fully dynamic scheme. The goal of our approach is to use just enough dynamic iterations to reschedule work delayed by noise, while using enough static iterations to prevent the communication phase from being delayed by queueing overhead.

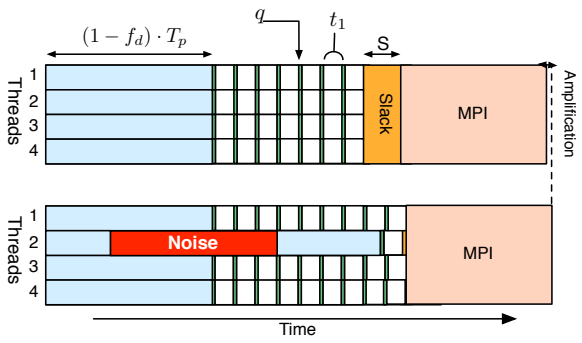

Figure 4.4: Hybrid Scheduling for a threaded computation region, with the slack factor added.

4.4 Extending the Model to Incorporate Slack

The question now becomes whether we can reduce scheduling overhead further by exploiting our understanding of slack.

We made the observation that processes have *slack*, or idle time spent waiting on another process inside an MPI operation. Slack acts as a *free* noise insulator, and we exploit it to reduce the dynamic scheduling necessary to mitigate the impact of noise. Note that the slack is different on different nodes. Thus, we need to extend the model by specializing the dynamic fraction on each node depending on its slack.

We describe how to further reduce the average dequeue overhead while still bounding the impact of noise by $\frac{\delta}{p-1}$. We refer to the resulting scheduling scheme as *Slack-conscious Hybrid Static/Dynamic* scheduling. What is the relationship between the delay to the critical path α_i and the computational delay η? If the collective operation at the end of each iteration started immediately, any computational delay will lead to extension of the critical path, i.e., $\alpha_i = \eta$. However, we know from Section 4.3 that different processes have different amounts of slack. Their slack relaxes the deadline on each node. Slack gives us some extra time to absorb part of the computational delay.

Let S_i be the amount of slack on a node i. Per Equation (4.5), on the critical path, the slowdown in the computation region *and* the amplification are both α_i. For the remainder of this section, we distinguish between *impact to the critical path* (α_i) and *computational delay* (η). α_i is η minus the slack:

$$\alpha_i = \eta - S_i \tag{4.6}$$

Slack provides free insulation from noise. On a node with slack S_i and

Model outputs	
f_d	Fraction of work scheduled dynamically
f'_d	Fraction of work scheduled dynamically, reduced for slack
Model inputs	
q	Overhead of dequeueing single iteration
S_i	Slack duration on process i
δ	Expected noise duration
T_p	Execution time on p cores with fully static scheduling and no noise
N	Total number of iterations across all threads
Change quantities	
Δ_f	Change in dynamic fraction
Δ_η	Change in execution time of computation region
τ	Sequential time for dynamic work moved
Other variables	
t_1	Duration of single iteration on a single thread, on one core
d	Duration of single dynamic iteration on a single thread
η	Compute delay due to noise and queue overhead
α_i	Delay added to the critical path by node i

Table 4.3: Overview of all model parameters.

without any dynamic scheduling, we could withstand noise events of up to length S_i without delaying the critical path. Here, we exploit this to reduce on-node dequeue overhead by decreasing the amount of dynamic scheduling f_d based on slack. We do this while still bounding each node i to at most α_i amplification in the expected case. We begin by replacing f_d with a new per-process fraction f'_{di}, or simply f'_d, where $f'_d < f_d$. Let $\Delta_f = f_d - f'_d$. When we reduce the dynamic fraction, we trade off dynamically scheduled work for statically scheduled work. We model the expected impact to the critical path by node i to ensure that it does not exceed α_i. Assume that there is noise of length δ. In this scenario, reducing the dynamic fraction reduces the work in the dynamic section of the threaded computation region. The time that one processor would take to do this work with no queue overhead is denoted τ:

$$\tau = Nt_1\Delta_f \tag{4.7}$$

When we remove this work from the dynamic section, we can no longer insulate ourselves from $pT_p\Delta_f$ noise. The change in the length of the com-

putation region (η) due to this scheduling change when noise occurs is:

$$\Delta_\eta = -\frac{\tau}{p} + \tau - \Delta_f N q \tag{4.8}$$

The first two terms model the change in computational load, and the last term models the change in queuing overhead. Now, we have enough information to choose f_d' so that the node's impact to the critical path is still α_i in the expected case. Let α_i', or simply α', be the amplification encountered using f_d'. α' is equal to amplification using f_d plus Δ_η, minus the slack:

$$\alpha' = \alpha + \Delta_\eta - S \tag{4.9}$$

Set the above equal to α and solve for $f_d{}'$:

$$\begin{aligned}
\alpha &= \alpha + \Delta_\eta - S \\
S &= -\frac{\tau}{p} + \tau - \Delta_f N q \\
S &= -pNt_1\Delta_f + T_p\Delta_f + \Delta_f N q \\
S &= -\Delta_f((p^2-1)Nt_1 + \frac{Nt_1}{p} + Nq) \\
-\frac{S}{(p^2-1)\frac{Nt_1}{p} + Nq} &= f_d - f_d' \\
f_d' &= f_d - \frac{S}{(p^2-1)\frac{Nt_1}{p} - Nq}
\end{aligned} \tag{4.10}$$

This dynamic fraction will ensure that amplification in the expected case does not exceed α, i.e., it is no worse than for nodes that are on the critical path. Indeed, it can be observed trivially that when we are on the critical path, $S = 0$ and $f_d' = f_d$. As slack grows, we reduce the dynamic scheduling used when a node is unaffected by noise. We prefer to use slack for insulation when it is available because dequeue overhead of dynamic scheduling can amplify even when there is no noise.

This formulation allows f_d' to be negative when slack is large, but in reality we cannot use less than 0% dynamic scheduling. We revise Equation (4.10) to:

$$f_d' = \min\left(f_d - \frac{S}{(p-1)\frac{Nt_1}{p} - Nq}, 0\right) \tag{4.11}$$

4.5 Slack-Conscious Hybrid Static/Dynamic Scheduling

The percentage of dynamic work that minimizes the *average-case* runtime of a threaded region in a noisy system depends on each node's communication deadline. This fact implies that optimizing the performance of a

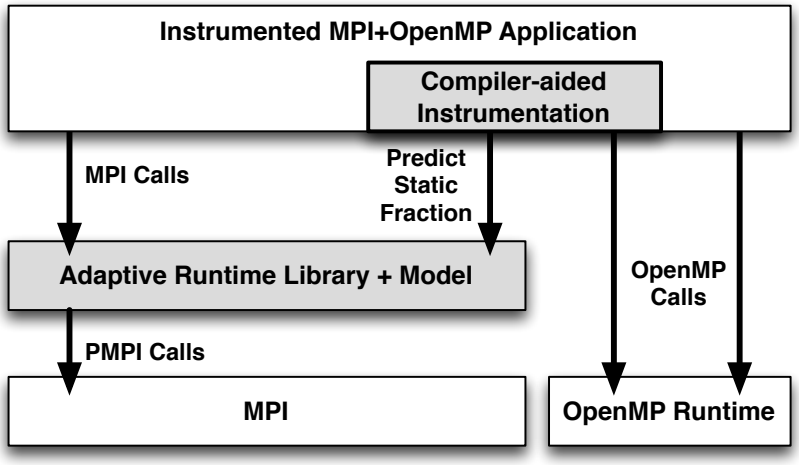

Figure 4.5: Runtime framework with our contributions in grey.

hybrid MPI+OpenMP application is not a simple matter of optimizing the distributed memory, e.g., MPI, and shared memory, e.g., OpenMP, runtime systems independently. Rather, we must dynamically tune the shared memory runtime based on the behavior of the distributed memory runtime. Inspired by this observation, we have devised a software system that performs this tuning automatically. Our prototype implementation uses a compiler-based approach to instrument MPI+OpenMP programs. Specifically, we have developed a runtime library to compute an optimized dynamic fraction for an OpenMP phase.

An overview of our architecture is shown in Figure 4.5. The white rectangles taken by themselves show the interaction between MPI+OpenMP application code and the MPI runtime and the OpenMP runtime. The gray components are our contributions. We can automatically employ our techniques within an application to take advantage of our library using a source-to-source transformation, of our own design. The source-to-source transformation adds calls to our adaptive runtime library, and these calls are used to guide the OpenMP runtime.

Our runtime library uses its slack prediction, its noise estimation, and its dequeue overhead estimation to compute the minimal dynamic fraction for each node. The computation of the slack-conscious dynamic fraction, i.e., implementation of the equation (4.11), is done within the `decide_dynamic_fraction()` call, on the arrow going from Compiler-aided Instrumentation to the Adaptive Runtime Library + Model.

We note that we choose MPI+OpenMP for the baseline codes, the most

popular hybrid programming combination, to demonstrate our techniques. However, our techniques generalize to other bulk-synchronous distributed memory applications, e.g., UPC or CAF, that are combined with on-node runtimes that support static scheduling, e.g., TBB. We detail these components of the framework below.

4.5.1 Automatic Compiler Transformation

```
for(int timestep=0; timestep<1000; timestep++)
{
#pragma omp parallel for
   for (int i = 0; i < n; i++)
     c[i] += a[i]*b[i];

   MPI_Allreduce(...);
}
```

(a) OpenMP loop with static scheduling.

```
static LoopTimingRecord *lr = NULL;
double fs; ...
for (int timestep=0;timestep<1000;timestep++)
  {
    fs = decide_static_fraction(&lr);
#pragma omp parallel
    {
#pragma omp for nowait
      for (int i=0;i<fs*n;i++)
  c[i] += a[i]*b[i];
#pragma omp for schedule(dynamic)
      for (int i=fs*n;i<n;i++)
  c[i] += a[i]*b[i];
      end_timing(&lr);
    }
    endLoop(&lr, n);
    MPI_Allreduce(...);
  }
```

(b) OpenMP loop tranformed for Slack-Conscious Hybrid Static/-Dynamic scheduling.

Figure 4.6: Transformation of an OpenMP loop to use our approach.

To allow developers to use Slack-Conscious Hybrid Static/Dynamic scheduling quickly, we have implemented a ROSE compiler transformation that instruments standard OpenMP code to use Slack-Conscious Hybrid Static/Dynamic scheduling and to call into our runtime library. Our transform splits loops like the one pictured in Figure 6.2 into two loops. The transformed code is shown in Figure 6.3. In the transformed code,

the first OpenMP loop's iterations are statically scheduled, and the second OpenMP loop's iterations are dynamically scheduled. The compiler inserts the `nowait` clause on the statically scheduled OpenMP loop to allow its threads to start the dynamic region immediately, without synchronization. Before the OpenMP region, the ROSE transformation adds the `predict_dynamic_fraction()` call and other instrumentations, the results of which are used to determine the bounds of our static and dynamic loops. Our approach relies heavily on cooperation between the MPI and OpenMP runtimes, and the `predict_dynamic_fraction()` call is where the two communicate. Without this call, OpenMP would be unable to get the information it needs from MPI to enable Slack-Conscious Hybrid Static/Dynamic scheduling.

4.5.2 Runtime Parameter Estimation

Within the `predict_dynamic_fraction()` call, observed slack values and measured parameters of computation time per thread $\frac{N \cdot t_1}{p}$, dequeue overhead q, and noise length δ are needed to calculate this per-process dynamic fraction, as determined in Equation 4.11 in Section 5.2. Below, we explain how these values are obtained during runtime.

Basic Scheduler Measurements

The `record` parameter stores the values of $\frac{N \cdot t_1}{p}$, q and δ. The scheduling overhead q is measured with a dynamically scheduled OpenMP loop at the initialization of the library. This loop runs multiple dynamically scheduled short iterations to estimate the dequeue overhead q. The expected noise event length δ is observed by running multiple measurement iterations in a tight loop containing within its body a square root calculation. The difference between the minimum and maximum runtimes is used to estimate δ. We estimate $\frac{N \cdot t_1}{p}$ by obtaining the minimally observed time taken for the statically scheduled section from previous invocations of the loop. We obtain t_1 by dividing this time by the number of iterations executed by a thread statically, and use it to calculate $\frac{N \cdot t_1}{p}$.

We denote the time taken in some arbitrary invocation as T_p, and the time taken for invocation i as $T_{p,i}$. The time for executing a single invocation of a loop depends on the application workload. Thus, we measure it for each OpenMP parallel loop. The mechanism is shown in Figure 6.3. The `endLoop()` function records time taken for the loop of the precedent invocation of the OpenMP region, and we collect the timing for each invocation

in the `LoopTimingRecord` struct.

This struct contains a configurable number of past loop invocations. For each of those past invocations, the framework computes the time for the parallel execution $T_{p,i}$ of the workload in invocation i; this is computed using the known dynamic fraction for this invocation. The new dynamic fraction for the next invocation now uses the minimally observed T_p across all previous invocations. Because we keep only the minimum of $T_{p,i}$, the memory to store the history is $\mathcal{O}(1)$. The first invocation will run with a fixed 10% dynamic fraction and the new dynamic fraction for the next invocations is then computed using these available runtime measurements from the previous invocations, along with the process-local slack, as described in the next section.

Process-local Slack Measurements

Process-local slack is measured during runtime. We use the PMPI profiling interface to intercept all calls to MPI collective routines. When the library intercepts a collective call, it measures the time spent inside the call, which it records in a historical slack trace. We have based our slack tracing on the Adagio tool [81], which uses similar instrumentation to predict slack for power optimizations. Since there is a tradeoff between runtime overhead for the slack measurement and the performance advantage due to Slack-Conscious Hybrid Static/Dynamic scheduling, we investigate three different granularities for slack measurement:

Callpath. The Adagio tool uses this mode. When we run this way, our library will unwind the call stack when it encounters an MPI operation, and it will associate slack with a particular call stack. This is our finest granularity. A call path represents specific context within a program, including the MPI call and all its ancestors. Callpath granularity can capture behaviors that differ depending on which part of the application is using MPI.

Collective. Rather than storing a full callpath, which requires the overhead of unwinding the stack, we can also associate slack trace values with *only* the type of the collective operation that had the slack. This allows us to capture different communication patterns per collective, but it does not capture application load imbalances or other behaviors extrinsic to MPI.

Naive. With the Naive prediction strategy, we forego runtime tracing altogether and predict slack based on a precomputed experiment. In this mode, we run 1,000 invocations of a simple `MPI_Allreduce()` with a message size of 4 bytes on all MPI processes before the application begins, i.e., right after `MPI_Init()`. The average slack across all invocations of

`MPI_Allreduce()` is then used to predict slack later. This is not an intelligent scheme, but the overhead of prediction is low, and it serves as an effective control to compare it with the adaptive case. When using the Collective or Callpath prediction schemes, this Naive prediction scheme is used for the slack prediction of the first invocation of a particular collective in an application.

4.6 Experimental Evaluation

Figure 4.7 compares the default OpenMP static and dynamic loop schedules with our approach. By using a minimally dynamic scheduling strategy, we improve the scalability of the application and achieve a 26.8% improvement over a stock OpenMP runtime for large-scale runs.

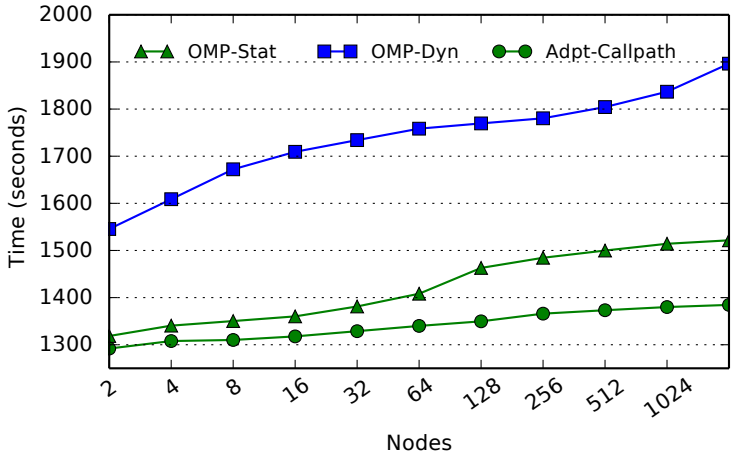

Figure 4.7: Scaling PF3D on a Intel Westmere 12-core cluster.

We now compare the effectiveness of our Slack-Conscious Hybrid Static/Dynamic scheduling scheme to the OpenMP static, dynamic, and guided scheduling policies, as well as static-hybrid scheduling. For our experimentation, we considered three different machines. Sierra is an Intel Westmere cluster with 12 Xeon EP X5660 cores on each node and the CHAOS 5 Linux-based operating system. Cab is a 16-core Intel Westmere cluster with the CHAOS 4.4 Linux-based operating system. Rzuseq is a Blue Gene/Q (BG/Q) system with 16 cores at each node running IBM's Compute Node Kernel OS. A 17th core on this machine is dedicated to servicing the MPI progress engine and to handling some OS events.

We test our strategies by applying them to bulk-synchronous MPI+OpenMP codes. First, we use all three NAS multi-zone benchmarks,

which are hybrid MPI+OpenMP versions of the traditional NAS benchmarks [50]. We use problem class D for these codes. We also consider the AMG2006 Algebraic multigrid application that solves a Laplace problem with Jacobi relaxation [5]. We run AMG for 13 load-balanced time steps using 100×100 elements per core. Finally, we consider the PF3D application [43], which is a laser-plasma interaction simulation. It alternates between successive 2-D FFT `MPI_Alltoall` communication on subcommunicators and computation regions consisting of multiple OpenMP loops. For all applications, we use one MPI process per node and fully occupy each compute core with an OpenMP thread.

4.6.1 System-Specific Noise Signatures

We utilized the tools offered by Hoefler et al. [46] to produce scatter plots of the noise signatures of each our test systems. The Blue Gene/Q system is noise-free. Cab and Sierra exhibit 0.18% and 0.16% serial noise, respectively. Our runtime system reports 0.6% and 0.7% performance improvement, respectively, showing consistency of our runtime system measurements with a commonly used benchmark. Figure 4.8 shows the noise signatures for the three systems.

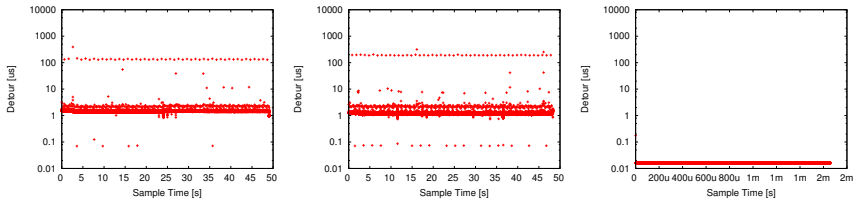

(a) Sierra. (b) Cab. (c) Blue Gene/Q.

Figure 4.8: Noise signatures for our test systems.

4.6.2 Slack Prediction Accuracy and Overhead

Our Slack-Conscious Hybrid Static/Dynamic scheduling techniques rely heavily on slack prediction to be effective. To test the efficacy of our predictors, we ran our slack predictors (described in Section 4.5) with each of our test applications and measured the average error and overhead, across all MPI processes. Figures 4.9a, 4.9b, and 4.9c show the results for slack error.

As expected, the Naive approach has the worst slack prediction error of the three approaches. This is because different collective operations exhibit different slack profiles at runtime. Slack prediction based on collective type

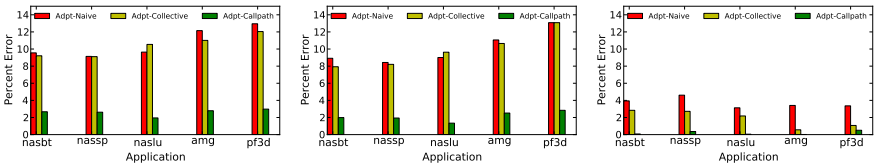

(a) Sierra. (b) Cab. (c) Blue Gene/Q.

Figure 4.9: Average error of runtime's slack prediction across all MPI processes, for different applications.

is only slightly better: from 8-15% on the Cab machine, and from 2-4% on Blue Gene/Q. On all three machines, callpath-based slack prediction, where a separate prediction is made for each *occurrence* of a collective, is by far the most accurate. This prediction scheme is able to predict slack for each MPI call to within 1.5% on Cab and within 1% on Blue Gene/Q. Figure 4.9b and Figure 4.9c show that Blue Gene/Q is much more consistent than Cab. Even the Naive approach seems to work reasonably well (2-4% error) on the Blue Gene/Q machine.

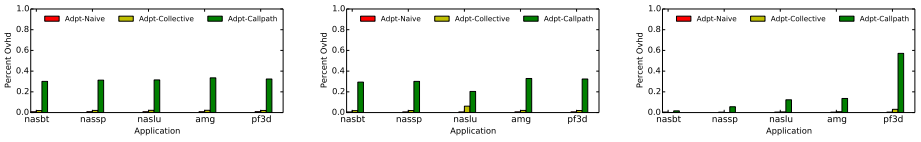

(a) Sierra. (b) Cab. (c) Blue Gene/Q.

Figure 4.10: Average overhead of implementation of slack prediction library function across all MPI processes for different applications.

Slack prediction is not useful if its use adds too much overhead to the run. For each application, we measured the overhead of our various slack prediction techniques. Figures 4.10a, 4.10b and 4.10c show the results. Overheads are an average over five independent runs of each application. On all three machines, the slack overheads are low; no machine exceeds 1% overhead for even the most expensive technique. We therefore use the most accurate, i.e., callpath-based, prediction technique.

4.6.3 Comparing Slack-conscious Scheduling with Best Static Fraction

In this section, to highlight the need for adaptivity, we compare our Slack-Conscious Hybrid Static/Dynamic scheduling strategy with an optimally

configured *non-adaptive* strategy. Here, the non-adaptive strategy makes the fraction of statically scheduled work constant for all loops on all nodes, and we compute the best such configuration by running each application many times with different static fractions. Figure 4.11a shows the performance of each run in our parameter sweep on Cab, using 1024 nodes. In all cases, the best *non-adaptive* static fraction is between 0.8 and 0.9. We performed the same set of runs at different scales, and Figure 4.11b shows the best (minimum) result from each ensemble. The best static fraction decreases as the scale increases. Using the data from Figs. 4.11a and 4.11b as an oracle, we compared the performance of Slack-Conscious Hybrid Static/Dynamic scheduling with each best performing non-adaptive run. From the outset, this comparison makes the non-adaptive approach look better than it realistically could, because knowing the optimal fixed static fraction would require too many experiments to be practical.

Figure 4.11c shows the results for the five applications on the cab machine. In all cases, Slack-Conscious Hybrid Static/Dynamic scheduling performs *better* than the optimal non-adaptive strategy. We achieve up to 10% improvement with NAS LU on 1024 nodes. Moreover, the advantage of our technique *increases* as we scale up. Clusters with on the order of 100,000 nodes already exist, and they are expected to be commonplace in the next few years. We expect the advantage of our approach to be even greater at such scales. Our approach enables large performance gains without burdening the programmer with the task of tuning each application for each scale, unlike prior work.

4.6.4 Implementation Strategy Assessment

We now compare the speedup over baseline static scheduling obtained with a) dynamic scheduling, b) static-hybrid scheduling, and c) the slack-aware scheduling strategies using different slack prediction techniques. Figure 4.12 shows the results of using these different implementation strategies for our applications run at full scale on each of our machines (1024 nodes on Sierra and Cab, and 512 nodes on Blue Gene/Q). The performance is reported as a speedup with respect to the default runtime of OpenMP static scheduling. The OpenMP dynamic scheduling policy has a slowdown rather than speedup on all of the plots. Thus, the dequeue overhead in dynamically scheduled applications far outweighs any noise resilience it may afford. We are better off simply accepting the noise than switching to this strategy. On Cab and Sierra, we see that our static-hybrid scheduling improves perfor-

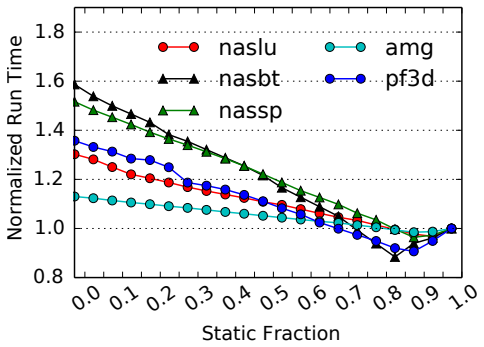

(a) Performance for different static fractions, normalized to static fraction of 1.0, on 1024 nodes.

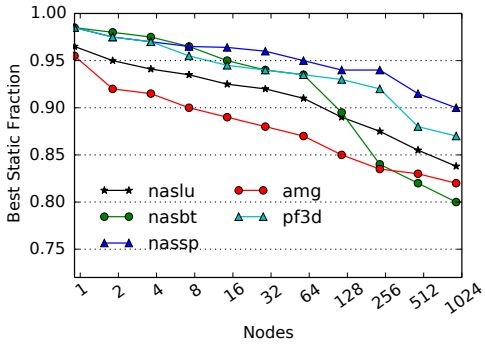

(b) Best static fraction for different scales.

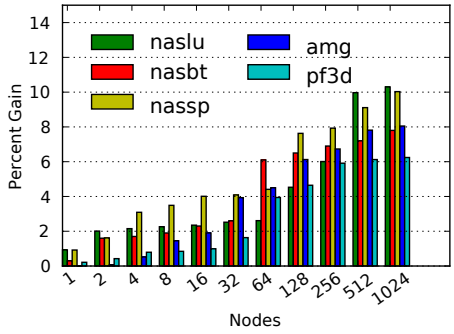

(c) Comparison of performance for best performing global static fraction with Slack-Conscious Hybrid Static/Dynamic scheduling.

Figure 4.11: Comparison of our scheduling technique with using the best static fraction on Cab.

mance by 10-20% over static scheduling, while our Slack-Conscious Hybrid Static/Dynamic scheduling techniques improve the performance further by 15-26%. On Blue Gene/Q, the techniques perform better in roughly the same rank order, but they decrease the performance degradation rather

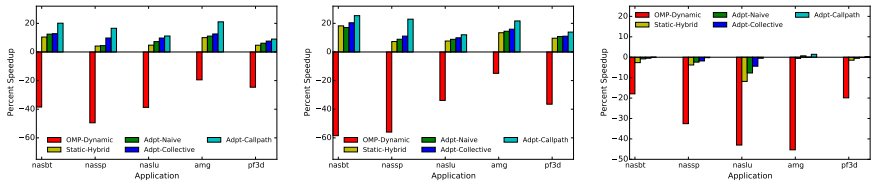

(a) Sierra. (b) Cab. (c) Blue Gene/Q.

Figure 4.12: Performance for different scheduling strategies shown as percentage speedup over OpenMP static scheduling.

than getting more speedup.

Overhead Analysis

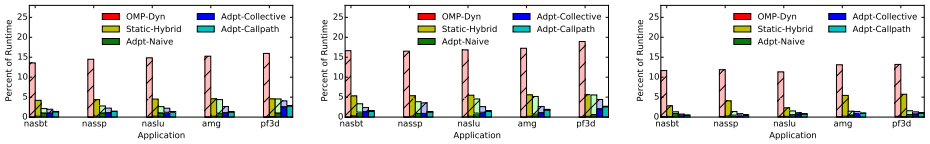

(a) Sierra. (b) Cab. (c) Blue Gene/Q.

Figure 4.13: Overheads for different scheduling strategies as a percent of total runtime. Dequeue overhead is hashed, and thread idle time is solid.

To understand better how different adaptation strategies balance transient load imbalances and scheduler overhead, we measure the total time spent across all threads in scheduler overhead and thread idle time during execution. Figures 4.13a, 4.13b and 4.13c show the percent costs (cost is in units of CPU-seconds) spent in thread idle time and scheduling overhead time for Sierra, Cab and BlueGene/Q, respectively. The general trend we see is that with the fully dynamic scheduling strategy, we incur high percentage costs mainly due to scheduling overhead. As we use more aggressively lightweight scheduling strategies (with *Adpt-Callpath* being most aggressive), we increase costs of thread idle time slightly, but the cost of scheduling overhead is greatly decreased. We also note that with Sierra, which has lower dequeue overhead than Cab, the *Adpt-Callpath* strategy is still beneficial in reducing scheduling overhead costs.

4.6.5 Overall Application Performance

Figures 4.14a, 4.14b, and 4.14c show the relative speedup we attain over OpenMP static scheduling for all five applications using our Slack-Conscious Hybrid Static/Dynamic scheduling with callpath-based slack prediction. On

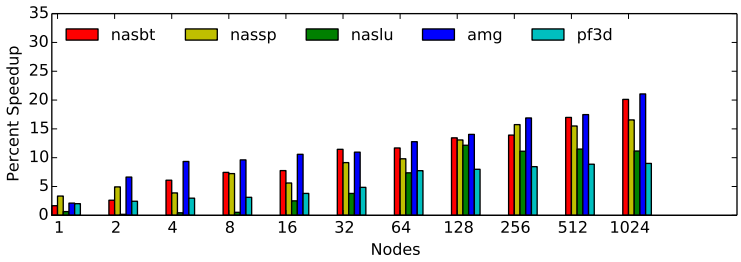

(a) Sierra.

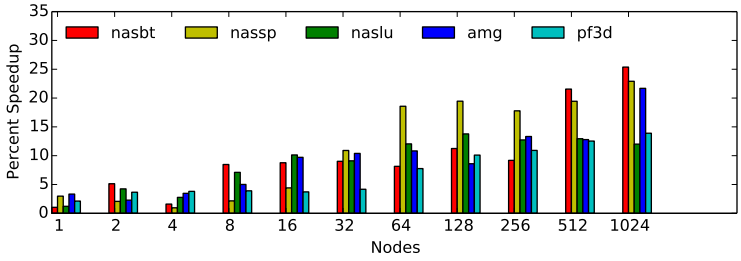

(b) Cab.

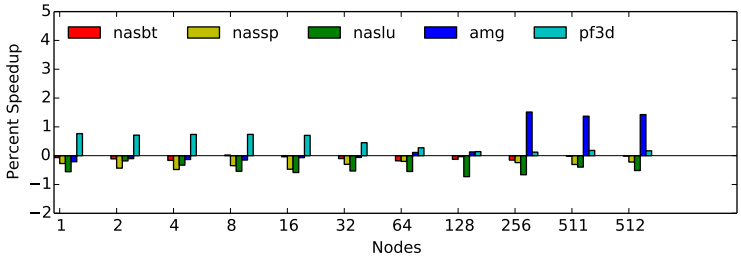

(c) Blue Gene/Q.

Figure 4.14: Scaling runs of all five applications.

Cab, Slack-Conscious Hybrid Static/Dynamic scheduling improves performance in all cases. We are able to improve performance by up to 26.8% for the NAS BT benchmark running on 1024 nodes. For real-world applications like AMG and PF3D, we are able to achieve a 20% performance gain on 1,024 nodes. Notably, the amount of improvement *increases* as we scale up, which is consistent with the idea of noise resiliency: there is more likelihood that *some* node will encounter noise at scale, so the benefit of our tech-

niques increases. On the Blue Gene/Q machine, we see that our techniques have much less effect. At most scales, our benchmarks and applications are slowed down by a fraction of a percent. This is likely because we add a small overhead to scheduling in the complete absence of noise. However, at large scale, we are able to improve AMG performance by a few percent. AMG has load imbalances in the sparse phases of the solve at larger scales, and we attribute these gains to being able to compensate for these imbalances. Because our Slack-Conscious Hybrid Static/Dynamic scheduler manages the transient delays while also reducing dequeue overhead, we are actually able to improve performance on a nearly "noiseless" machine, showing that our technique can be beneficial for transient load imbalances that come from the application and not just the platform. The key observation here is that even on a machine with little or no noise, we do not hurt performance, and for load imbalanced applications we can often improve it. For machines where noise is prevalent, we achieve significant speedups with Slack-Conscious Hybrid Static/Dynamic scheduling.

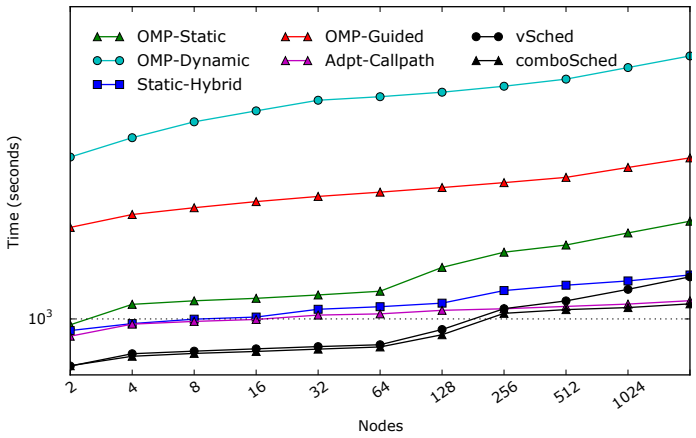

Figure 4.15: Scalability of PF3D with different schedulers on cab.

Figure 4.15 shows the raw runtimes for the PF3D application on cab. On this system, OpenMP dynamic scheduling performs noticeably worse than the other strategies. On Cab, both static and guided scheduling perform roughly 10% faster than dynamic scheduling, with guided scheduling sometimes tying and sometimes coming in slightly faster. Using our static-hybrid scheduling policy, we are able to perform faster than any built-in OpenMP scheduling policy by approximately 9%, and using *Slack-conscious* scheduling to exploit knowledge of the MPI runtime, we are able to run up to 18%

faster than stock OpenMP.

4.7 Conclusion

In this work, we have developed fundamental techniques that enable programmers to overcome the scaling wall, induced by within-node transient delays, for hybrid parallel applications. We demonstrated a general method that adaptively tunes itself, and which shows increasing performance improvement on increasingly large systems. We also implemented an automated source-to-source transformation framework for MPI+OpenMP hybrid applications that transforms such applications in a way that is transparent to the application programmer.

Our results showed performance gains of 26.8% over basic static scheduling for NAS BT MZ running on 1,024 nodes (16,384 cores) of a NUMA cluster. We showed that our Slack-Conscious Hybrid Static/Dynamic scheduler will not hurt performance significantly on a low-noise machine, and may improve the performance of load imbalanced applications even when there is no noise. Most importantly, we showed that our performance gains *increase* for increasingly large scales, indicating that our approach will yield even more improvement on future systems.

Chapter 5

Spatial Locality in Dynamically Assigned Iterations

The hybrid static/dynamic scheduling scheme provides many performance benefits. In particular, the statically allocated iterations exhibit higher spatial and temporal locality. In consecutive outer iterations, each thread executes the same inner loop iterations and therefore touches the same data on each outer iteration. In addition, statically allocated iterations for a given thread constitute a contiguous region, and thus exhibit spatial locality (this assumes consecutive iterations access nearby data, which is the common case in most applications). However, for dynamically allocated iterations, spatial as well as outer-loop temporal locality is lost. In this chapter, we develop a technique to restore locality for these iterations.

To handle a larger class of load imbalances so as to make our approach useful to a broad range of applications, we consider modifications to our existing hybrid static/dynamic scheduling scheme to improve data locality. Specifically, we implement a scheduling scheme in which we change the layout of the iterations that are static and the iterations that are dynamic, in order to improve spatial locality. We also add an additional tunable constraint in the dequeue function of the scheduler, in order to reduce coherence cache misses on a multi-core node. The constraint is quantified as a fraction of dynamically scheduled work, and thus can be determined through performance modeling and theoretical analysis in the same way as done in [27].

The contributions of this chapter are:

1. Analysis of the tradeoff between locality and load balance for coarse-grained application-generated imbalances;

2. Improvement of spatial locality for scheduling in current static/dynamic scheduling schemes;

3. Techniques (constraints) for the portion of work that is dynamically scheduled, so as to reduce both coherence cache misses and contention on the shared memory interconnect.

Through experimentation of an N-body code on modern multi-core architectures, our technique gives 19.42% performance gains over dynamic scheduling, and an overall 48.63% gain over standard static scheduling.

5.1 Problem Statement

The scheduling strategy in this chapter builds upon the basic hybrid static/dynamic scheduling strategy of Chapter 2. So, we begin with a recap of that strategy. We assume a bulk-synchronous hybrid MPI+OpenMP or MPI+pthread application, where each thread runs on one core of an SMP node (and each MPI process runs on one node). A bulk-synchronous code consists of several application timesteps, with each application timestep surrounded by two successive global MPI collective invocations. Within each timestep are one or more threaded computation regions, e.g., a loop performing a dot product with a `#pragma omp parallel for` surrounded by it. Unless otherwise noted, a threaded computation region ends with a thread barrier. There may be load imbalance across threads, not just of the magnitude of one loop iteration, i.e., fine-grained, but also of the magnitude of multiple loop iterations, i.e., coarse-grained. This load imbalance may come from either system noise or from the application. The characteristic of load imbalance may be transient, i.e., without a fixed pattern across application timesteps, or persistent, i.e., with a fixed pattern across application timesteps.

A simple technique to handle the load imbalance within a node during the execution of an application timestep is to use dynamic scheduling rather than standard static scheduling. We assume a dynamic scheduling strategy where, during each invocation of a threaded computation region, threads pull sets of loop iterations, or *tasklets*, from a shared work queue. These tasklets have locality tags associated with them that indicate the thread on which that tasklet ran in the last application timestep. The scheduler attempts to give a thread a tasklet that the thread executed in the previous outer iteration, to the extent possible. Let us assume that when a thread retrieves a tasklet from the shared work queue, it incurs some scheduler overhead, consisting of dequeue overhead due to locking (including waiting for the lock) and unlocking the queue to retrieve a tasklet, along with the possible cost of data movement overhead due to coherence cache misses required to retrieve data corresponding to iterations specified by the tasklet from another core.

To reduce these costs of dynamic load balancing, a hybrid static/dy-

namic scheduling scheme can be used. In this scheme, depicted in Figure 5.1, threads first execute pre-assigned iterations from a fraction of iterations of the compute loop.The threads then, without waiting at a thread barrier, execute the remaining fraction of iterations dynamically by retrieving tasklets from a shared work queue. The x-axis in the figure is iterations, and not time. The point in the computation at which the threads switch from static scheduling to dynamic scheduling is either empirically tuned or determined through performance modeling and theoretical analysis.

5.2 Scheduling Strategy

We explain the locality optimizations of the hybrid static/dynamic scheduling strategies that we use to improve performance. In the following, let p be the number of cores on an SMP node. Let n be the number of iterations in a loop. Let f_s be the fraction of statically scheduled iterations of the loop. Let t be the thread ID of a particular thread participating in a threaded computation region.

5.2.1 Modifications to Allocation of Iterations

A key problem of spatial locality exists with hybrid static/dynamic scheduling. Figure 5.1 shows the allocation of iterations to threads. In the diagram, the x-axis is loop iteration number. Consider the dynamically scheduled set of loop iterations, starting with the iteration numbered $\frac{n \cdot f_s}{p}$, in Figure 5.1. As the labeling indicates, iterations are executed by arbitrary threads depending on the order in which the threads requested work.

Across outer iterations, the same inner iteration will typically be executed by different threads, and therefore will access data that was used by a different thread earlier. Heuristically, we can assume that consecutive iterations access adjacent data. This is because programmers typically write code to preserve spatial locality. Note that in the dynamic section, this spatial locality is also lost, where the consecutive sets of loop iterations get allocated to different threads arbitrarily.

Can we control the arbitrariness of the allocation of dynamic iterations to reduce the above problem? Consider the case of transient noise. We note that on a given node, on most outer iterations, there will be no noise. Yet, the dynamic scheduler will necessarily be arbitrary given the order in which the threads will enter the critical section to fetch their dynamic allocations. We prefer that the dynamic iterations executed by a thread be contiguous to its static allocation, to the extent possible.

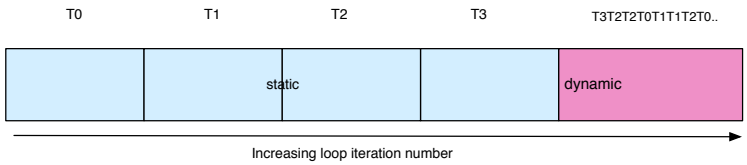

Figure 5.1: Allocation of iterations to threads for Hybrid Static/Dynamic Scheduling.

Therefore, we rearrange the static and dynamic iterations so that for each thread, the dynamic iterations are placed after the static iterations. That is, when a thread completes its last statically scheduled iteration i, the first dynamically allocated iteration it receives is likely to be $i+1$. This new layout is shown in Figure 5.2. Now, thread t begins its static section at $\frac{n \cdot t}{p}$, and ends it before $\frac{n \cdot (t+f_s)}{p}$. Most importantly, each thread t maintains a separate queue of tasklets that corresponds to iterations contiguous to its static iterations, namely from $\frac{n \cdot (t+f_s)}{p}$ to $\frac{n \cdot (t+1)}{p}$.

Each thread first executes its static iterations, and then dynamically allocates iterations from its own dynamic queue. Only after that does it attempt to steal work from other queues. When there is no imbalance, each thread will execute a contiguous set of iterations (static + dynamic) just as an OpenMP static scheduler will. Even when a core is overloaded by noise, the rest of the cores execute their own dynamic iterations first before helping the overloaded cores. Therefore, most dynamic iterations retain outer iteration locality as well as spatial locality.

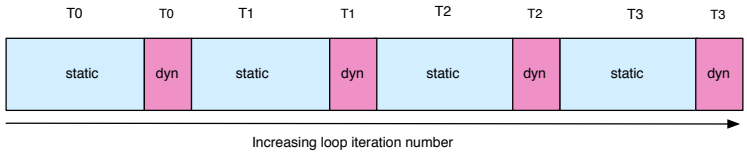

Figure 5.2: Allocation of loop iterations to threads for Staggered Hybrid Static/Dynamic Scheduling.

5.2.2 Choosing the Thread From Which to Steal

A basic problem with the dynamic scheduling section of hybrid static/dynamic scheduling is that it incurs overhead due to scheduling from a shared queue, as is done in many dynamic scheduling implementations. This causes additional locking and synchronization overhead, especially as the number

of cores increases. To address this, we will use a queue per thread rather than a shared queue, as described later.

A basic way to implement work-stealing is to steal tasklets from a randomly chosen thread. This randomization in stealing increases the chance of off-chip coherence cache misses. To avoid such coherence cache misses, we use a non-random strategy which better handles the tradeoff between load balance and scheduler overhead. For a thread t, we steal the tasklet from the queue belonging to a thread with either thread ID $t-1$ or $t+1$. To choose between thread $t-1$ and $t+1$, thread t steals from the queue which has the most tasklets to be completed. If no tasklets are available to steal from on these two threads, then thread t tries to steal from either thread $t-2$ and $t+2$. We continue this process until the thread t has found a queue with a tasklet that can be stolen, or has searched through all threads and found no tasklet to steal.

5.3 Implementation

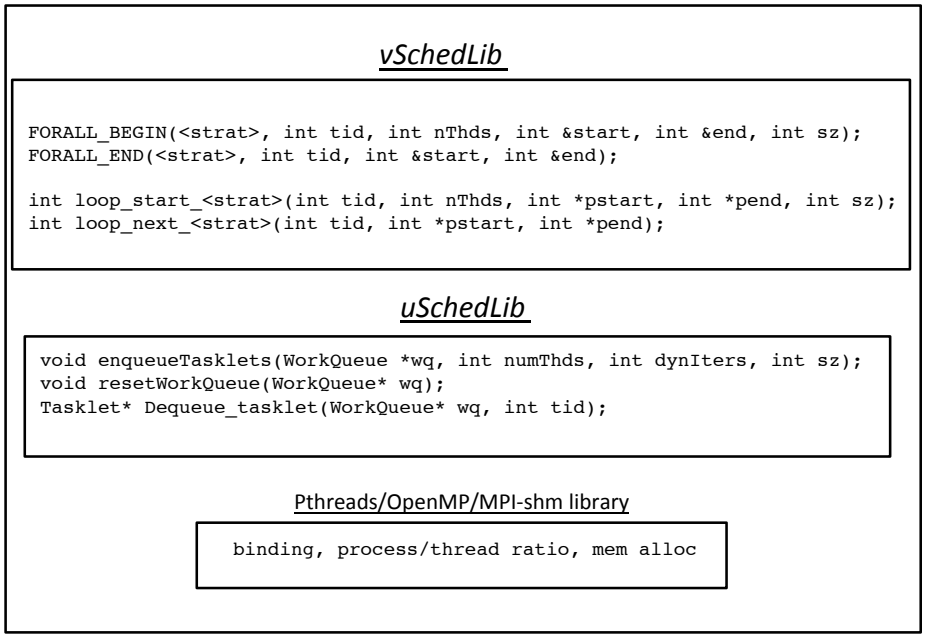

Figure 5.3: Framework for our modified portion of the thread library.

5.3.1 Framework and Usage

Our scheduling library software architecture is shown in Figure 5.3. This architecture shown is an extension to the library discussed in Chapter 4. The user's within-node code can be written in pthreads or OpenMP. The *vSched* module contains the macro functions `FORALL_BEGIN` and `FORALL_END` that the user would invoke (these functions are for ease of expressivity in applications). The only other change to the user's code is the inclusion of the header file `vSched.h`.

The macro functions invoke the scheduling functions `loop_start_<strat>()` and `loop_next_<strat>()`, called within the *vSched* library. The *uSched* module contains the back-end dequeuing functions, enqueuing functions, work queue data type definition, tasklet data type definition, and utility functions that can be used to print profiling and statistics about the scheduler library execution.

To illustrate usage, consider the following threaded computation region, as shown in Figure 6.2, which computes a dot product. The original computation region in this application program changes to that shown in Figure 6.3 when using our library. The application programmer can choose a particular scheduling strategy in our library through specification of the strategy name `<strat>` in the first parameter of the `FORALL_BEGIN` and `FORALL_END` functions.

5.3.2 Implementation of Locality Optimized Static/Dynamic Scheduling

The per-thread queues for the dynamic scheduling portion are implemented using a C struct. The per-thread struct contains a pthread mutex. Each thread locks this mutex when retrieving a tasklet from its private queue. When some other thread attempts to steal from this thread, it uses this lock to retrieve the tasklet from the queue.

For the *sd* and *sds* strategies, the dynamic fraction is calculated in the `loop_start_sd()` and `loop_start_sds()` functions, respectively. We calculate the value of the dynamic fraction at compile time, and store it in that thread's queue data structure. For the execution of the dynamic tasklets, the per-thread struct contains a variable storing the starting index of the next chunk of iterations, along with the chunk size to identify the end index of that chunk; these two values identify the work in the queue that a thread can do next when it tries to retrieve work from the queue. When the chunk of work is completed by a thread, the index of the next chunk is

```
#pragma omp parallel
{
  int myTid = omp_get_thread_num();
  int numThreads = omp_get_num_threads();
  for (int i=myTid/numThreads; i<((myTid+1)/numThreads)*n;
      i++)
    c[i] += a[i]*b[i];
}
```

(a) OpenMP loop with static scheduling.

```
int start, end = 0;

#pragma omp parallel
{
   int myTid = omp_get_thread_num();
   int numThreads = omp_get_num_threads();
   FORALL_BEGIN(sds, myTid, numThreads, 0, n, start, end)
      for(int i=start; i<end; i++)
         c[i] += a[i]*b[i];
   FORALL_END(sds, myTid, start, end)
}
```

(b) OpenMP loop transformed for Locality-Optimized Hybrid Static/Dynamic Scheduling.

Figure 5.4: Transformation of a loop to use our approach.

updated by the thread. The updating of the variable identifying the next chunk to be completed is protected by the per-thread mutex.

In the stealing function, when we obtain the thread ID one greater than and one less than the given thread ID (or k greater and k less than the given thread ID), we avoid the use of a modulo operation, which can be costly on most architectures [54], and instead do a comparison test to first check whether the thread ID is below the minimum thread ID number 0, and then a comparison test to check whether a thread id is above the maximum thread ID number $p - 1$.

5.4 Experimental Evaluation

We now show experimentation of our locality-optimized static/dynamic scheduling strategy. We first show runtime implementation overheads using a dot product computation, dot product square root computation, and a Barnes-Hut code. We then focus on the evaluation of our locality-optimized strategy, comparing it with both OpenMP dynamic scheduling and OpenMP guided scheduling. Results are shown for the 16-core Intel Westmere cluster

Code	Pct. ovhd
dotProd	3.14%
dotProdSqrt	2.31%
Barnes-Hut	1.71%
Regular Mesh	2.12%

Table 5.1: Overheads of our scheduling runtime shown as the percentage difference between our library's static scheduling and OpenMP static scheduling.

with a CHAOS 4.4 Linux-based operating system.

For the Barnes-Hut code, we show in Figure 5.5 the main modification done. Specifically, the modified code is shown within the `#ifdef CDY_` ... `#else` portion of the code. The original pthreads code is shown in the `#else`... `#endif` portion of the code. The `start` and `end` variables, which are private to each thread, are calculated from within our scheduler library.

5.4.1 Implementation Overhead

Table 5.1 shows the comparison between our library's static scheduling and OpenMP static scheduling for three different codes. The first code is a dot product calculation, denoted dotProd. To increase the computation per step of this dot product code, we applied a square root function to each product, denoted dotProdSqrt. We also show the result for the Barnes-Hut code, denoted by its name below. The comparison between our library implementation and the OpenMP library implementation is done by taking the percentage loss in execution time of our static scheduling method (100% static) with respect to OpenMP static scheduling.

The overheads in our implementation are small even for the code with very little work in each timestep (1000 timesteps were done), i.e., for the dot product computation, and decreases slightly when we increase the computation done, specifically for the square rooted dot product computation. We also see that the overheads are notably low for Barnes-Hut code, where the computation per step is significantly larger than both the dotProd and dotProdSqrt. From this, we can justify that our library is adequately optimized. Further optimizations can be done to reduce other overheads of library operation, but these small overheads do not add significant performance degradation to application execution when using our runtime.

5.4.2 Application Performance

We next compare the performance of the new strategy with the previously described strategies, namely OpenMP dynamic, OpenMP guided, hybrid static/dynamic (Chapter 2), and the staggered hybrid static/dynamic scheduling strategy described in this chapter.

Figure 5.8 show speedup over OpenMP static scheduling for different dynamic scheduling strategies mentioned above for the Barnes-Hut code on one node of Cab. Dynamic scheduling by itself is beneficial, compared with static, because of importance of load balancing for this computation. The benefit of the dynamic strategy decreases with increasing problem size. This is not because dynamic scheduling is doing worse, but because static scheduling is doing better. For larger problem sizes, static scheduling is able to balance load somewhat better than for smaller problem sizes. This improved load balance for smaller problem sizes is likely because when each thread is assigned a larger number of iterations, the law of large numbers tends to bring the load per thread closer to the average load per thread. However, even with the benefits for load balancing that the dynamic scheduling strategy provides, the strategy still incurs the non-negligible and significant cost of scheduler overhead.

Consider the 16-core data in Figure 5.8. When we use hybrid static/-dynamic scheduling to reduce these overheads (denoted *sd* in the graphs), performance improves 8.5% over dynamic scheduling for the smallest problem size, and 10.5% over dynamic scheduling for the largest problem size. When we use our locality-optimized hybrid static/dynamic scheduling (denoted *sds* in the graphs) scheme, performance improves 14.5% over dynamic scheduling for the small problem size, and 19.8% over dynamic scheduling for the largest problem size.

The performance improvement of staggered static/dynamic scheduling over OpenMP static scheduling for the largest problem size is approximately 60% on 16 cores, but only 30% on 4 cores.

This shows the importance of dynamic scheduling with increasing number of cores, and suggests that our benefits will be even higher on future larger multicore nodes. Note though that the dynamic scheduling strategy gives approximately 10% improvement on 4 cores, and only about 20% improvement on 16 cores.

This is due to the additional synchronization overhead with a larger number of threads, which our scheme is better able to handle than the purely dynamic scheduling, due to the scheme using a hybrid strategy as

well as its use of localized work queues.

Comparing with Guided Scheduling: Our strategy improves performance 10.1% over OpenMP guided scheduling for the smallest problem size, and 14.3% for the largest problem size. Guided scheduling incurs additional data movement because it does not respect outer iteration locality as well as spatial locality, whereas our scheduling scheme limits this dequeue overhead through the use of partially static scheduling.

Table 5.2 shows the standard deviations of execution times across 15 trials of the Barnes-Hut code, where a trial is a single job submission of the code. The dynamic and guided scheduling schemes exhibit over 6.2% standard deviation, and the *sd* strategy improves the standard deviation to 4.1%. Our *sds* scheduling further reduces the standard deviation to 1.9%. This is likely due to its superior outer iteration locality in both static and dynamic sections of iterations. This low standard deviation shows performance consistency, which is beneficial for bulk-synchronous codes, as shown in [27, 54].

```
static void* Process(void* arg)
{
   register const int slice = (long) arg;
   int start, end;
#ifdef CDY_ // constrained dynamic scheduling
   int tid = (long) arg;
   int i;
   setCDY(fd, myConstraint, chunkSz);
   FORALL_BEGIN(sds, 0, nbodies, start, end, tid, thds)
      for (i=start; i<end; i++)
         body[i]->ComputeForce(groot, gdiameter);
   FORALL_END(sds, start, end, myTid)
#else  // normal pthreads code
      start = slice * nbodies / threads;
   end = (slice + 1) * nbodies / threads;
  // the iterations can be executed in any order
   for (int i = start; i < end; i++) {
     // compute the acceleration of each body
     //(consumes most of the runtime)
      body[i]->ComputeForce(groot, gdiameter);
   }
#endif
   return NULL;
}
```

Figure 5.5: Barnes-Hut code main modification using Slack-Conscious Hybrid Static/Dynamic scheduling.

We briefly explain the impact of the *sds* strategy on load balanced computations. Recall that we consider dynamic strategies for such computations is because of transient imbalances, a.k.a. noise. We have explained and experimented with the relationship between single-node performance and multi-node performance going to a large number of nodes, in the presence of noise. We therefore focus on single-node performance in this chapter. Specifically, for load balanced computations, our objective is to show that our schemes do not add significant overhead to static scheduling. This can help to ensure that on large number of nodes, the dynamic component of our schemes will control the amplification as described in Chapter 2. In this context, we show the performance of multiple scheduling strategies on the stencil computation of Chapter 2 in Figure 5.9. The *sds* strategy does slightly, but consistently better than the *sd* strategy because of the improved locality in the dynamic section. The guided scheduling strategy does slightly better on the two smallest problem sizes, but much worse on the largest problem size, compared with *sds*. This again shows the consistency benefit of *sds*. We believe that the benefit of *guided* can be overcome by increasing the chunk size in *sds*.

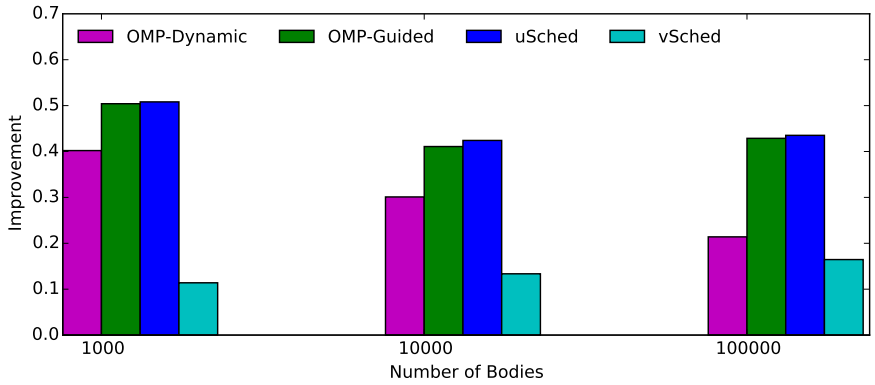

Figure 5.6: Improvement obtained over OpenMP static scheduling for different scheduling strategies applied to Barnes-Hut, shown for 4 of 16 cores of Cab.

5.5 Conclusion

In this work, we showed different techniques to increase locality further and to reduce costs of scheduling in the hybrid static/dynamic scheduling technique, which allows for reducing performance degradation at scale for

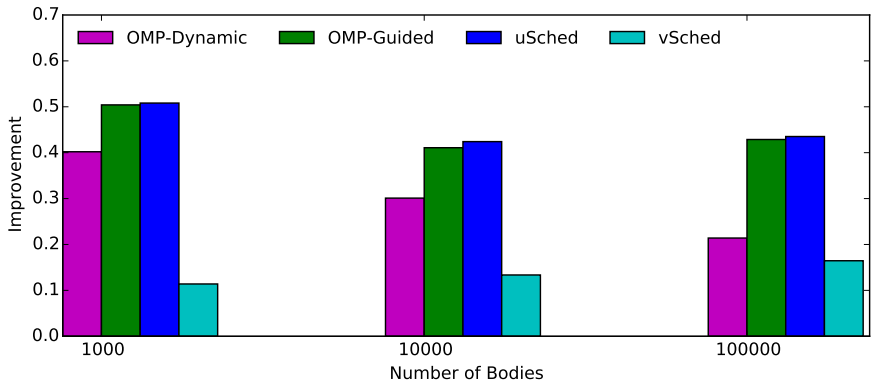

Figure 5.7: Improvement obtained over OpenMP static scheduling for different scheduling strategies applied to Barnes-Hut, shown for 8 of 16 cores of Cab.

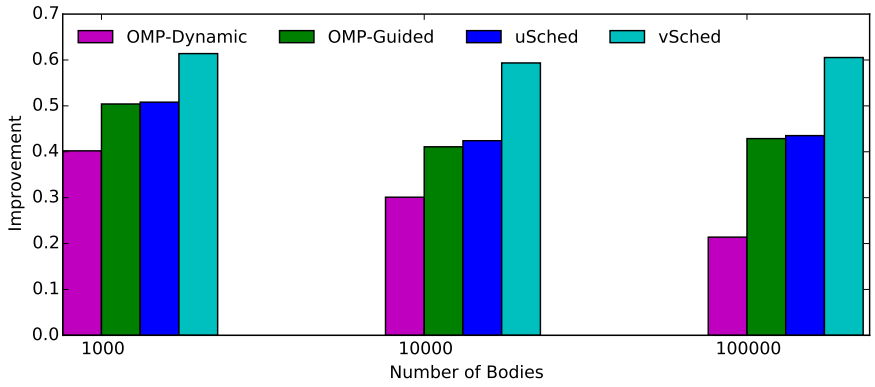

Figure 5.8: Improvement obtained over OpenMP static scheduling for different scheduling strategies applied to Barnes-Hut, for 16 cores of Cab.

Strategy	**Runtime dev.**
dynamic	10.68%
besf	3.49%
stag	1.42%
guided	6.92%

Table 5.2: Barnes-Hut standard deviations of execution times across 15 trials, where a trial is a job submission of the code.

bulk-synchronous MPI applications. We improved spatial locality by rearranging the data layout of hybrid static/dynamic scheduling. We used a sophisticated stealing function that avoided off-chip coherence cache misses.

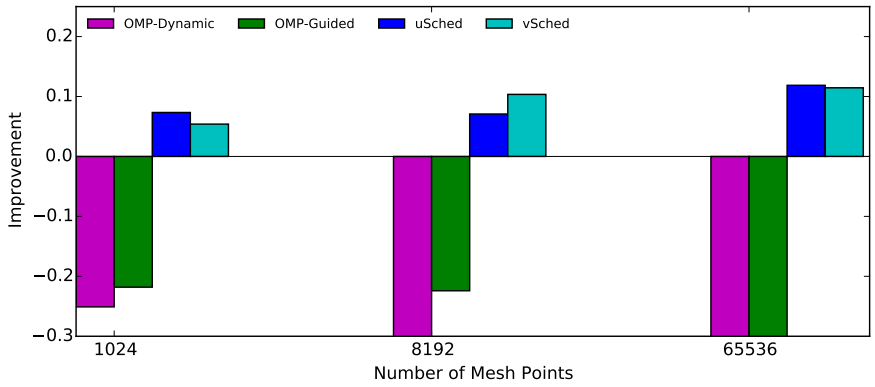

Figure 5.9: Improvement obtained over OpenMP static scheduling for different scheduling strategies applied to a stencil code, running on 16 cores of Cab.

We demonstrated our techniques on a Barnes-Hut code on a noisy machine, which provided the challenge of coarse-grained, persistent load imbalance from the application along with fine-grained, transient load imbalance due to noise induced by the OS and architecture. Our methods achieved 19.62% gain over dynamic scheduling, and a 48.63% gain over dynamic scheduling on a 16-core NUMA machine.

For future work, we plan to have alternate strategies for staggering the static and dynamic iterations, along with providing alternative stealing functions. We also plan to develop a more sophisticated performance model and theoretical analysis for determining the constraint for our dequeue function. Finally, we aim to make our library freely available to provide it for integration within a popular shared memory programming model such as OpenMP or the MPI shared memory extensions [44].

Chapter 6

Composing Multiple Scheduling Strategies

In the previous chapters, we discussed the reasons for using basic hybrid static/dynamic scheduling techniques, and discussed additional optimizations over hybrid static/dynamic scheduling. However, for real applications running on real-world architectures, several different factors of the machine and application are involved. Thus, we need to find a way to handle all of the problems discussed, simultaneously. In this chapter, we discuss a methodology to combine the scheduling schemes to make it available for the user.

To do this, we first identify the general types of scheduler techniques we have discussed up to this point, and combine them to make them usable for the application programmer within software. We discuss implementation a scheduler composition containing all the different schedulers implemented up to this point. With this, we show results for 3 new application codes on different architectures, shown for different types of scheduling strategies discussed up to this point. We include notes and data on architecture-specific tuning for the scheduler and application programmer usability. Finally, we conclude the chapter through discussion of scheduling techniques and the composed scheduler described in this chapter as it could be used for in the context of running applications on next-generation architectures.

6.1 Scheduling Strategies Overview

We have examined several schedulers in the previous chapters. In different circumstances, features of different schedulers will be more useful. It is desirable to combine features of different schedulers to make more sophisticated schedulers with better performance.

To do this, we first describe categories of circumstances, features of schedulers, methods of tuning their parameters, and performance factors.

1. circumstances: these are the architecture and application characteristics that affect the choice of the scheduling strategies.

2. scheduler features: these are the individual techniques that were used in putting together the schedulers of previous chapters. Our attempt will be to judiciously choose and combine features from individual schedulers.

3. methods for selecting parameters.

4. performance facets: the different features impact the performance via affecting specific performance facets.

Circumstances: The application-platform combinations that we encounter can be classified based on the following *circumstances*:

- noise
- application imbalance
- different iterations take different amounts of time
- effective core speed variation
- number of nodes
- number of cores per node

Features: Each of the schedulers from the previous chapters was built using a combination of scheduling techniques. Each scheduling technique can be thought of as a separate feature that can often be independently combined.

- hybrid static/dynamic scheduling
- chunking of iterations,(task quantization)
- variable-sized tasklets, as in guided and tasklet library.
- separate calculation of f_d for each node.(forgetting about slack)
- exploiting slack
- weighted scheduling
- staggered

Methods for selecting parameters: Many of the features described above can be refined further by selection of parameters. Also, when we combine features from different schedulers, needs for balancing the tradeoffs involved can be satisfied by creating additional parameters that can be adjusted. For example, the tradeoff between idle time and grain size, or the tradeoff between idle time and locality.

- model-driven determination
- experimental tuning
- runtime adjustment

Performance facets: Different scheduling strategies impact overall application performance in multiple ways. Although execution time is the most important metric, several intermediate metrics provide useful insights. Specific scheduling strategies may worsen one metric while improving another. Understanding these tradeoffs is critical to design combined schedulers that serve any specific purpose such as the needs of an application class of interest. We describe below the most important performance facets, i.e., the intermediate metrics.

- idle time
- synchronization
- spatial locality (in dynamic section)
- spatial locality (static section)
- temporal locality (across outer iterations)

6.2 Techniques for Composing Schedulers

To illustrate how to combine schedulers, we show a particular sequence of composition of a subset of the schedulers from previous chapters. In the process, we will generate a new scheduler, which we call *comboSched*, that combines several features from each of the baseline schedulers. The sequence of development of these schedulers is shown in Figure 6.1.

We first review the definition of the basic lightweight scheduling technique, as it is described in previous chapters. With this defined, we explain each of three schedulers, each based on a scheduler we have described in the previous chapter. In some cases, these are improved versions of the corresponding schedulers. We give a description of each scheduler, and its specific features, especially from the point of view of how to combine them with each other.

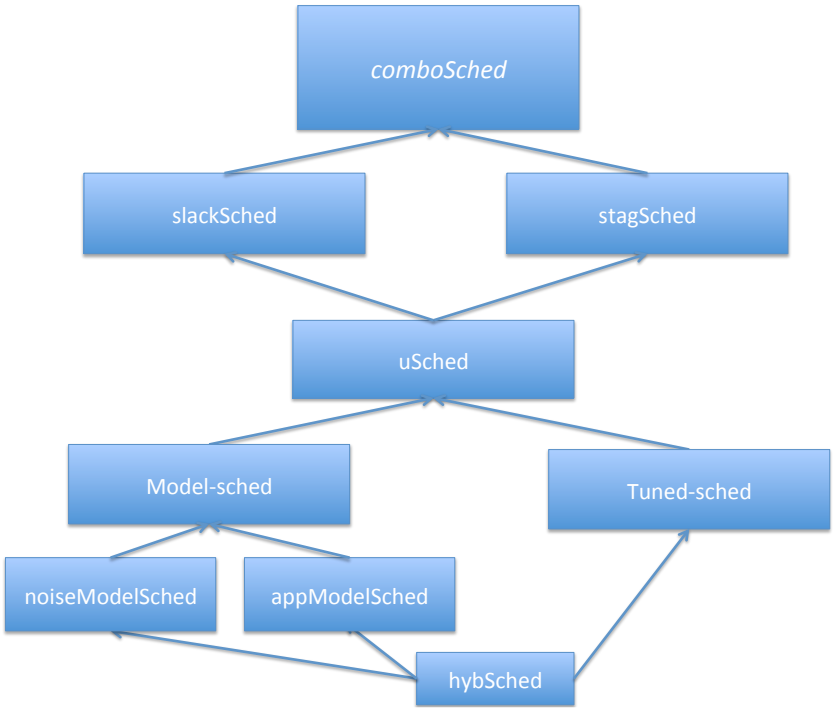

Figure 6.1: Composition of 8 schedulers that make *comboSched*.

6.2.1 hybSched

We begin with the simplest scheduler that embodies the idea of static/dynamic hybrid scheduling. As the name suggests, this scheduler itself combines features from two schedulers: OpenMP static scheduling and OpenMP dynamic scheduling. It divides the iterations in two parts, static and dynamic. It is designed to address both low-frequency noise and application imbalance. This is a loop scheduling strategy operating across threads within an MPI process, where each thread first does a pre-defined portion of the iterations in the static partition, and then dequeues iterations from the dynamic partition. The number of iterations executed statically can be adjusted per threaded computation region and per MPI process. The static fraction, denoted f_s, is the fraction of all iterations that are allocated statically. This scheduling parameter is exposed to the application programmer.

6.2.2 tunedSched

This scheduler builds upon hybSched by adding a parameter selection method of auto-tuning the static fraction. Specifically, the static fraction is determined after measuring the performance with different values of static

fractions.

6.2.3 NoiseModelSched

Builds upon the hybSched by using a model for execution time given parameters of the duration of noise δ_{noise}. See Chapter 4 for how the static fraction is calculated using this model. For each node used for the application run, we obtain the noise event length, t_{noise}, and time for dequeue operation, t_q. Note that t_q and t_{noise} is obtained before the application begins. We obtain the overhead due to noise and overhead due to dequeue operations as described in Section 5.3 of Chapter 4. In Chapter 2 and Chapter 4, we referred to the value of the noise event length as δ, but here, we will call it δ_{noise} so that we can distinguish load imbalance due to noise and load imbalance due to any other source.

6.2.4 AppModelSched

Builds upon the hybSched by developing a model for execution time in presence of application imbalance. This involves replacing the δ_{noise} by a measure of within-node application imbalance, δ_{app}.

To obtain δ_{app}, we first run 1 step of the application twice: one using static scheduling and the other using dynamic scheduling. Specifically, we run the application code with OpenMP static scheduling on process 0, and then run the application code with OpenMP dynamic scheduling on process 0. For each process, we calculate the average idle time across threads within the process from the previous application timestep. The scheduling overhead, t_{ovhd}, is computed by multiplying the iterations per thread d by the time for a dequeue operation t_q, where t_q is obtained from the measurements of dynamic scheduling as above.

Let the time for the statically scheduled run be t_{static}, the time for the dynamically scheduled run be $t_{dynamic}$, and the time for scheduler overhead be t_{ovhd}. The magnitude of the additional duration induced by load imbalance coming from the application, δ_{app}, is t_{static} - $t_{dynamic}$ - t_{ovhd} [1]. We estimate the parallel outer iteration time as T_p by running the application in a mode where only one core of each node is used, i.e., we remove the OpenMP parallelism. We obtain the execution time on node 0, as a sample, and divide it by the total number of cores used for the run. Instead of using node 0 as a sample, we could use an average across all the nodes, by doing

[1] Alternatively, δ_{app} can be calculated via the method used in Figure 1.2.

a global reduction. Now that we have all the parameters needed by the new model, we can calculate the static fraction to be used.

6.2.5 modelSched

The previous two schedulers handled two different circumstances: (a) low-frequency noise in an otherwise balanced application (noiseModelSched), (b) application imbalance on a non-noisy machine. We would like to handle circumstances where application imbalance exists on a noisy machine.

A simple way of doing this is to replace the δ in the basic model by a sum of δ_{noise} and δ_{app}. This is a conservative (or pessimistic) approach. It aims to handle the situation when noise happens on the heaviest loaded core. The least conservative (or optimistic) approach is to assume noise always happens on a core that is not the most overloaded. In that case, we can modify the model to use $\max(t_{noise}, t_{app})$ as δ.

6.2.6 uSched

This scheduler first measures the parameters, such as iteration time and noise duration. It then uses modelSched(handling both application imbalance and noise) to determine a reasonable baseline value of the static fraction f_s. After this, we compose a feature from expTunedSched: we conduct an exhaustive search in a small neighborhood around f_s. Specifically, we try different static fractions 0.05 below and 0.05 above a given static fraction, with the given static fraction being $f_{s_{tot}}$, as calculated from above. This increment can be adjusted by the application programmer and requires knowledge of iteration granularity. The resulting static fraction is $fs_{totTuned}$, which is the static fraction used for *uSched*. This is the static fraction used for all nodes.

6.2.7 slackSched

This scheduler is an optimization over *uSched*. This is a slack-conscious scheduling strategy described in Chapter 4. In particular, this is the variant that uses the call path method for predicting the slack for each collective call. Recall that MPI slack is the deadline that each process has to finish its work, before this process extends the applications critical path, thereby increasing the cost of application execution. The scheduler is put together and works as follows:

1. On each process, start with the static fraction f_s obtained in *uSched*.

(a) On each process, retrieve that process's invocation of the last MPI collective, where the invocation of the last MPI collective is retrieved through the callsite slack-prediction method (see paper for details on implementation details of slack prediction).

(b) Given the identifier of the last the MPI collective call invoked, estimate that collective call's slack value from the history of slack values stored by the slack-conscious runtime. The slack estimate is based on the slack value recorded in the previous MPI collective invocation, as is done in the cited work of Adagio.

2. On each process, adjust its dynamic fraction based on the slack value. This adjustment is done using the formula 5 in section 3 of Chapter 4 (final formula defining the slack-conscious dynamic) and implementation of section 4 of Chapter 4. The static fraction used in the loop bound is 1- f_d.

Note that the *dynamic fraction*, rather than the *static fraction* (used in Chapters 2, 3, and 5) was used in Chapter 4 to make the slack-conscious scheduling technique more intuitive. Additionally, doing the theoretical analysis in that chapter using the dynamic fraction rather than the static fraction helped more to minimize the calculations needed for slack-conscious runtime adjustment of the hybrid static/dynamic scheduling during execution of an MPI application.

6.2.8 vSched

This scheduler is based on Chapter 5. The motivation of this scheduler is to improve the spatial locality in the dynamically scheduled iterations. In uSched, the dynamically scheduled iterations are assigned to threads arbitrarily based on the order in which threads happen to request dynamic work (see Figure 5.2). The focus of this scheduler is to use different dimensions of the tradeoff between load balance and locality to improve upon basic hybrid static/dynamic scheduling.

We start with the hybrid static/dynamic scheduling strategy with the static fraction obtained from *uSched* above, and then apply the strategy of staggering of iterations to this.

6.2.9 ComboSched

The comboSched scheduling strategy is stagSched, i.e., locality-optimized scheduling, with slackSched, i.e., slack-conscious scheduling, added into it.

In other words, one optimization over uSched, slackSched, is composed with another optimization over uSched, stagSched, to form the comboSched scheduling strategy. We add further optimizations to just the dynamic scheduling section, e.g., using variable task sizes, only after the slack-conscious scheduling adjustment is done.

In summary, we described a series of schedulers. We also illustrated how new schedulers can be designed by composing features from multiple schedulers, or by extending an existing scheduler by adding new features to it. We next compare the performance of several of these schedulers.

6.2.10 Code Transformation

```
#include <omp.h>

int main(int argc, char* argv[])
{
  int timestep = 0;
  void *status;
  int numprocs;
  int rank;

  MPI_Init(&argc,&argv);
  MPI_Comm_size(MPI_COMM_WORLD,&numprocs);
  MPI_Comm_rank(MPI_COMM_WORLD,&rank);

  // ...

  while(timestep < 1000)
  {
#pragma omp parallel
    {
#pragma omp for
      for(int i = 0; i<n; i++)
  c[i] += a[i]*b[i];
    }
    MPI_Allreduce(&sum, &global_sum, 1, MPI_DOUBLE, MPI_SUM
        , MPI_COMM_WORLD);
    timestep++;
  }

  MPI_Finalize();
}
```

Figure 6.2: Original code with OpenMP loop.

Figure 6.2 shows an application program containing a basic OpenMP loop. Note that the original full application code file is shown here, rather than in the code snippet from previous chapters. We do this to show the application programmer's lines of code changed. When we put the implementation together, we get the following code shown in Figure 6.3 below.

The code shows an application program containing the OpenMP loop transformed to use our Composed Scheduler. Specifically, the code shows how to implement a composition of schedulers, using our existing scheduling techniques from previous chapters. The implementation changes needed for the composition are done within our macro-based scheduler. In the above code, the slack-conscious scheduling scheme is shown in lines 40 and 48. Considering the implementation of slack-conscious scheduling in Section 4 of Chapter 4, no changes were needed for the slack prediction runtime or source-to-source transformation for this scheduler composition.

6.3 Results

With the above composition of schedulers, the main question we ask is: does our composition of the schedulers and adjustment of the scheduler parameters help provide further performance improvement than each of the schedulers in isolation? Specifically, how close is the sum of the performance gains obtained by using the individual schedulers in the scheduler composition to the performance gain obtained by the composed schedulers?

To answer the above, we experimented with three different MPI+OpenMP application codes. The first application code is Rebound [79], an MPI+OpenMP N-body simulation that simulates bio-molecular interactions. The second application code is the CORAL SNAP code [86], a regular mesh code which has computation used in the context of heat diffusion. The third application code is the CORAL miniFE code [40], an MPI+OpenMP finite element code involving computation on an unstructured mesh used in the context of earthquake simulations. We performed the experiments on Cab, an Intel Xeon cluster with 16 cores per node, 2.66 GHz clock speed, a 32 KB L1 data cache, a 256 KB L2 cache, 24 MB shared L3 cache, the TOSS operating system, an InfiniBand interconnect with a fat-tree network topology.

Figure 6.4 shows the results for the MPI+OpenMP N-body code Rebound [79] run on Cab, with different schedulers applied to Rebound. In this code, every particle loops through its neighborhood of particles to calculate forces applied to it, identifying the position in the next application

```
#include "mpi.h"
#include <omp.h>
#include "vSched.h"
// ...

// In the below macros, strat is how we specify the library
    .
#define FORALL_BEGIN(strat, s,e, start, end, tid, numThds )
      loop_start_ ## strat (s,e ,&start, &end, tid, numThds)
    ;  do {

#define FORALL_END(strat, start, end, tid)  } while(
    loop_next_ ## strat (&start, &end, tid));

int main(int argc, char* argv[])
{
  int timestep = 0;
  int rank, numprocs;
  int numThrds;
  int start, end = 0;
  double fd, fs;
  static LoopTimeRecord *record = NULL;
  MPI_Init(&argc,&argv);
  MPI_Comm_size(MPI_COMM_WORLD,&numprocs);
  MPI_Comm_rank(MPI_COMM_WORLD,&rank);
  vSched_init(numThrds);
  // ...

  while(timestep < 1000)
  {
    fd = predict_dynamic_fraction(&record); fs = 1.0 - fd;
#pragma omp parallel
    {
  int tid = omp_get_thread_num();
  int numThrds = omp_get_num_threads();
  FORALL_BEGIN(sds,tid,numThrds, 0, n, start, end, fs)
    for(int i=start;i<end;i++)
      c[i] += a[i]*b[i];
  FORALL_END(sds,tid,start,end)
    }
      end_timing(&record, n);
      MPI_Allreduce(&sum, &global_sum, 1, MPI_DOUBLE,
          MPI_SUM, MPI_COMM_WORLD);
      timestep++;
  }
 endLoop(&lr, (int) (n*fd));
 vSched_finalize(numThrds);
 MPI_Finalize();
}
```

Figure 6.3: Code transformed to use composed scheduler.

timestep; there is geometric locality in this application. This geometric locality is reflected by the order in which the particles are organized in the tree. For example, nearby particles tend to interact with the same sets of particles with a few exceptions. Therefore, the *vSched* strategy of keeping nearby iterations on the same thread in the dynamic section provides performance benefits. The *slackSched* benefits are the generic benefits of reducing the dynamic fraction and its associated overheads. The benefits are not as large for other applications because of its relatively large grain-size of each iteration. For Rebound at 1024 nodes, the *comboSched* improves 45% over OpenMP static scheduling. The percent gains of each of the scheduling strategies are significant even at low node counts. Specifically, at 2 nodes, performance improves 35% over OpenMP static scheduling when we apply only *uSched* to the Rebound code. Using *slackSched* on Rebound gets limited gains of 5.6% over the *uSched* scheduling strategy. Using *vSched*, performance improves 8.5% over *uSched*. This is likely because *vSched* can take advantage of the geometric locality in this application. Using the *comboSched* strategy, which combines *slackSched* and *vSched*, the Rebound code gets an overall 44% over the OpenMP static scheduled version of Rebound.

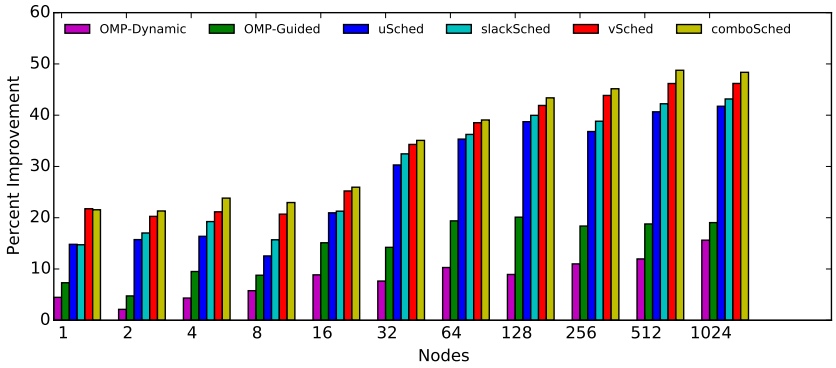

Figure 6.4: Rebound(N-body): Performance improvement obtained over OpenMP static scheduling.

Figure 6.5 shows the results for miniFE [40] run on Cab, with different schedulers applied to miniFE. Here, iteration to iteration spatial locality is relatively low because of indirect access caused by the unstructured mesh; for unstructured meshes, the spatial locality across iterations is not as strong as looping over a 1-D array. However, with reasonable variable ordering of mesh elements, there is still a significant amount of spatial locality that *vSched* exploits. Because of imperfect data partitioning of the problem across nodes, moderate load imbalances across nodes exist. Due to law of

large numbers, the imbalances across cores are larger at larger number of nodes. Thus, dynamic and guided scheduling by itself should be able to provide significant performance gains. Consider the results for miniFE running at 1024 nodes of Cab. The *vSched* scheduling strategy gets 15% performance improvement over OpenMP static scheduling, while the *slackSched* gets 19% performance gain over OpenMP static scheduling. The *comboStrat* gets 23% performance improvement over OpenMP static scheduling, and also gets 9.0% performance improvement over OpenMP guided scheduling. By putting together *vSched* and *slackSched*, we are able to improve performance further, to make our scheduling methodology perform better than *guided*. The benefits of *vSched* and *slackSched* are not completely additive. Composing the scheduling strategies along with tuning of parameters could increase performance benefits, and could yield better performance for the *comboSched*.

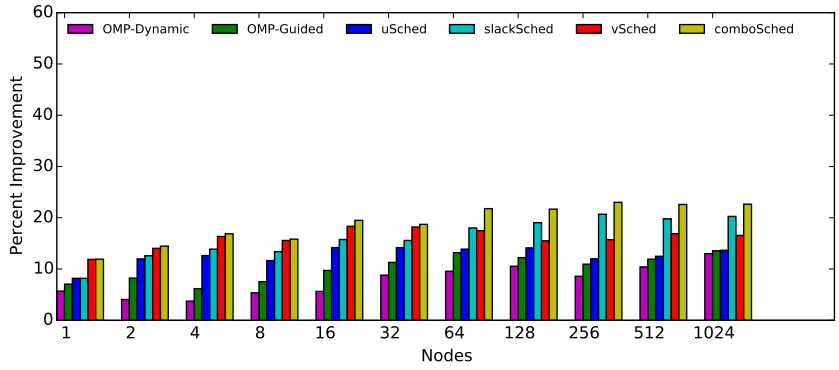

Figure 6.5: miniFE (finite element): Performance improvement obtained over OpenMP static scheduling.

Figure 6.6 shows the results for the regular mesh code SNAP [86] run on Cab, with different schedulers applied to the SNAP code. The regular mesh computation has no application load imbalance; the only load imbalance during application execution is that due to noise. Note that the regular mesh computation has inherent spatial locality (because the computation's sweep operation works on contiguous array elements). At 1024 nodes of Cab, performance improves 10% over OpenMP static with *slackSched*, and we get a reasonable performance gain of 16% over static scheduling with *vSched*. The *comboSched* scheduler gets 19% performance improvement over OpenMP static scheduling. This result of *comboSched* specifically helps to show that the optimizations of *vSched* and *slackSched* composed in *comboSched* do not cancel out each other's performance benefits, and that the

performance are additive. (Recall that this is because each optimization is aimed at solving complementary problems, as discussed in Section 2 of this chapter.)

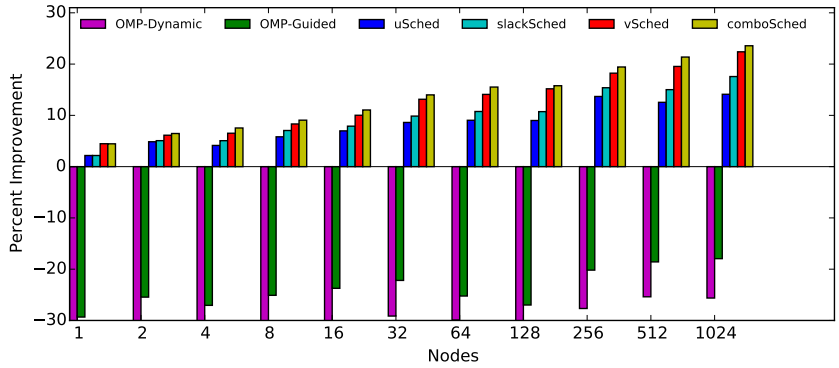

Figure 6.6: SNAP (regular mesh): Performance improvement obtained over OpenMP static scheduling.

6.3.1 Application Programmer Effort

We assess how easy it is to use our methodology for the application programmer. Figure 6.7 shows the lines of code changed for each of the different applications. We specifically show the lines of code changed per OpenMP region, and the total lines of code changed for the application. As seen in

Application	Rebound	SNAP	FE
ΔLOC per region	+10	+7	+12
Pct. LOC changed	12.31%	6.3%	14.22%

Figure 6.7: Total lines of code changed and average lines of code changed per threaded computation region for the Rebound N-body, CORAL SNAP and CORAL miniFE.

Figure 6.7, the application programmer effort is minimal for all three codes. Additionally, source-to-source transformation support from software such as ROSE [77] can reduce or eliminate application programmer effort needed to use our technique.

6.4 Relevance to Future Architectures

Now that we have examined how various circumstances motivate specific scheduling techniques and how different techniques impact specific perfor-

mance metrics, we examine the relevance of this work in the context of future exascale machines.

As we go to exascale, the number of nodes in a parallel machine will increase. This increases the likelihood of amplification. More importantly, static and dynamic variability of future processor chips is likely to be much higher. To complicate matters further, applications at exascale are likely to be strong scaled [9]. Because of memory costs, the total amount of memory will not increase as much as the number of FLOP/s. For example, the 10 petaflop MIRA, has about 0.8 petabytes of memory [88]. Summit, which will be operational in 2017-2018, will have 15 times more floating-point performance (150 PF), but only about 2.5 times more memory (2 PetaBytes). This means the size of the problem in terms of memory will not increase significantly, but it will have to be solved much faster to utilize this floating-point capacity available. This is strong scaling. Separately, application scientists are also increasingly seeking strong scaling. For many application domains, scientists would want to solve the same problem faster rather than a larger problem at the same speed.

Strong scaling implies that outer iteration durations for most applications will get smaller, e.g., of the order of a few milliseconds. We know that for longer outer iterations, the impact of irregularities and noise-like events can be absorbed without significant impact, but for shorter iterations, the impact will be more significant. This raises the importance of dynamic scheduling further. The locality cost differentials will also be higher in future because of the large number of cores in a node, and necessarily deeper memory hierarchy. Therefore, dynamic scheduling must be balanced carefully with locality considerations. Our scheduling strategies are designed to handle exactly this balance.

Future machines will also have a large number of cores per node. These may include heavier Xeon-like cores, or NVIDIA accelerator-like cores. Our scheduling strategies are designed to utilize the abundance of cores to mitigate the scaling bottlenecks arising from variability, load imbalances, or noise. So, our scheduling strategies distribute excess work on any core to other cores, without significantly affecting locality.

Of course, exascale is still many years away. There will be many unknown circumstances, in the combination of applications and architectures. Yet, we have identified a large number of scheduling features in this work. We expect many of the features to be relevant at exascale. Further, we have demonstrated an extensible software infrastructure. We can combine the features in different ways, as illustrated in this chapter. This extensibility,

combined with invention of new scheduling features inspired by specific exascale circumstances, will ensure that our approach will remain viable for exascale.

Chapter 7

Related Work

The topics related to this dissertation research have received significant attention by researchers in recent years. Some of the categories we discuss in this chapter include noise and its amplification, MPI+X hybrid programming, loop scheduling strategies, task scheduling strategies, dependent tasks, cache-obliviousness, etc.

Several studies provide an in-depth analysis of noise and its impact on large-scale systems [45, 68, 72, 82, 90]. Beckman *et al.* [8] discuss a benchmark for quantification of noise referred to as the selfish benchmark. This benchmark has enabled a more accurate and proper study of noise in several follow-up studies, and has allowed one to quantify noise on a system in a standardized fashion.

The study by Petrini *et al.* of OS system services on ASCI Q investigates how to mitigate noise [72]. Noise mitigation is achieved through system service suppression, i.e., the sources of system noise (in the form of OS daemons) are identified, and then each non-critical service is stripped away from the machine. Stripping away OS services was key to enabling better performance of ASCI Q. They also suggest using co-scheduling to make existing noise more coordinated. Furthermore, the study discusses several lessons learned from their studies, particularly the impact that noise mitigation solutions have on different classes of applications. The solutions discussed in Petrini *et al.* are lower-level and specific to the platform used to run the application. They are not portable to enable applicability to a larger class of machines and a larger set of applications. As discussed in [54], a higher-level solution is necessary to take advantage of the compute power of emerging clusters of multi-cores. In particular, the application programmer should have control over how the application should be implemented and tuned, ensuring that characteristic noise has minimal impact on a particular problem. A paper discussing experimentation of a molecular dynamics simulation code NAMD on a noisy system argues that effects of noise in the communication sub-system can be mitigated by data-driven execution [73].

However, not all applications can use this technique. For some applications, overlap of communication and computation is not possible due to inherent strict dependencies across application time steps.

A study of the impact of noise for MPI applications was done by Hoefler *et al.* [46]. This showed how noise can have a large impact for a particularly large number of MPI processes. This assessment of performance loss is done for several key scientific applications, and many different experiments are carried out to understand changes in performance as the amount of system noise is increased. Such studies have provided insight on how to mitigate noise, and several studies show its usage.

An early study by Lusk with MPI+OpenMP focuses on the comparison between MPI-everywhere and MPI+OpenMP codes [63]. Cappello et al [19] show how MPI-everywhere performs better than MPI+OpenMP codes. OpenMP has improved significantly since then, but some of the issues still remain valid. The lack of locality-awareness in OpenMP programming is the main reason for the performance problems. Rabenseifner et al [78] provides an important introduction to the issues involved in hybrid programming. They note that dynamic or guided loop scheduling is suboptimal because of its memory access performance, especially in a NUMA context. We believe that the work in this thesis has addressed the challenge referenced by this paper.

Application load balancing has been studied in [20, 47, 51]; these strategies take advantage of the principle of persistence in load imbalance in many applications. The problem with a system using measurement-based load balancing on multi-core systems with transient load imbalance induced by system noise is that it is difficult to predict the load imbalance in each timestep. Thus, it is important to use a dynamic scheduling scheme which reacts to changes in load during the application timestep, rather than proactively assigning work to threads based on patterns in past application timesteps. Load imbalances aren't persistent across cores. The same goes for Charm++ [51, 57] persistence across nodes, as these are uncoordinated load imbalances.

Dynamic scheduling has been supported in OpenMP since the early days of OpenMP [69]. Guided self-scheduling can reduce scheduler overhead compared with it, while trying to maintain good load balance through exponentially decreasing the chunk sizes [62, 75] as threads execute chunks of work. However, guided scheduling (along with other work-stealing schemes) may not necessarily take into account outer iteration locality, or the temporal locality of data across application timesteps. This means that in one timestep,

the i^{th} iteration is assigned to thread k, while in a subsequent timestep, the i^{th} iteration may be assigned to some other thread k'. Such patterns are prevalent in a large number of HPC codes. In this work, the idea of the tasklet aims to handle this outer iteration locality by storing within the tasklet data structure a field denoting the last thread that the tasklet executed on.

The work in Olivier et al. [71] discusses incorporation of affinity in OpenMP scheduling for load imbalanced codes. This work considers optimizations specific to the OpenMP runtime. A key distinction between our scheduling strategies and this work is that our method tunes the balance between locality and load imbalance for each application and architecture rather than having a general runtime solution for handling locality for scheduling. The importance of tuning the scheduler, given a particular application and architecture, with the guidance of a simple model to validate results, was shown in [27].

Chapman *e*t al. [69] provide a system for OpenMP affinity-based locality parameters for each architecture, and finding the right placement of data. This is done through detection of architecture parameters provided in hardware. The system does not however tune to find the balancing of scheduler overhead and load imbalance in an application, and also doesn't consider slack. Each combination of application and architecture can make this tradeoff different, and tuning the application/architecture pairs provides a solution that can handle the different tradeoffs.

Zhang *et al.* [47] describe an adaptive OpenMP loop scheduler that addresses synchronization and load imbalance issues that arise out of hyper-threading (symmetric multi-threading), and it uses a NUMA-aware hierarchical scheduling strategy.

Loop iterations are a form of independent tasks. Several programming models support creation of independent tasks directly. One of the key shortcomings of work-stealing [13,14,35] is that work-stealing incurs an overhead due to the cost of a lock and the cost of coherence cache misses, both of which depend on the number of cores and the shared memory interconnect of the node architecture [18, 85]. Scalable work-stealing [25] is beneficial in a distributed memory context, but it mainly focuses on steals across a large number of nodes. We try to avoid the cost of overhead by doing only within-node scheduling. Further work might include scheduling across neighboring nodes. UPC scheduler [49] load imbalances across nodes are not large enough to justify across node data movement.

SLAW (2010) [59] is a locality-aware scheduling scheme for Cilk. Its main

contribution is orthogonal to locality, a synthesis of work-first and help-first scheduling. It addresses locality in a hierarchical sense, by dividing cores into groups and prioritizing within-group steals first.

Threaded Building Blocks [80] use templates for common parallel iteration patterns, written in terms of tasks, and supports dynamic load balancing.

Recently, many systems have started supporting creation of tasks that depend on remote data as well as completion of other tasks. Examples of such systems include DaGue and DPLASMA [15]. Galois for irregular parallelism also represents a similar task creation mechanism [58]. These scheduling strategies provide dynamic load balancing, but it is unclear if they can address locality affectively. Concurrent Collections is another task scheduling language that supports data-dependent and control-dependent tasks [22] via graphs.

Much work has been done to improve scalability of bulk-synchronous MPI applications on large-scale clusters of SMPs in the presence of the changes in architectures and interconnect topologies [4, 87]. In the general context of performance tuning of applications on multicore architectures, several application papers investigate performance tuning of the application timesteps for maximum efficiency in the compute phase of the bulk-synchronous application. Some studies have aimed to find the best code that maps to an architecture by enumerating the search space of all codes, and then use machine learning to find the optimal code within the search space [4, 55, 93]. Other application studies [19, 63, 78] on Hybrid Parallel Programming have tried to document the techniques that programmers can use to to harness the power of large-scale clusters through using a mixture of different programming libraries. There are two main differences between the approaches taken in the above work and the approach taken in this work. First, each of these studies take a static approach and improve performance locally within a node. In this work, we consider transient variations within an SMP node, and maintain resiliency to unexpected noise on a core of a node throughout the execution of the application. Second, these studies focus on the compute phase within one particular node, without consciousness of MPI collective communication across nodes. In this work, we do consider the collective communication for tuning the computation within each node.

The importance of spatial locality, specifically for static schedules, is discussed in [34, 44], and also discussed in work demonstrating the importance of block-cyclic data distributions [7, 76] in the context of static scheduling. This work is complementary but orthogonal to our work, and we note that

it does not handle rearrangement or staggering of static and dynamic iterations. In this work, we optimize for spatial locality through data placement in the context of hybrid static/dynamic scheduling, as illustrated through the use of a staggered approach.

Chapter 8

Conclusions

The broad problem that this thesis is concerned with is how to assign work to compute elements in a synchronous data parallel program. Such a program contains outer iterations, such as timesteps, and inner loop iterations, typically over the data elements of the program. Application imbalances arise when the time for different loop iterations are different. These imbalances may be persistent or irregular. The machine imbalance could be caused by noise, i.e., transient irregularities on specific cores, or it could be persistent when some cores are slower than the others. Imbalances affect performance of such programs significantly because all the processors wait for the most loaded processor in every outer iteration.

One approach to solving this problem is to move data and work across nodes. Typical MPI applications require an invasive reprogramming to do this. This work focused on within-node load balancing. As we showed in Chapter 1, given the large number of cores on each node, within-node load balancing has a significant impact on global load imbalance, i.e., if you can perfectly balance work within each node, much of the global imbalance will be taken care of.

Although this seems like a straightforward solution, we demonstrated that we are faced with three major challenges. While idle time can be significantly reduced using OpenMP dynamic or guided scheduling, the synchronization overhead, and data movement costs stop us from realizing the full potential of this idea This work was aimed at developing scheduling strategies the three challenges simultaneously, and demonstrates scalability of applications to a large number of nodes.

Our basic approach is to fix a percentage of iterations that are executed statically, and the remainder dynamically. The presence of a statically scheduled iterations helped to restore locality and reduce the above synchronization and data movement costs to a much smaller level, while the dynamically scheduled iteration allowed mitigation of load imbalance. This design principle is carried out throughout this thesis.

Dynamically scheduled iterations add synchronization costs due to coordination among thread to allocate iterations. More importantly, it disturbs the locality in two different ways: (a) outer iteration locality: whether an inner iteration continues to be scheduled on the same thread across outer iterations, and (b) spatial locality within data parallel loops: whether consecutive inner iterations are executed consecutively on the same thread. Both of these metrics are close to perfect with static scheduling, except that it suffers from load imbalances. The series of strategies in the chapters can be seen as increasingly sophisticated methods for improving both of these locality factors.

In Chapter 2, we show how a careful selection of dynamic fraction, i.e., the percentage of iterations allocated dynamically improves performance significantly. This was done in the context of both load imbalanced and load balanced codes. This selection helps us balance the costs of idle time due to imbalances and data movement overhead due to dynamic load balancing. We showed the amplification problem arising from OS noise in the context of a 3D regular mesh computation, analyzing it through histogramming of outer iteration times, and how our strategy mitigates it. We also showed how the scheduling of work benefits core computations in numerical linear algebra, particularly dense matrix factorizations.

Chapter 3 showed how to schedule work given the persistent imbalance observed among cores, typically because of high-frequency low-amplitude noise events. This is done by changing the number of statically allocated iterations to each thread, based on the recent history of outer iterations. We also showed how to combine this *weighted* scheduling strategy with the hybrid scheduling strategy of Chapter 2.

In Chapter 4, we showed how to reduce the search space for the dynamic fraction through theoretical analysis coupled with a small runtime adjustment. Further, by allowing the dynamic fraction to be different on different MPI processes, we were able to take advantage of slack in MPI collective operations, thus reducing the dynamic fraction further. This reduces the dynamic scheduling overhead further, as demonstrated on multiple benchmarks and application codes.

Although the previous techniques improve spatial locality and outer iteration locality in the static section, the dynamically scheduled iterations lose the benefits of locality. By staggering the allocations of iteration space, i.e., into alternate bands of statically and dynamically allocated iterations, the dynamically scheduled iterations executed by a thread are made likely to be contiguous to its statically scheduled iterations. This strategy was

described and demonstrated In Chapter 5.

Chapter 6 identified the problem that each of the performance issues addressed individually in previous chapters may exist together when running applications on a cluster SMPs, notably for next-generation (most imminently exascale) supercomputers. Given this, we showed an example compositions of our schedulers (developed in prior chapters), and showed, for three representative MPI+OpenMP application codes, how this synthesis of scheduling techniques can provide more performance benefits than that of each of the individual schedulers that it was composed of.

Our runtime does not introduce significant overheads. Thus, even if runtime slowdowns due to performance irregularity are negligible, it can still be used, i.e., even when the user is unsure whether noise or imbalances affect the application, they may use our scheduler without any concerns of adding overhead.

Some specific ideas that immediately follow from this dissertation include the following: (a) the usage of our technique in MPI+X applications(including applications written with MPI-3 shared memory extensions), as opposed to only MPI+OpenMP applications, and (b) developing additional examples of composite strategies and describing the circumstances under which such strategies can be useful.

We showed how scheduling strategies within a node will be important in the coming years as we get increasingly larger and more complex nodes. We believe that our scheduling strategies, along with their potential for extension and composition, will contribute significantly to efficient utilization of large-scale machines consisting of such nodes.

References

[1] Specifications of the MIRA Supercomputer. `http://www.alcf.anl.gov/user-guides/mira-cetus-vesta`, Jun 2011.

[2] Specifications of the Titan Supercomputer. `https://www.olcf.ornl.gov/titan/`, Oct 2012.

[3] L. Adhianto, S. Banerjee, M. Fagan, M. Krentel, G. Marin, J. Mellor-Crummey, and N. R. Tallent. HPCToolkit: Tools for Performance Analysis of Optimized Parallel Programs. *Concurrency and Computation: Practice and Experience*, 22(6):685–701, 2010.

[4] D. H. Bailey, J. Chame, C. Chen, J. Dongarra, M. Hall, J. K. Hollingsworth, P. Hovland, S. Moore, K. Seymour, J. Shin, A. Tiwari, S. Williams, and H. You. PERI Auto-tuning. *Journal of Physics: Conference Series*, 125(1):012089, 2008.

[5] A. H. Baker, T. Gamblin, M. Schulz, and U. M. Yang. Challenges of Scaling Algebraic Multigrid Across Modern Multicore Architectures. *IEEE International Parallel and Distributed Processing Symposium*, pages 275–286, 2011.

[6] M. Bauer, S. Treichler, E. Slaughter, and A. Aiken. Legion: Expressing Locality and Independence with Logical Regions. In *Proceedings of the International Conference on High Performance Computing, Networking, Storage and Analysis*, SC '12, pages 66:1–66:11, Salt Lake City, UT, USA, 2012. IEEE Computer Society Press.

[7] D. Becker, M. Faverge, and J. Dongarra. Towards a Parallel Tile LDL Factorization for Multicore Architectures. Technical report, University of Tennessee at Knoxville, April 2011. ICL-UT-11-03.

[8] P. Beckman, K. Iskra, K. Yoshii, S. Coghlan, and A. Nataraj. Benchmarking the Effects of Operating System Interference on Extreme-scale Parallel Machines. *Cluster Computing*, 11:3–16, March 2008.

[9] K. Bergman, S. Borkar, D. Campbell, W. Carlson, W. Dally, M. Denneau, P. Franzon, W. Harrod, J. Hiller, S. Karp, S. Keckler, D. Klein, R. Lucas, M. Richards, A. Scarpelli, S. Scott, A. Snavely, T. Sterling, R. S. Williams, K. Yelick, K. Bergman, S. Borkar, D. Campbell, W. Carlson, W. Dally, M. Denneau, P. Franzon, W. Harrod, J. Hiller, S. Keckler, D. Klein, P. Kogge, R. S. Williams, and K. Yelick. ExaScale Computing Study: Technology Challenges in Achieving Exascale Systems. Technical Report 0, University of Notre Dame, Computational Science and Engineering Department, September 2008.

[10] A. Bhatelé, L. V. Kalé, and S. Kumar. Dynamic Topology-Aware Load Balancing Algorithms for Molecular Dynamics Applications. In *23rd ACM International Conference on Supercomputing*, ICS '09, Yorktown Heights, NY, USA, 2009. ACM.

[11] A. Bhatele, L. Wesolowski, E. Bohm, E. Solomonik, and L. V. Kale. Understanding Application Performance via Micro-benchmarks on Three Large Supercomputers: Intrepid, Ranger and Jaguar. *International Journal of High Performance Computing Applications (IJHPCA)*, 2010. http://hpc.sagepub.com/cgi/content/abstract/1094342010370603v1.

[12] A. Blanchard. Practical Experiences with OS Jitter. `http://www.ibm.com/developerworks/wikis/display/LinuxP/OS+Jitter+Mitigation+Techniques`, 2010.

[13] R. D. Blumofe, C. F. Joerg, B. C. Kuszmaul, C. E. Leiserson, K. H. Randall, and Y. Zhou. Cilk: An Efficient Multithreaded Runtime System. In *Journal of Parallel and Distributed Computing*, 1995.

[14] R. D. Blumofe and C. E. Leiserson. Scheduling Multithreaded Computations by Work Stealing. In *In Proceedings of the 35th Annual Symposium on Foundations of Computer Science (FOCS)*, pages 356–368, Santa Fe, NM, USA, 1994.

[15] G. Bosilca, A. Bouteiller, A. Danalis, M. Faverge, A. Haidar, T. Hérault, J. Kurzak, J. Langou, P. Lemarinier, H. Ltaief, P. Luszczek, A. Yarkhan, and J. J. Dongarra. Distibuted Dense Numerical Linear Algebra Algorithms on Massively Parallel Architectures: DPLASMA. In *Proceedings of the 25th IEEE International Symposium on Parallel and Distributed Processing Workshops and PhD Forum (IPDPSW'11), PDSEC 2011*, pages 1432–1441, Anchorage, Alaska, USA, May 2011.

[16] F. Broquedis, J. Clet Ortega, S. Moreaud, N. Furmento, B. Goglin, G. Mercier, S. Thibault, and R. Namyst. hwloc: a Generic Framework for Managing Hardware Affinities in HPC Applications. In *PDP 2010 - The 18th Euromicro International Conference on Parallel, Distributed and Network-Based Computing*, Pisa, Italy, 02 2010.

[17] S. Browne, J. Dongarra, N. Garner, G. Ho, and P. Mucci. A Portable Programming Interface for Performance Evaluation on Modern Processors. *International Journal of High Performance Computing Applications*, 14(3):189–204, Aug. 2000.

[18] J. M. Bull. Measuring Synchronisation and Scheduling Overheads in OpenMP. In *In Proceedings of First European Workshop on OpenMP*, pages 99–105, Lund, Sweden, 1999.

[19] F. Cappello and D. Etiemble. MPI versus MPI+OpenMP on IBM SP for the NAS Benchmarks. In *Proceedings of the 2000 ACM/IEEE conference on Supercomputing (CDROM)*, Supercomputing '00, Dallas, TX, USA, 2000. IEEE Computer Society.

[20] U. Catalyurek, E. Boman, K. Devine, D. Bozdag, R. Heaphy, and L. Riesen. Hypergraph-based Dynamic Load Balancing for Adaptive Scientific Computations. In *IEEE International Parallel and Distributed Processing Symposium*, Long Beach, CA, USA, 2007. IEEE.

[21] E. Chan. Runtime Data Flow Scheduling of Matrix Computations. Technical Report FLAME Working Note 39, University of Texas at Austin, 2009.

[22] A. Chandramowlishwaran, K. Knobe, and R. Vuduc. Performance Evaluation of Concurrent Collections on High-performance Multicore Computing Systems. In *2010 IEEE International Symposium on Parallel and Distributed Processing*, pages 1–12, Atlanta, GA, USA, April 2010.

[23] L. Dagum and R. Menon. OpenMP: An Industry-Standard API for Shared-Memory Programming. *IEEE Computational Science & Engineering*, 5(1), January-March 1998.

[24] J. Dempsey. i7-980x Details on Latencies of Caches and TLB and Buffers. `https://software.intel.com/en-us/forums/topic/287236`, June 2013.

[25] J. Dinan, D. B. Larkins, P. Sadayappan, S. Krishnamoorthy, and J. Nieplocha. Scalable Work Stealing. In *Proceedings of the Conference on High Performance Computing Networking, Storage and Analysis*, SC '09, pages 53:1–53:11, Portland, OR, USA, 2009. ACM.

[26] S. Donfack, J. Dongarra, M. Faverge, M. Gates, and J. Kurzak. On Algorithmic Variants of Parallel Gaussian Elimination: Comparison of Implementations in Terms of Performance and Numerical Properties, 2013.

[27] S. Donfack, L. Grigori, W. D. Gropp, and V. Kale. Hybrid Static/Dynamic Scheduling for Already Optimized Dense Matrix Factorizations. In *IEEE International Parallel and Distributed Processing Symposium*, IPDPS 2012, Shanghai, China, 2012.

[28] S. Donfack, L. Grigori, and A. Gupta. Adapting Communication-Avoiding LU and QR Factorizations to Multicore Architectures. In *2010 IEEE International Parallel and Distributed Processing Symposium*, pages 1–10, Atlanta, GA, USA, April 2010.

[29] J. Dongarra, P. Beckman, T. Moore, P. Aerts, G. Aloisio, J.-C. Andre, D. Barkai, J.-Y. Berthou, T. Boku, B. Braunschweig, F. Cappello, B. Chapman, X. Chi, A. Choudhary, S. Dosanjh, T. Dunning, S. Fiore, A. Geist, B. Gropp, R. Harrison, M. Hereld, M. Heroux, A. Hoisie, K. Hotta, Z. Jin, Y. Ishikawa, F. Johnson, S. Kale, R. Kenway, D. Keyes, B. Kramer, J. Labarta, A. Lichnewsky, T. Lippert, B. Lucas, B. Maccabe, S. Matsuoka, P. Messina, P. Michielse, B. Mohr, M. S. Mueller, W. E. Nagel, H. Nakashima, M. E. Papka, D. Reed, M. Sato, E. Seidel, J. Shalf, D. Skinner, M. Snir, T. Sterling, R. Stevens, F. Streitz, B. Sugar, S. Sumimoto, W. Tang, J. Taylor, R. Thakur, A. Trefethen, M. Valero, A. Van Der Steen, J. Vetter, P. Williams, R. Wisniewski, and K. Yelick. The International Exascale Software Project Roadmap. *International Journal of High Performance Computing Applications*, 25(1):3–60, Feb. 2011.

[30] P. Du, A. Bouteiller, G. Bosilca, T. Herault, and J. Dongarra. Algorithm-based Fault Tolerance for Dense Matrix Factorizations. *SIGPLAN Not.*, 47(8):225–234, Feb. 2012.

[31] A. E. Eichenberger, C. Terboven, M. Wong, and D. an Mey. The Design of OpenMP Thread Affinity. In *International Workshop on OpenMP*, pages 15–28, Rome, Italy, Jun 2012.

[32] A. Faraj, P. Patarasuk, and X. Yuan. A Study of Process Arrival Patterns for MPI Collective Operations. In *Proceedings of the 2006 ACM/IEEE Conference on Supercomputing*, SC '06, Tampa, FL, USA, 2006. ACM.

[33] E. Frachtenberg, D. G. Feitelson, F. Petrini, and J. Fernandez. Adaptive Parallel Job Scheduling with Flexible Coscheduling. *IEEE Transactions of Parallel and Distributed Systems*, 16(11):1066–1077, Nov. 2005.

[34] M. Frigo, C. E. Leiserson, H. Prokop, and S. Ramachandran. Cache-Oblivious Algorithms. In *Proceedings of the 40th Annual Symposium on Foundations of Computer Science*, FOCS '99, pages 285–, New York, NY, USA, 1999. IEEE Computer Society.

[35] M. Frigo, C. E. Leiserson, and K. H. Randall. The Implementation of the Cilk-5 Multithreaded Language. *SIGPLAN Not.*, 33(5):212–223, May 1998.

[36] L. Grigori, J. Demmel, and H. Xiang. Communication-Avoiding Gaussian Elimination. In *International Conference on High Performance Computing, Networking, Storage and Analysis, 2008. (SC 2008)*, pages 1–12, Atlanta, GA, USA, Nov 2008.

[37] B. T. Gunney, A. M. Wissink, and D. A. Hysom. Parallel Clustering Algorithms for Structured AMR. *Journal of Parallel and Distributed Computing*, 66(11):1419 – 1430, 2006.

[38] J. Habich, C. Feichtinger, H. Köstler, G. Hager, and G. Wellein. Performance Engineering for the Lattice Boltzmann Method on GPGPUs: Architectural Requirements and Performance Results. *Computers and Fluids*, abs/1112.0850, 2011.

[39] B. Hadri, H. Ltaief, E. Agullo, and J. Dongarra. Tall and Skinny QR Matrix Factorization Using Tile Algorithms on Multicore Architectures. Technical report, University of Tennessee at Knoxville, September 2009. ICL-UT-09-03.

[40] M. Heroux. MiniFE Documentation. `http://www.nersc.gov/users/computational-systems/cori/nersc-8-procurement/trinity-nersc-8-rfp/nersc-8-trinity-benchmarks/minife/`.

[41] J. Hess and A. Smith. Calculation of Potential Flow About Arbitrary Bodies. *Progress in Aerospace Sciences*, 8(0):1 – 138, 1967.

[42] J. L. Hess. Panel Methods in Computational Fluid Dynamics. *Annual Review of Fluid Mechanics*, 22:255–274, 1990.

[43] D. Hinkel, D. Callahan, N. Meezan, L. Suter, C. Still, D. Strozzi, E. Williams, and A. Langdon. Analyses of Laser-plasma Interactions in NIF Ignition Emulator Designs. In *Journal of Physics: Conference Series*, volume 244, page 022019. IOP Publishing, 2010.

[44] T. Hoefler, J. Dinan, D. Buntinas, P. Balaji, B. Barrett, R. Brightwell, W. Gropp, V. Kale, and R. Thakur. MPI + MPI: A New Hybrid Approach to Parallel Programming with MPI plus Shared Memory. *Computing*, 95(12):1121–1136, 2013.

[45] T. Hoefler, T. Schneider, and A. Lumsdaine. The Impact of Network Noise at Large-Scale Communication Performance. In *Proceedings of the 23rd IEEE International Parallel & Distributed Processing Symposium, LSPP'09 Workshop*, Rome, Italy, May 2009.

[46] T. Hoefler, T. Schneider, and A. Lumsdaine. Characterizing the Influence of System Noise on Large-Scale Applications by Simulation. In *International Conference for High Performance Computing, Networking, Storage and Analysis (SC'10)*, New Orleans, LA, USA, Nov 2010.

[47] S. F. Hummel, J. Schmidt, R. N. Uma, and J. Wein. Load-sharing in Heterogeneous Systems via Weighted Factoring. In *Proceedings of the Eighth Annual ACM symposium on Parallel Algorithms and Architectures*, SPAA '96, pages 318–328, Padua, Italy, 1996. ACM.

[48] Intel. Intel Math Kernel Library. `https://software.intel.com/en-us/intel-mkl/`, 2011.

[49] S. jai Min, C. Iancu, and K. Yelick. Hierarchical Work Stealing on Manycore Clusters. In *In Fifth Conference on Partitioned Global Address Space Programming Models*, New York, NY, USA, 2010.

[50] H. Jin and R. F. Van der Wijngaart. Performance Characteristics of the Multi-zone NAS Parallel Benchmarks. *Journal of Parallel and Distributed Computing*, 66(5):674–685, May 2006.

[51] L. Kalé and S. Krishnan. CHARM++: A Portable Concurrent Object Oriented System Based on C++. In A. Paepcke, editor, *Proceedings of OOPSLA'93*, pages 91–108. ACM Press, September 1993.

[52] V. Kale, A. Bhatele, and W. D. Gropp. Weighted Locality-Sensitive Scheduling for Mitigating Noise on Multicore Clusters. In *18th Annual IEEE International Conference on High Performance Computing (HiPC 2011)*, Bangalore, India, December 2011.

[53] V. Kale, S. Donfack, L. Grigori, and W. D. Gropp. Lightweight Scheduling for Balancing the Tradeoff Between Load Balance and Locality. 2014.

[54] V. Kale and W. Gropp. Load Balancing for Regular Meshes on SMPs with MPI. In *Proceedings of the 17th European MPI Users' Group Meeting Conference on Recent Advances in the Message Passing Interface*, EuroMPI '10, pages 229–238, Stuttgart, Germany, 2010. Springer-Verlag.

[55] S. Kamil, C. Chan, S. Williams, L. Oliker, J. Shalf, M. Howison, and E. W. Bethel. A Generalized Framework for Auto-tuning Stencil Computations. In *In Proceedings of the Cray User Group Conference*, 2009.

[56] T. Klug, M. Ott, J. Weidendorfer, C. Trinitis, and T. U. Mnchen. autopin, Automated Optimization of Thread-to-Core Pinning on Multicore Systems, 2008.

[57] S. Krishnan and L. V. Kale. Automating Runtime Optimizations for Load Balancing in Irregular Problems. In *Proc. Conf. on Parallel and Distributed Processing Technology and Applications*, San Jose, CA, USA, August 1996.

[58] M. V. Kulkarni. *The Galois System: Optimistic Parallelization of Irregular Programs*. PhD thesis, Cornell University, 2008.

[59] V. Kumar, Y. Zheng, V. Cave, Z. Budimlic, and V. Sarkar. HabaneroUPC: a Compiler-free PGAS Library, 2014.

[60] D. Levinthal. Intel Xeon Processor Architecture. `https://software.intel.com/en-us/`, Jun 2013.

[61] Y. D. Liu. Green Thieves in Work Stealing. In *Seventeenth International Conference on Architectural Support for Programming Languages and Operating Systems*, ASPLOS 2012, London, United Kingdom, 2012.

[62] S. E. Lucco. *Adaptive Parallel Programs*. PhD thesis, EECS Department, University of California, Berkeley, Aug 1994.

[63] E. Lusk and A. Chan. Early Experiments with the OpenMP/MPI Hybrid Programming Model, 2004.

[64] E. Lusk, N. Doss, and A. Skjellum. A High-performance, Portable Implementation of the Message Passing Interface Standard. *Parallel Computing*, 22:789–828, 1996.

[65] P. D. V. Mann and U. Mittaly. Handling OS Jitter on Multicore Multithreaded Systems. In *Proceedings of the 2009 IEEE International Symposium on Parallel and Distributed Processing Symposium*, Rome, Italy, 2009. IEEE Computer Society.

[66] J. D. McCalpin. STREAM: Sustainable Memory Bandwidth in High Performance Computers. Technical report, University of Virginia, Charlottesville, VA, USA, 1991-2007. A continually updated technical report.

[67] R. G. Minnich, M. J. Sottile, S.-E. Choi, E. Hendriks, and J. McKie. Right-weight Kernels: An off-the-shelf Alternative to Custom Lightweight Kernels. *SIGOPS Oper. Syst. Rev.*, 40(2):22–28, Apr. 2006.

[68] A. Morari, R. Gioiosa, R. Wisniewski, F. J. Cazorla, and M. Valero. A Quantitative Analysis of OS Noise. In *Proceedings of the IEEE International Parallel and Distributed Processing Symposium*, Anchorage, AK, USA, May 2011.

[69] A. Muddukrishna, P. A. Jonsson, V. Vlassov, and M. Brorsson. Locality-Aware Task Scheduling and Data Distribution on NUMA Systems. In A. P. Rendell, B. M. Chapman, and M. Miller, editors, *OpenMP in the Era of Low Power Devices and Accelerators*, volume 8122 of *Lecture Notes in Computer Science*, pages 156–170. Springer Berlin Heidelberg, 2013.

[70] A. Nataraj, A. Morris, A. D. Malony, M. Sottile, and P. Beckman. The Ghost in the Machine: Observing the Effects of Kernel Operation on Parallel Application Performance. In *Proceedings of the 2007 ACM/IEEE Conference on Supercomputing*, pages 1–12, Reno, NV, USA, 2007. ACM.

[71] S. L. Olivier, B. R. de Supinski, M. Schulz, and J. F. Prins. Characterizing and Mitigating Work Time Inflation in Task Parallel Programs. In *Proceedings of the International Conference on High Performance Computing, Networking, Storage and Analysis*, SC '12, pages 65:1–65:12, Salt Lake City, UT, USA, 2012. IEEE Computer Society Press.

[72] F. Petrini, D. J. Kerbyson, and S. Pakin. The Case of the Missing Supercomputer Performance: Achieving Optimal Performance on the 8,192 Processors of ASCI Q. In *Proceedings of the 2003 ACM/IEEE Conference on Supercomputing*, Phoenix, AZ, USA, 2003. IEEE Computer Society.

[73] J. C. Phillips, G. Zheng, S. Kumar, and L. V. Kalé. NAMD: Biomolecular simulation on thousands of processors. In *Proceedings of the 2002 ACM/IEEE Conference on Supercomputing*, pages 1–18, Baltimore, MD, USA, September 2002.

[74] T. Pohl, F. Deserno, N. Thurey, U. Rude, P. Lammers, G. Wellein, and T. Zeiser. Performance Evaluation of Parallel Large-Scale Lattice Boltzmann Applications on Three Supercomputing Architectures. In *Proceedings of the 2004 ACM/IEEE Conference on Supercomputing*, SC '04, Pittsburgh, PA, USA, Nov 2004. IEEE Computer Society.

[75] C. D. Polychronopoulos and D. J. Kuck. Guided Self-scheduling: A Practical Scheduling Scheme for Parallel Supercomputers. *IEEE Transactions of Computing*, 36:1425–1439, December 1987.

[76] L. Prylli and B. Tourancheau. Fast Runtime Block Cyclic Data Redistribution on Multiprocessors. *Journal of Parallel and Distributed Computing*, 45(1):63 – 72, 1997.

[77] D. Quinlan. ROSE: Compiler Support for Object-Oriented Frameworks. *Parallel Processing Letters*, 10, January 2000.

[78] R. Rabenseifner. Hybrid Parallel Programming: Performance Problems and Chances. In *In Proceedings of the Forty-Fifth Cray User's Group Conference*, Columbus, OH, USA, May 2003.

[79] H. Rein and S. F. Liu. REBOUND: An Open-source Multi-purpose N-body Code for Collisional Dynamics. *Astronomy and Astrophysics*, 537:A128, 2012.

[80] J. Reinders. *Intel Threading Building Blocks: Outfitting C++ for Multi-Core Processor Parallelism*. O'Reilly Media, 2007.

[81] B. Rountree, D. K. Lowenthal, B. R. de Supinski, M. Schulz, V. W. Freeh, and T. Bletsch. Adagio: Making DVS Practical for Complex HPC Applications. In *Proceedings of the 23rd International Conference on Supercomputing*, ICS '09, pages 460–469, Yorktown Heights, NY, USA, 2009. ACM.

[82] S. Seelam, L. Fong, A. Tantawi, J. Lewars, J. Divirgilio, and K. Gildea. Extreme-scale Computing: Modeling the Impact of System Noise in Multicore Clustered Systems. In *Proceedings of the IEEE International Parallel and Distributed Processing Symposium*, pages 1–12, Atlanta, GA, USA, April 2010.

[83] J. R. Shewchuk. Triangle: Engineering a 2D Quality Mesh Generator and Delaunay Triangulator. In M. C. Lin and D. Manocha, editors, *Applied Computational Geometry: Towards Geometric Engineering*, volume 1148 of *Lecture Notes in Computer Science*, pages 203–222. Springer-Verlag, May 1996. From the First ACM Workshop on Applied Computational Geometry.

[84] F. Song, A. YarKhan, and J. Dongarra. Dynamic Task Scheduling for Linear Algebra Algorithms on Distributed-Memory Multicore Systems. In *Proceedings of the Conference on High Performance Computing Networking, Storage and Analysis*, Portland, OR, USA, 2009. ACM.

[85] P. Stenström. A Survey of Cache Coherence Schemes for Multiprocessors. *Computer*, 23(6):12–24, June 1990.

[86] A. Talamo. Numerical Solution of the Time Dependent Neutron Transport Equation by the Method of the Characteristics. *Journal of Computational Physics*, 240(0):248 – 267, 2013.

[87] Y. Tang, R. A. Chowdhury, B. C. Kuszmaul, C.-K. Luk, and C. E. Leiserson. The Pochoir Stencil Compiler. In *Proceedings of the Twenty-third Annual ACM Symposium on Parallelism in Algorithms and Architectures*, SPAA '11, pages 117–128, San Jose, CA, USA, 2011. ACM.

[88] T. Trader. Obamas 2016 Budget Boosts R & D Exascale Funding. `http://www.hpcwire.com/2015/02/04/obamas-2016-budget-request-holds-clues-exascale/`.

[89] L. N. Trefethen and I. David Bau. Numerical Linear Algebra.

[90] D. Tsafrir, Y. Etsion, D. G. Feitelson, and S. Kirkpatrick. System Noise, OS Clock Ticks, and Fine-grained Parallel Applications. In *Proceedings of the 19th annual international conference on Supercomputing*, ICS '05, pages 303–312, Cambridge, MA, USA, 2005. ACM.

[91] S. Vetter. Architecture of the IBM POWER7+ Technology-Based IBM Power 750 and IBM Power 760. `http://www.redbooks.ibm.com/Redbooks.nsf/RedbookAbstracts/tips0972.html`, Feb. 2013.

[92] M. S. Warren and J. K. Salmon. A Parallel Hashed Oct-Tree N-body Algorithm. In *Proceedings of the 1993 ACM/IEEE Conference on Supercomputing*, SC '93, pages 12–21, Portland, OR, USA, 1993. ACM.

[93] S. Williams, J. Carter, L. Oliker, J. Shalf, and K. A. Yelick. Optimization of a Lattice Boltzmann Computation on State-of-The-art Multicore Platforms. *Journal of Parallel and Distributed Computing*, 2009.

[94] G. Zheng. *Achieving High Performance on Extremely Large Parallel Machines: Performance Prediction and Load Balancing.* PhD thesis, Department of Computer Science, University of Illinois at Urbana-Champaign, 2005.